Palaeontologia Electronica
palaeo-electronica.org

Temperate to tropical palaeoclimates on the northwest margin of Europe during the middle Cenozoic

Jessica McCoy, Martha E. Gibson, Emma P. Hocking, Jennifer M.K. O'Keefe, James B. Riding, Raymond Roberts, Stewart Campbell, Geoffrey D. Abbott, and Matthew J. Pound

ABSTRACT

Globally, the middle Cenozoic (Oligocene to early Miocene, ~33.9–15.97 Ma) was characterized by a warmer, wetter climate than present. Reconstructing the climate of this stratigraphic interval helps us to better understand the implications of present and future anthropogenically-driven climate change in an Earth system with an established Antarctic ice mass and comparable pCO_2 levels (400–700 ppm). Relative to mainland Europe, little palaeoclimate work has been done on the British Isles for this time interval. Compiled middle Cenozoic palynology records from across the British Isles were used to quantitatively reconstruct palaeoclimate, which was then used to define Köppen-Geiger signatures for each palynomorph assemblage. These reconstructions were used to show the presence of a temperate, dry-winter and hot-summer *(Cwa)* Köppen-Geiger climate type before 31.8 Ma, which was possibly a short-lived event driven by precessional (~26 k.y.) forcing. We attribute reconstructions with dry-winter Köppen-Geiger classifications to combined eccentricity-obliquity-precession (~405 k.y.) forcing, after the Eocene–Oligocene Transition. Declines in Mean Annual Temperature, in Chattian sections, are associated with the *Svalbardella*-2 and 3 North Sea cooling events. The late Oligocene warming event is shown to have produced tropical rainforest *(Af)* Köppen-Geiger classification types in the British Isles. Following early Miocene glaciation, a temperate, no-dry-season, warm-summer *(Cfb)* signature was reconstructed. We suggest the present-day climate of the northwest margin of Europe is comparable to the early Miocene palaeoclimate. Under increased pCO_2 concentrations, based on projected twenty-first century anthropogenic warming scenarios, there is potential for wetter summers becoming more prevalent within the next century.

Jessica McCoy. Department of Engineering and Environmental Sciences, Northumbria University, Newcastle upon Tyne, UK. jessica.mccoy@northumbria.ac.uk
Martha E. Gibson. Department of Geology and Geography, West Virginia University, Morgantown, West Virginia, USA and PetroStrat, Parc Caer Seion, Conwy, UK. Martha.Gibson@petrostrat.com

Final citation: McCoy, Jessica, Gibson, Martha E., Hocking, Emma P., O'Keefe, Jennifer M.K., Riding, James B., Roberts, Raymond, Campbell, Stewart, Abbott, Geoffrey D., and Pound, Matthew J. 2024. Temperate to tropical palaeoclimates on the northwest margin of Europe during the middle Cenozoic. Palaeontologia Electronica, 27(2):a43.
https://doi.org/10.26879/1349
palaeo-electronica.org/content/2024/5275-mid-cenozoic-palaeoclimates-northwest-europe

Emma P. Hocking. Department of Engineering and Environmental Sciences, Northumbria University, Newcastle upon Tyne, UK. emma.hocking@northumbria.ac.uk
Jennifer M.K. O'Keefe. Department of Physics, Earth Science and Space Systems Engineering, Morehead State University, Morehead, Kentucky, USA. j.okeefe@moreheadstate.edu
James B. Riding. British Geological Survey, Keyworth, Nottingham, UK. jbri@bgs.ac.uk
Raymond Roberts. Natural Resources Wales, Chester Road, Flintshire, UK. raymond.roberts@cyfoethnaturiolcymru.gov.uk
Stewart Campbell. Natural Resources Wales, Chester Road, Flintshire UK. stewart.campbell@cyfoethnaturiolcymru.gov.uk
Geoffrey D. Abbott. School of Natural and Environmental Sciences, Newcastle University, Newcastle upon Tyne, UK. geoff.abbott@newcastle.ac.uk
Matthew J. Pound. Department of Engineering and Environmental Sciences, Northumbria University, Newcastle upon Tyne, UK. matthew.pound@northumbria.ac.uk

Key words: middle Cenozoic; British Isles; palaeobotany; palaeoclimate; palynology; Köppen-Geiger

Submission: 10 October 2023. Acceptance: 15 July 2024.

INTRODUCTION

Collapse of the Greenland ice sheet may occur within the next century, because of the weakening of ice shelf structure. This will produce a world with substantial ice sheets in the southern hemisphere only (Pattyn et al., 2018; Boers and Rypdal, 2021; Armstrong McKay et al., 2022; IPCC, 2022). The middle Cenozoic (Oligocene–early Miocene) was the last stratigraphic interval that had substantial ice solely in Antarctica (Wade and Pälike, 2004; Armstrong McKay et al., 2022). Following the formation of substantial ice in Antarctica during the Eocene–Oligocene Transition (Hutchinson et al., 2021), the Oligocene was an interval of fluctuating temperatures that included several warming intervals (such as the late Oligocene warming) and culminated in a major glaciation event around the Oligocene – Miocene boundary (Miller et al., 1991; Zachos et al., 1997; Wilson et al., 2008; Woods et al., 2014; Greenop et al., 2019).

There is a discrepancy in palaeoclimate reconstructions of the northwest margin of Europe during the Oligocene–Miocene time interval (Eldrett et al., 2009). The late Oligocene warming event (~25–24 Ma), in the North Atlantic marine record, corresponds with a reconstructed decline in pCO_2 (~450–200 ppm; Zachos et al., 2001a; O'Brien et al., 2020). However, this has not been resolved with the known role of atmospheric pCO_2 in global temperature change (Zachos et al., 2001a; Crowley and Berner, 2001; Scheffer et al., 2006). Here we provide new palaeoclimate reconstructions for the Oligocene to early Miocene from the United Kingdom and Ireland to document changes in terrestrial palaeoclimates during this interval. From the resulting reconstruction we present the magnitude of warming associated with the early Oligocene (Rupelian, 33.9–27.82 Ma) and the late Oligocene warming events, as well as the impacts of Early Miocene glaciation on this oceanographically sensitive terrestrial region.

BRIEF OVERVIEW OF PALAEOCLIMATES FROM THE EOCENE–OLIGOCENE TRANSITION TO THE EARLY MIOCENE

The Eocene–Oligocene Transition (circa 33.9 Ma) resulted in a global stepwise transition from greenhouse to icehouse conditions, within 0.4 Ma (Lear et al., 2000; Zachos et al., 2001a; Zachos and Kump, 2005; Katz et al., 2008; Zanazzi et al., 2007; Liu et al., 2009; Pound and Salzmann, 2017; Straume et al., 2022). A weakening of the North Atlantic overturning circulation and reductions in pCO_2 (1000–400 ppm, O'Brien et al., 2020) led to reductions in temperatures in the Northern Hemisphere (Straume et al., 2022). A southward expansion of the Hadley Cell led to intensified tropical-rain regimes and temperatures (where winter temperatures exceeded 20°C) to the Southern Hemisphere, causing an intensification of the North Atlantic circulation. This in turn resulted in Northern Hemispheric cooling (Straume et al., 2022). The Eocene–Oligocene Transition cooling, associated with the positive (>1 ‰) $\delta^{18}O$ excursion from the deep sea benthic foraminiferal record (Miller et al., 1991; Lear et al., 2000; Coxall et al., 2005; Wade et al., 2012; Brzelinski et al., 2023), led to the

establishment of the present-day Antarctic ice sheet (Kennett and Shackleton, 1976; Ehrmann and Mackensen, 1992; Ivany et al., 2006; Galeotti et al., 2016). Other Eocene–Oligocene Transition-timed cooling-drivers included eustatic sea-level fall (Katz et al., 2008; Ladant et al., 2014; Miller et al., 2020); tectonics (Dupont-Nivet et al., 2007; Karagaranbafghi and Neubauer, 2018), and the opening of the Tasmanian Gateway, which strengthened the developing Antarctic Circumpolar Current (Kennett, 1977; Pound and Salzmann, 2017). Eocene–Oligocene Transition-driven cooling, particularly in high latitudes (Liu et al., 2009) contributed to increased Northern Hemispheric seasonality, with a reduction in high-latitude winter temperatures by 4–5°C (Ivany et al., 2000; Eldrett et al., 2009) and a northward shift of the Intertropical Convergence Zone (Hyeong et al., 2016; Straume et al., 2022).

Köppen-Geiger signatures assigned to Rupelian assemblages, from Central Europe, suggest that there was no overall dry-season (Pross et al., 1998, 2001; Kovar-Eder, 2016; Maxwell et al., 2016). Dry-winter Köppen-Geiger climate types, driven by the Asian monsoon system, likely developed throughout the Eocene in India (Shukla et al., 2014) and remained prevalent in Asian regions throughout the Oligocene (Srivastava et al., 2012; Miao et al., 2013; Lin et al., 2015; Farnsworth et al., 2019; Bhatia et al., 2021; Ling et al., 2021; Li et al., 2023). However, the palaeo spread of *Podocarpium,* often attributed to monsoonal-climate conditions, moved into Europe throughout the Cenozoic (Han et al., 2020). We suggest that the summer-monsoonal system may have been established sometime in Oligocene Europe, particularly in the Rupelian, where the Upper Rhine assemblage (Germany) reconstructed a temperate palaeoclimate with hot summers, and a slightly monsoonal signal (*Cwb*; Kovar-Eder, 2016).

From the onset of the Oligocene, there was a transition to a bipolar deep-water circulation, leading to the deep-water formation in the North Atlantic (Via and Thomas, 2006). This led to the development of a proto-Gulf Stream, which contributed to enhanced warming at high Northern Hemispheric latitudes (Via and Thomas, 2006).

Global cooling and periods of ice-sheet expansion and decline surrounding the Oligocene–Miocene Transition occurred in 100 k.y. cycles, likely driven by short-term eccentricity (100 k.y.), paced episodes (Zachos et al., 2001b; Lear et al., 2004; Pälike et al., 2006; Beddow et al., 2016; Liebrand et al., 2017; Greenop et al., 2019). Short-lived (~500 k.y.), orbitally forced glacial events, characterised by increases in the deep-sea foraminiferal $\delta^{18}O$ record throughout the Oligocene and Miocene, were described as Oligocene isotope (Oi-) and Miocene isotope (Mi-) stages (Miller et al., 1991; Zachos et al., 2001b; Van Simaeys et al., 2005). Cooling events Oi-1a (~33.5 Ma, -1.3 $‰_o$) and Oi-2b, at the Rupelian-Chattian boundary (~27.82 Ma), and Mi-1 (~23.03 Ma) were driven by eccentricity minima (~405 k.y.) and low amplitude obliquity (1.2 m.y.) (Pälike et al., 2006; Jovane et al., 2006; Śliwińska and Heilmann-Clausen, 2011; Fenero et al., 2013). The influx of the Arctic-marker dinoflagellate cyst *Svalbardella cooksoniae,* in the North Atlantic, are associated with these cooling phases, and are labelled as *Svalbardella* events 3, 2, and 1, respectively (Van Simaeys et al., 2005; Śliwińska et al., 2010; Clausen et al., 2012; Śliwińska et al., 2014). Northern Hemispheric summer season warmth, throughout the Oligocene, was driven by Earth's position at perihelion (De Vleeschouwer et al., 2017). The late Oligocene warming events in Central Europe occurred within an interval of increased late Oligocene (Chattian, 27.82–23.03 Ma) temperatures (Zachos et al., 2001a; De Man and Van Simaeys, 2004; Utescher et al., 2015; Moreno-Domínguez et al., 2021). The late Oligocene warming event was marked by the first appearance of *Asterigerina*-type foraminifera in North Atlantic assemblages, and by a rise in eustatic sea-level (Doppert and Neele, 1983; King, 1983, 1989; Van Simaeys, 2004).

A warming trend was interrupted by a return to global glacial conditions with the transition from the Oligocene–Miocene at 23.03 Ma (Zachos et al., 1997; Lear et al., 2000; Brzelinski et al., 2023). A positive excursion in benthic foraminferal isotopic signatures suggested there was a reduction in mean global air temperatures, with a distinct gradient between the mid and high latitudes in air temperatures (Zachos et al., 2001b; Beddow et al., 2016; Liebrand et al., 2017; Torricelli et al., 2022). Following this cooling event, early Miocene European floral assemblages reconstructed well-drained riparian wetlands, with subtropical to tropical elements (Bessedik, 1984; Huguenery and Truc, 1976; Velitzelos et al., 2014). This Miocene warm palaeoclimate occurred when the summertime incoming solar radiation angle was at its maximum position (De Vleeschouwer et al., 2017).

To test whether these Central European reconstructions were consistent with the northwest margin of Europe, we set out to reconstruct the palaeoclimate of the British Isles, for the Oligocene

to early Miocene. From our palaeoclimate reconstructions, we aim to assign Köppen-Geiger classes to study sites to illustrate palaeoclimate change during this interval of unipolar glaciation.

GEOLOGICAL SETTING OF THE BRITISH ISLES

The current climate of the British Isles (used here to refer to the islands that make up the countries of Ireland and the United Kingdom) is warm with relatively dry summer conditions. This climate is maintained by high pressure westerlies, and east-moving polar jet streams, which are strengthened between the winter to early spring months and create common fog and drizzle (Mayes, 1991, 1996; Hulme and Barrow, 1997; Hall et al., 2015; Methner et al., 2020). Westerlies were believed to have been established from the middle Miocene (Serravallian, 13.65–11.63 Ma) according to Quan et al. (2014) and Pound and Riding (2016). Given the relatively low topography of the northwest margin of Europe during the Miocene (Roberts, 1975), westerlies may have driven a stronger, more intense precipitation regime than those reconstructed for southern Europe (Henrot et al., 2010). The Gulf Stream contributes to the present-day warmth of the British Isles, and it regulates a mild winter regime; the Gulf Stream was established by at least the middle Miocene (Denk et al., 2013; Pound and McCoy, 2021). With the onset of anthropogenically-driven climate change, the future climate of the British Isles is expected to develop hotter summers and wetter winters (Pope et al., 2021).

The British Isles have an abundance of onshore and offshore Oligocene siliciclastic deposits (Figure 1A–B). These are present in clay and lignite beds in the North Sea, the Republic of Ireland, Northern Ireland, Wales, and southern England (Figure 1A–B; Appendix 1). These units likely formed in shoreline environments, a result of the palaeo-shoreline being located ~75 km east during the Oligocene, relative to present-day (Murray, 1992; Walsh, 2001). Most of these strata lie along the Sticklepath-Lustleigh Fault that runs northwest from southwest England towards Northern Ireland and appears to have been a major influence on post-Eocene sediment accumulation (Tappin et al., 1994; King et al., 2016; Figure 1A–B). Therefore, the British Isles have a limited

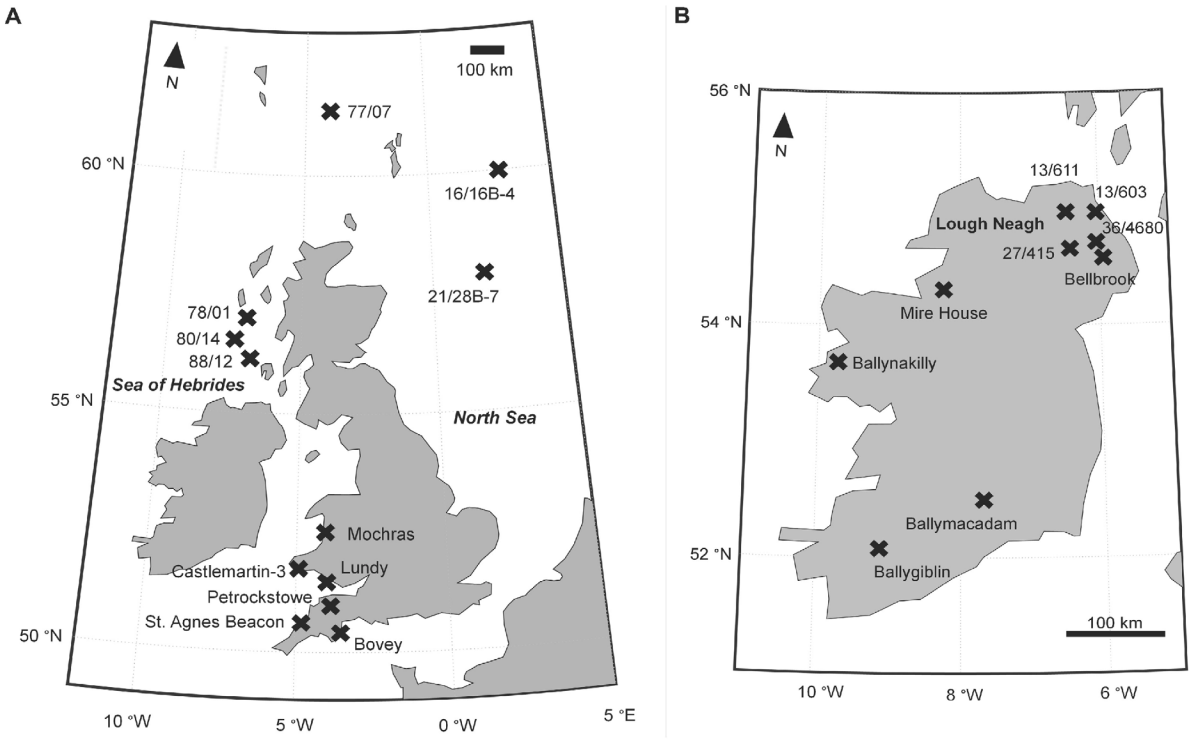

FIGURE 1. Locations of study sites (as marked by X) across the British Isles (Figure 1A) and in Northern Ireland and the Republic of Ireland (Figure 1B). Land outlines created using MATLAB Mapping Toolbox (The Mathworks Inc., 2021).

amount of onshore Utescher et al. (2024) sediment of post-Eocene age available for palaeoclimate reconstruction. Offshore coring expeditions have retrieved abundant post-Eocene siliciclastic deposits (Wilson, 1996).

METHODS

Data Synthesis

Seventy-eight published onshore and offshore Oligocene to early Miocene pollen assemblages (Figure 2), from the British Isles, were compiled into a presence-absence matrix (Appendix 2; King et al., 2016).

Details of each site, including coordinates, borehole names, lithology/sedimentology, and previous palynological reconstructions, are available in Appendix 1. The biostratigraphical ranges of dinoflagellate cysts, recovered from assemblages 16/16B-4, and 21/28B-7 by Wilson (1996), were reviewed and updated to reflect current biostratigraphical correlations (Wilson, 1996; Egger et al., 2016; King et al., 2016) of the concerned dinoflagellate cysts. Fossil form names were synonymised, where possible, following Stuchlik et al. (2001, 2002, 2009, 2014) and Utescher et al. (2024) (Appendix 3). Due to the morphological similarities between pollen-types belonging to the Cupressaceae family (Bortenschlager, 1990; Bouchal and Denk, 2020), genera belonging to the Cupressaceae family (e.g., *Sequoiapollenites*) were assigned “Cupressaceae” for their NLR.

The relict taxon *Sciadopitys*-type was removed from reconstructions. This is because their modern biogeography is limited in comparison to their Cenozoic environmental distribution, which was much broader (Mosbrugger et al., 1994; Figueiral et al., 1999; Utescher et al., 2014).

Palaeoclimate Reconstruction

The Climate Reconstruction SofTware (CREST, *crestr* R package) probability density function-based (pdf) model was used to reconstruct climate variables, based on the present-day distributions of contemporary taxa and the corresponding climatic tolerance ranges of assigned nearest-living relatives of pollen (Table 1, page 39); Chevalier et al., 2014; Chevalier, 2019; Chevalier, 2022). Modern floral distribution data was taken from the Global Biodiversity Information Facility (GBIF, 2020a–g). CREST-based outputs delivered an optimised value, based on the WorldClim2 climate dataset (Fick and Hijmans, 2017) with 50% and 95% uncertainty ellipses defined (Chevalier et al., 2014).

Full details of the CREST model, R code, and background can be found in Chevalier et al. (2014) and Chevalier (2022). To assign Köppen-Geiger climate-types to assemblages, CREST was used to reconstruct the Mean Annual Temperature (MAT), Mean Temperature of the Warmest Quarter (MTWQ), Mean Temperature of the Coldest Quarter (MTCQ), Mean Annual Precipitation (MAP), Precipitation of the Driest Quarter (MPDry); Precipitation of the Warmest Quarter and Precipitation of the Coldest Quarter (Fick and Hijmans, 2017).

Assignment of Köppen-Geiger classes, using output variables from CREST was adapted from the Köppen-Geiger assignment method (Beck et al., 2018). Tropical rainforest signatures *(Af)* were

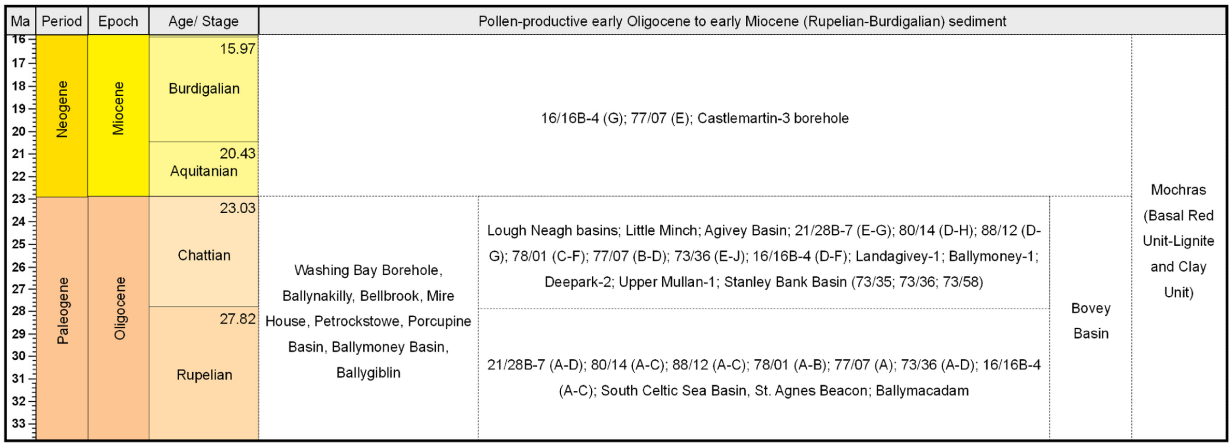

FIGURE 2. Previously assigned ages of selected onshore and offshore Oligocene-Miocene succession from the British Isles, based on King et al. (2016).

assigned to sites where MTCQ reconstructions exceeded 18°C, and where seasonal MAP, minus the Precipitation of the Driest Quarter, gave a positive value, thus indicating no dry season. Assemblages which reconstructed MTCQ values between 0–18°C were assigned a subtropical-temperate climate signature *(C).* Palaeoclimate types with a dry season were determined by differences between the Precipitation of the Warmest Quarter and the Precipitation of the Coldest Quarter, and their comparison to the annual rainfall, as adapted by Beck et al. (2018) (Table 2, page 45). Where reconstructions of the Precipitation of the Warmest Quarter exceeded the Precipitation of the Coldest Quarter by 10 mm, a dry-winter signal was assigned *(Cw).* Where the difference between the Precipitation of the Coldest and Warmest Quarter reconstructions did not exceed 10 mm, reconstructions were assigned a no-dry-season signal *(Cf).* Subtropical signatures were assigned hot summer (–*a*) and warm summer (–*b*) signals, where MTWQ reconstructions were >22°C and 12–22°C, respectively.

MPDry reconstructions were unsuccessful where particular families were included, i.e., Anacardiaceae; Asteraceae; Caprifoliaceae; Fabaceae; Lythraceae; Malvaceae; Poaceae and Solanaceae (Table 1). These taxa were removed from MPDry model runs. This was because their tolerance ranges, regarding MPDry, included 0 and so this resulted in a zero-based error being carried forward throughout model runs, resulted in an impossible division of a value by 0. As a result of the removal of these families, MPDry reconstructions may have been skewed towards wetter reconstructions.

RESULTS

Palaeoclimate Reconstruction

In text, palaeoclimate reconstructions are presented with their reconstructed optima, followed by their largest 50% confidence interval, marked after "±". Model results, with 50% uncertainty ranges with differences from optima, are provided in Appendix 4.

Mean annual temperature. Rupelian Mean Annual Temperature (MAT) reconstructions were lowest in the southernmost localities, i.e., the St. Agnes Beacon and Bovey Basin, where the optimal MAT reconstruction was 13.37 ±1.51°C (Figure 3). The Ballymacadam Rupelian assemblage reconstructed a higher MAT value of 16.38°C ±1.51°C (Figure 4). We note that overlaps in 50% statistical uncertainties occurred in reconstructions of 16/16B-4 (associations A–B); 88/12 (associations A–B) and 73/36 (D–E), other discussed MAT reconstructions throughout sequences below showed no overlap, and therefore showed statistically significant change (Appendix 4).

Between associations A–B of site 73/36 (>31.8 Ma), reconstructed MATs increase from 13.37 (±1.51)–20.91 (±1.51)°C; no other MAT increases are reported from other Rupelian reconstructions (Figure 5). Between associations A–B, of well 16/16B-4 there is a reduction in MAT, from 19.40 (±1.51)–17.89 (±1.51)°C, where associations are assigned to 32.1–31.7 Ma (Figure 5). Significant, non-overlapping cooling from 20.91 (±1.51)–14.87 (±1.51)°C occurred from 32.1–31.7 Ma at site 21/28B-7, as shown by reconstructions from associations B–C of well 21/28B-7 (Figure 5). Similar reductions in MAT were reconstructed using assemblages from: associations A–B of site 88/12, (14.87 [±1.51]–11.86 [±1.51]°C, deposited >31.5 Ma); associations A–C of borehole 80/14, (22.41 [±0.00]–19.40 [±1.51]°C, deposited <31.8 Ma), and from associations D–E of borehole 73/36 (19.40 [±1.51] –17.89 [±0.00]°C, deposited <31.8 Ma) (Figure 5). Associations A–B of site 77/07 did not reconstruct cooling during this time (Figure 5).

All Chattian MAT reconstructions exceed their present-day MAT values (Figures 3–5; Table 2). MAT reconstructions surrounding Lough Neagh produce similar optimal values, ranging from 13.37–14.87°C in boreholes 13/603, 13/611, 27/415, and 36/4680 (Figure 4). Associations B–D of Well-28 reconstructed a decline in MAT (22.42 [±0.00] –14.87 [±1.51]°C) that occurred between ~31.65–25.8 Ma (Figure 4). MAT reconstructions from associations A–G of 78/01 suggest MAT increased from 17.89 [±1.51]–22.41 [±1.51]°C without interruption between 33.9–24.8 Ma (Figure 5).

The Mochras Basal Red Unit reconstructed an increase in MAT, from 17.89 ±1.51°C to 23.92 ±1.51°C at depths 515.42 m and 408.43 m, respectively (Figure 5). Between the Mochras Basal Red Unit (408.43 m) and the Transitional Unit (368.80 m), reconstructions indicate a decline in MAT from 23.92 ±1.51°C to 14.87 ±1.51°C (Figure 5). Reconstructed MAT decline to 8.84 ±0.00°C at depth 368.20 m, then increase to 11.86 ±1.51°C at depth 324.61 m (Figure 5). The assemblage from Association E of 77/07 (<23.03 Ma) and the Castlemartin-3 assemblage (<23.03 Ma) reconstruct MATs of 11.86 (± 1.51)°C (Figure 3).

Mean temperature of the warmest quarter. All Chattian MTWQ reconstructions exceed the variables of their present-day location (Table 2).

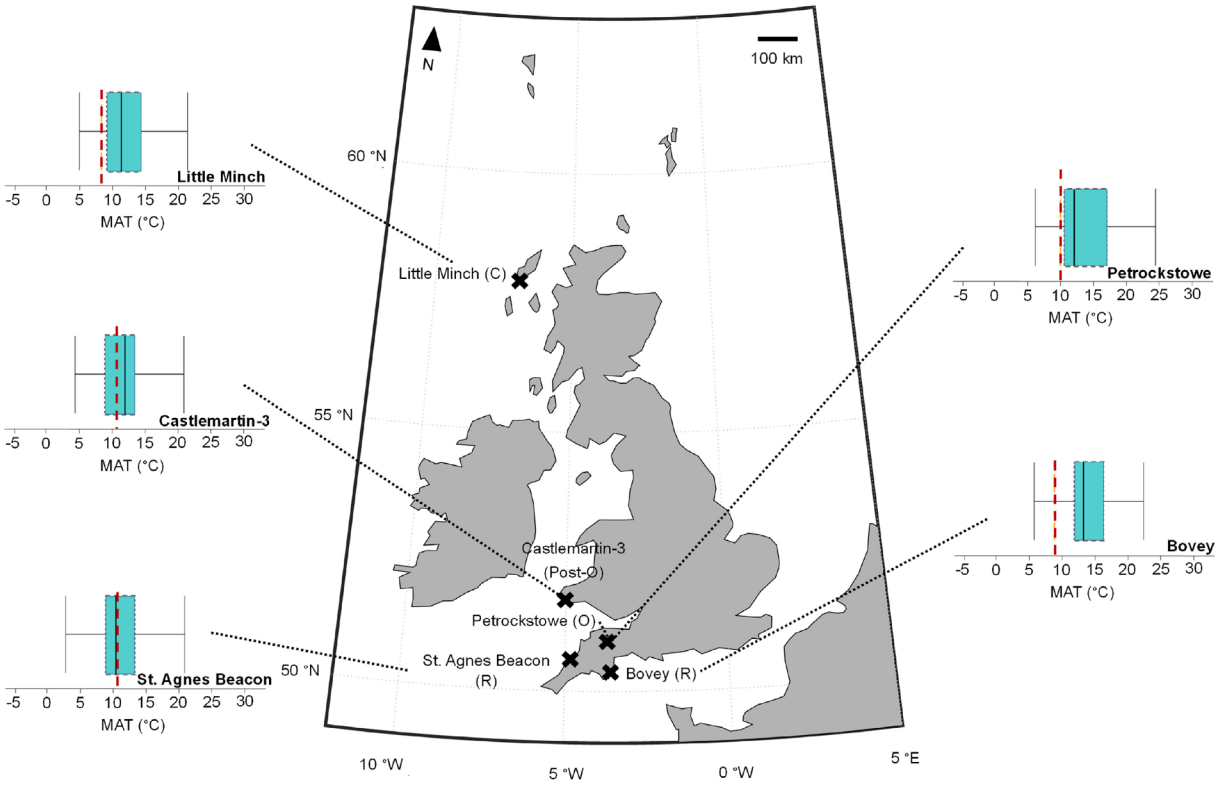

FIGURE 3. Mean Annual Temperature (MAT) reconstructions based on study sites where only one pollen assemblage was available. The red dotted line shows the present-day MAT. Solid black lines show the value of the reconstructed optima. The grey dotted lines and grey solid lines show the respective uncertainty ranges of 50 % and 95 %. Rupelian, Chattian, and Oligocene sites are labelled (R), (C), and (O), respectively.

Sequences show no change to their optima reconstructions, from their Rupelian counterparts (Figure 6). Of the discussed changes in MTWQ below, we acknowledge overlap in uncertainty ranges in studied depths of the Mochras borehole, from in 77/07 (associations D–E).

Chattian MTWQ reconstructions from associations C–D of borehole 77/07 remain unchanged from 24.62 (±0.00–1.41)°C prior to 37.1 Ma (Figure 6). MTWQ optimal reconstructed from the borehole 73/35 and borehole 73/58 assemblages overlap with the reconstructed optima from association A of borehole 73/36 with overlap occurring between, 33.9–31.8 Ma (Figure 6). Depths 515.42–408.43 m of the Mochras Basal Red Unit reconstructed a shared MTWQ of 26.03 ±0.00°C (Figure 6). Between the Basal Red Unit and the Transitional Unit of the Mochras borehole, reconstructed MTWQ decline to 24.62 ±1.41°C (Figure 6). MTWQ declines to 16.18 ±1.41°C at depth 368.20 m of the Transitional Unit (Figure 6). At depth 324.61 m, reconstructed MTWQ increase to 17.59 ±1.41°C (Figure 6). Reconstructed MTWQ declined from 24.62 ±1.41°C to 21.81 ±1.41°C between Association D–E of borehole 77/07 (Chattian to early Miocene) (Figure 6).

Mean temperature of the coldest quarter. At >31.8 Ma, Rupelian assemblages from associations A–B of borehole 80/14 reconstructs a decline in MTCQ from 21.00 (±0.00) –19.40 (±1.61)°C (Figure 7). Associations A–B of borehole 88/12, reconstruct a decline in MTCQ from 9.74 (±3.21) –4.92 (±1.61)°C (Figure 7). Associations B–C of well 21/28B-7 (~32.1–32 Ma) reconstruct a substantial decline in MTCQ values from 19.40 (±1.61) –8.14 (±1.61)°C; after association C (<32 Ma) MTCQ values increase to 16.18 (±1.61)°C, in association D (Figure 7). Overlap between 50% uncertainty ranges were observed in 80/14 (associations A–B), 88/12 (associations A–B), 77/07 (associations B–C) and between depths in the Mochras borehole (Appendix 4).

Coldest MTCQ reconstructions were noted for the reconstruction of the southernmost sites: the

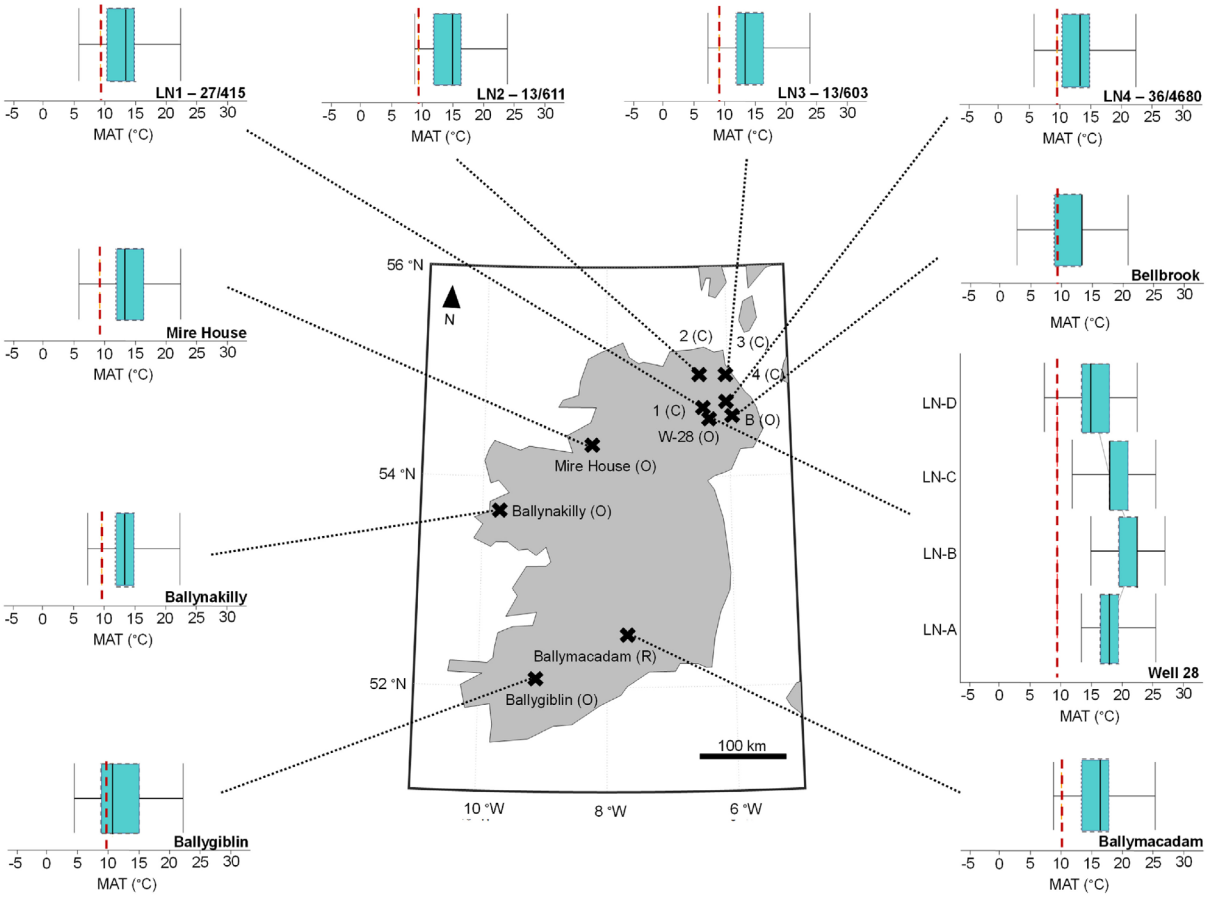

FIGURE 4. Mean Annual Temperature (MAT) reconstructions, based on pollen assemblages from Northern Ireland and the Republic of Ireland. The red dotted line shows the present-day MAT. Solid black lines show the value of the reconstructed optima. The grey dotted lines and grey solid lines show the respective uncertainty ranges of 50 % and 95 %. Rupelian, Chattian and Oligocene sites are labelled (R), (C), and (O), respectively. "B" and "W-28" are abbreviated for "Bellbrook" and "Well-28", respectively.

St. Agnes Beacon (4.92 ±1.60°C) and the Bovey Basin (6.53 ±1.61°C) (Figure 8). Assemblages from boreholes 13/603 and 36/4680 both reconstructed MTCQ values of 6.53 ±1.61°C, respectively (Figure 9). Assemblages from boreholes 27/415, 13/603, and 36/4680 reconstructed respective MTCQ values of 4.92 ± 1.60°C, 6.53 ± 1.61°C and 6.53 ±1.61°C (Figure 9). Well-28 reconstructed a step-like decline in reconstructed MTCQ, from 19.40 (±1.61) –9.75 (±3.22)°C between Associations B–D (Figure 9). Declines in MTCQ reconstructions were also seen in reconstructions taken from assemblages B–C of borehole 77/07 (31.7–26.8 Ma) where MTCQ temperatures declined from 16.18 (±1.61)–14.57 (±1.61)°C (Figure 7). Reconstructed MTCQ values decline from 19.40 (±3.21)–8.14 (1.61)°C for associations F–H of 80/14 (25.8–25.5 Ma) (Figure 7).

Lowest early Miocene MTCQ optimal reconstructions of 4.92 (±3.21)°C and 4.92 (±1.60)°C and 4.92 ±1.61°C were taken from the respective assemblages from Association E of borehole 77/07, the Castlemartin-3 borehole, and from depths 73–62.5 m of Little Minch (Figures 7–8; Table 2). A significant decline in optimal values from 16.18 (±1.61)°C to 4.92 (±3.22)°C from borehole 77/07 at Associations D–E (26.8–23.03 Ma) was reconstructed (Figure 7).

The Mochras Basal Red Unit reconstructs MTCQ values of 9.75 (±1.61)°C and 9.75 (±3.22)°C at depths 515.42 m and 408.43 m, respectively (Figure 7). MTCQ values decline to 6.53 (±3.21)°C at the Transitional Unit (368.80 m) then MTCQ reconstructions decline to 3.32 (±1.61)°C (at 368.20 m) (Figure 7). MTCQ reconstructions increase to 6.53 ±1.61°C (at 324.61 m) (Figure 7).

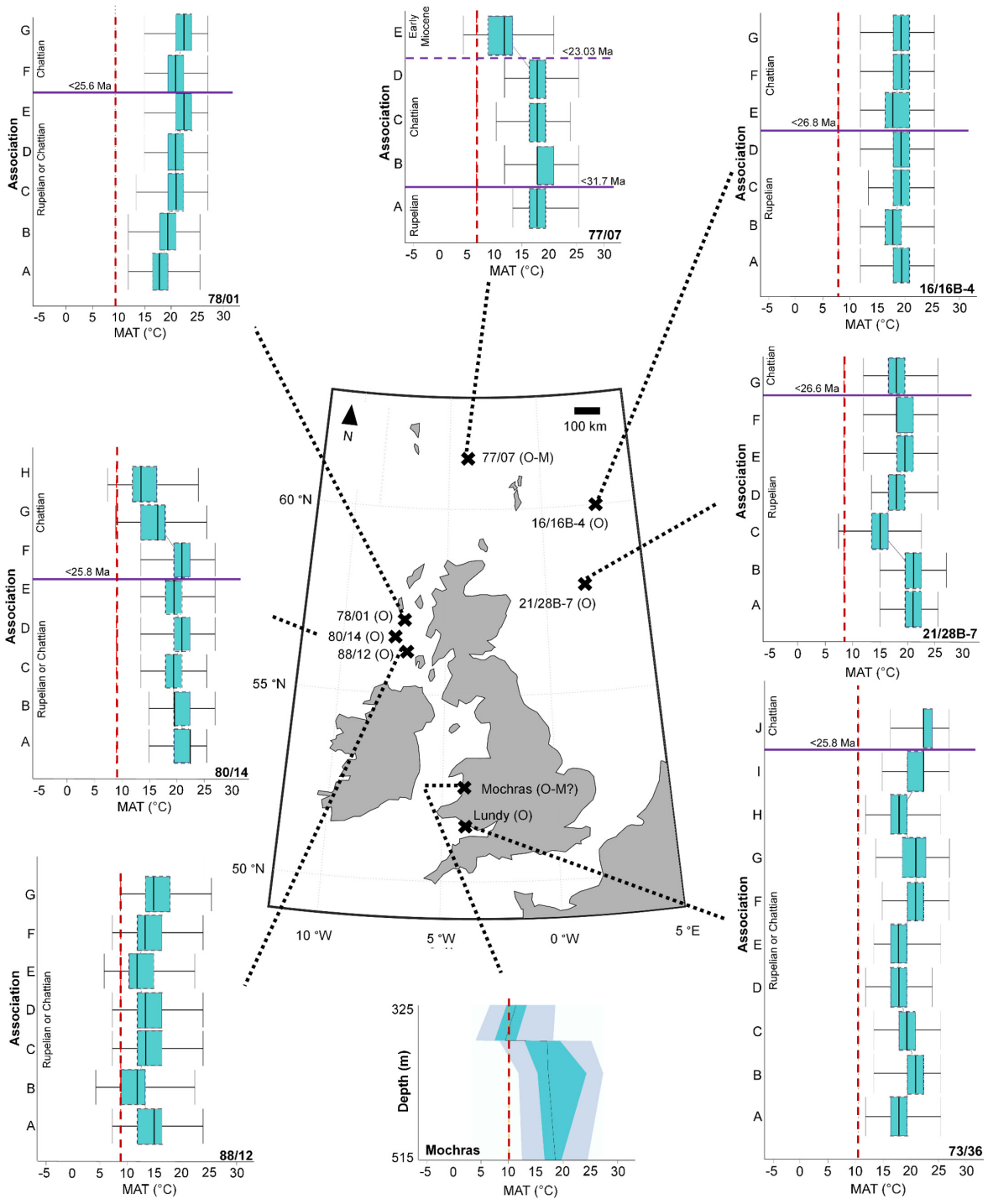

FIGURE 5. Mean Annual Temperature (MAT) reconstructions from the sequential boreholes. The red dotted line shows the present-day MAT. Solid black lines show the value of the reconstructed optima. The grey dotted lines and grey solid lines show the respective uncertainty ranges of 50 % and 95 %. Purple solid lines and purple dotted lines separate Rupelian from Chattian, and Chattian from early Miocene associations, respectively, based on dinoflagellate cyst zonation. The uppermost/ lowermost ages of depicted boundaries between epochs, based on dinoflagellate cyst zonation, have been labelled where possible. Oligocene and ?Miocene sites are labelled (O) and (M?), respectively.

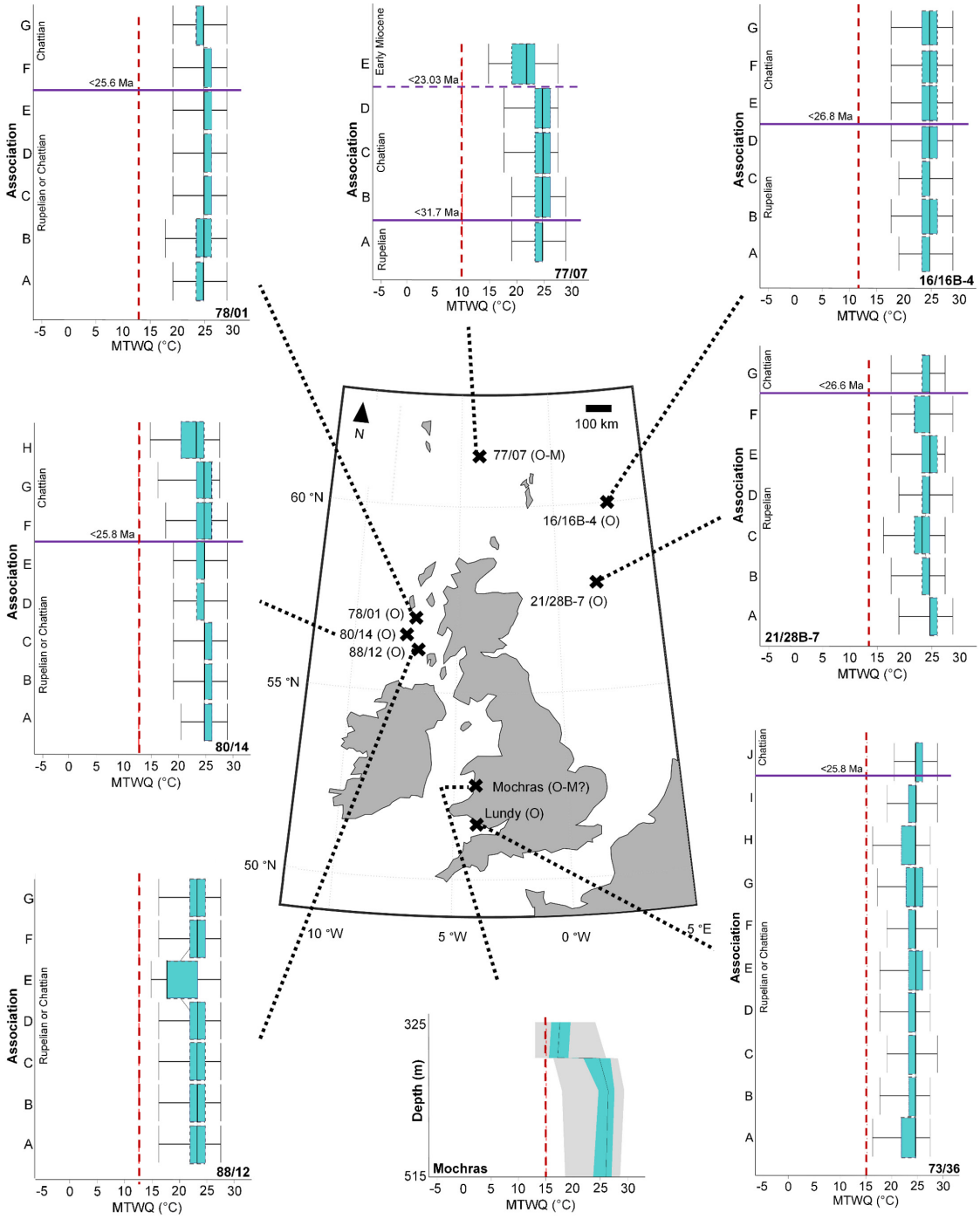

FIGURE 6. Mean Temperature of the Warmest Quarter (MTWQ) reconstructions from the sequential boreholes. The red dotted line shows the present-day MTWQ. Solid black lines show the value of the reconstructed optima. The grey dotted lines and grey solid lines show the respective uncertainty ranges of 50 % and 95 %. Oligocene and ?Miocene sites are labelled (O) and (M?), respectively. Purple solid lines and purple dotted lines separate Rupelian from Chattian, and Chattian from early Miocene associations, respectively, based on dinoflagellate cyst zonation. The uppermost/ lowermost ages of depicted boundaries between epochs, based on dinoflagellate cyst zonation, have been labelled where possible.

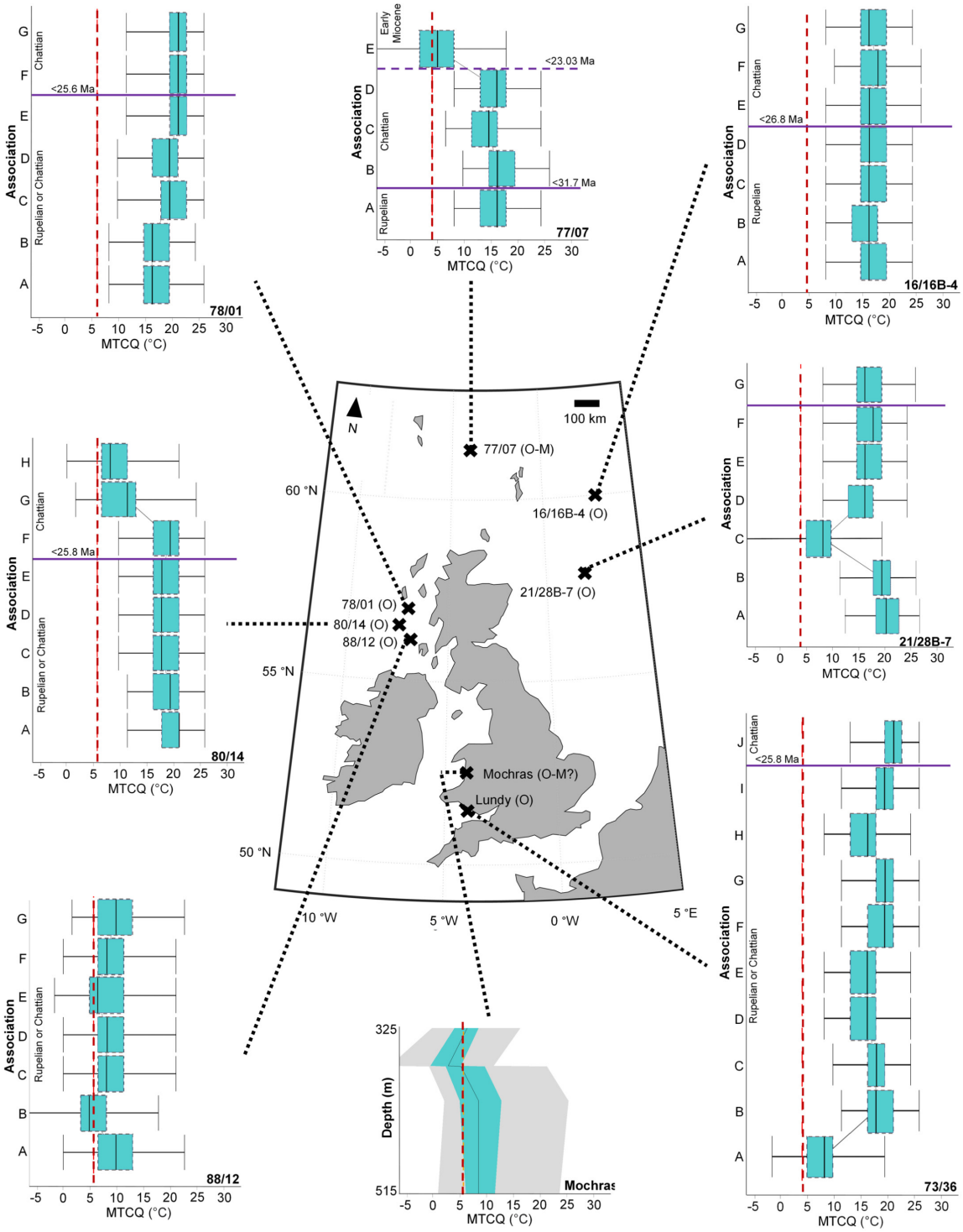

FIGURE 7. Mean Temperature of the Coldest Quarter (MTCQ) reconstructions from the sequential boreholes. The red dotted line shows the present-day MTCQ. Solid black lines show the value of the reconstructed optima. The grey dotted lines and grey solid lines show the respective uncertainty ranges of 50 % and 95 %. Oligocene and ?Miocene sites are labelled (O) and (M?), respectively. Purple solid lines and purple dotted lines separate Rupelian from Chattian, and Chattian from early Miocene associations, respectively, based on dinoflagellate cyst zonation. The uppermost/ lowermost ages of depicted boundaries between epochs, based on dinoflagellate cyst zonation, have been labelled where possible.

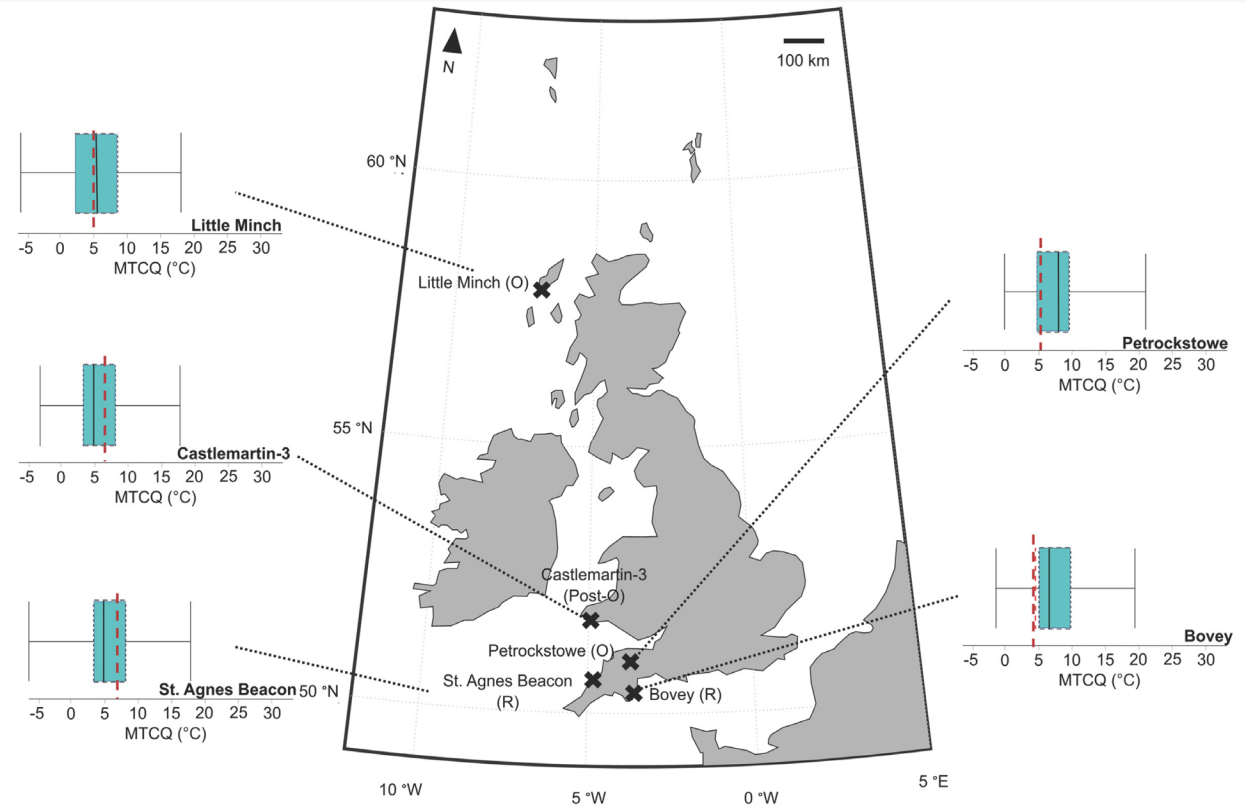

FIGURE 8. Mean Temperature of the Coldest Quarter (MTCQ) reconstructions, based on study sites where only one pollen assemblage was available. The red dotted line shows the present-day MTCQ. Solid black lines show the value of the reconstructed optima. The grey dotted lines and grey solid lines show the respective uncertainty ranges of 50 % and 95 %. Rupelian and Oligocene and ?Miocene sites are labelled (R) and (O), respectively.

Mean annual precipitation. Overlaps in uncertainties are recorded in reconstructions, which compare 16/16B-4 (associations A–B); 80/14 (associations A–B); 77/07 (associations B–C); 78/01 (associations A–F); and between depths 515.42–408.43 m in the Mochras borehole (Appendix 4). The assemblages from associations A–B of well 21/28B-7 reconstruct a minor increase in MAP from 1195 (±227)–1422 (±284) mm (~33–32 Ma). MAP declines from 1308 [±228]–1251 [±284] mm, between associations A–B at site 80/14 (~31.8–31.5 Ma, Figure 10) A minor decline in MAP is reconstructed (1251 [±228]–1195 [±228] mm) between associations B–C of borehole 77/07 (31.7–26.8 Ma) (Figure 10). Associations A–F of borehole 78/01 reconstructed a minor increase in MAP (from associations A–F) from 1138 (±228)–1536 (±398) mm at >24.8 Ma (Figure 10). Association E of borehole 77/07 reconstructs a decline in MAP (to 1081 ±227 mm) (Figure 10).

The Mochras Basal Red Unit reconstructs respective MAP values of 1308 ±171 mm and 1308 ±341 mm for depths 515.42 m and 408.43 m (Figure 10). MAP reconstructions decrease from 1138 ±228 mm to 739 ±114 mm (between depths 368.80–368.20 m) before then increasing to 1251 ±284 mm (324.61 m) (Figure 10).

Higher MAP values, than those reconstructed from the Mochras borehole, were reconstructed from the Beacon Cottage Farm Outlier section of St. Agnes Beacon (796 mm ± 170 mm) to the Bovey Basin (1138 ±228 mm) to the Ballymacadam (1195 ±285 mm) study site (Figures 11–12).

Mean precipitation of the driest month. Of discussed changes in MPDry reconstructions, we highlight that overlaps in uncertainties are recorded in 80/14 (associations A–C) and in 16/16B-4 (associations C–D) (Appendix 4). Associations A–C of well 21/28B-7 reconstructs a decline in MPDry from 68 (±11)–42 (±8) mm (~33–32 Ma) (Figure 13). Reconstructed MPDry from borehole 80/14 (associations A–C) reconstructs an increase in MPDry from 48 (±6)–54 (±8) mm (>31.8 Ma); reconstructions increase into site 80/14's Chattian

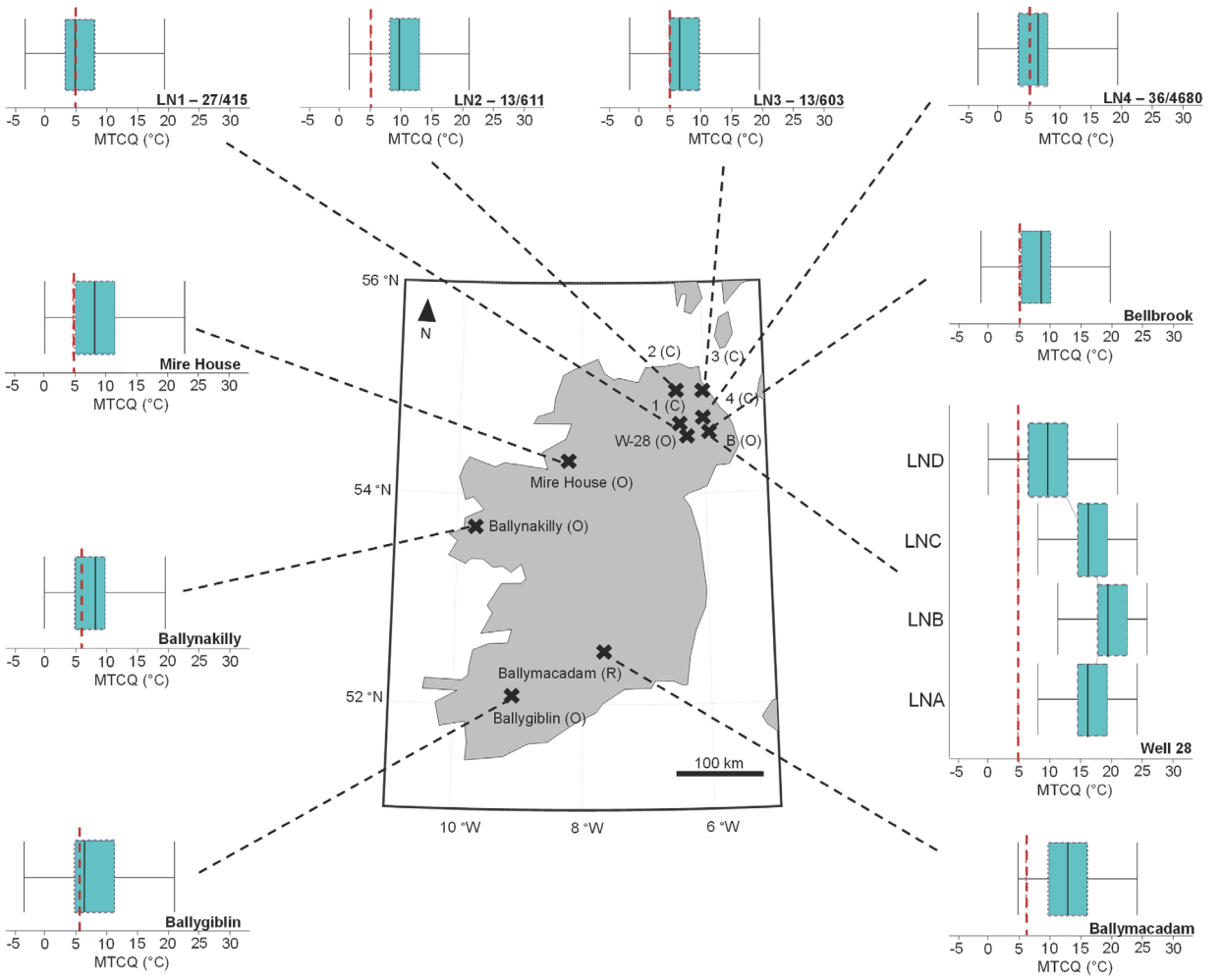

FIGURE 9. Mean Temperature of the Coldest Quarter (MTCQ) reconstructions based on pollen assemblages from Northern Ireland and the Republic of Ireland. The red dotted line shows the present-day MTCQ. Solid black lines show the value of the reconstructed optima. The grey dotted lines and grey solid lines show the respective uncertainty ranges of 50 % and 95 %. Rupelian, Chattian, and Oligocene sites are labelled (R), (C), and (O), respectively. "B" and "W-28" are abbreviated for "Bellbrook" and "Well-28", respectively.

associations (Figure 13). Similar MPDry reconstructions, 42 (±8)–62 (±11) mm and 48 (±8)–56 (±11) mm, are reconstructed from associations C–F of well 21/28B-7 (~32–31.05 Ma) and for associations C–D of well 16/16B-4 (31.7–31.05 Ma), respectively (Figure 13).

Early Miocene assemblages reconstruct MPDry values that range from 45 (±11) mm to 48 (±9) mm, based on respective reconstructions from the Castlemartin-3 and the 77/07 (Association E) boreholes (Figure 14). Association E of the 77/07 borehole, in comparison to its earlier-dated reconstructions in associations A–D, reconstructs a decline in MPDry to 48 ±9 mm (Figure 13).

Tropical Taxa-Types

Eight taxa-types classified to genus level, with subtropical-tropical signatures were present. Of these, *Cycas* is the sole conifer-type; the remaining seven genera are angiosperms (Figure 15). *Anacolosa*-types were not present in the northwest European palaeovegetation record during the Rupelian, whereas all other taxa-types were present (Figure 15). All tropical taxa-types were likely to have been present throughout the Chattian, and the warming events throughout the late Oligocene (Figure 15). *Anacolosa*-types were only recorded from the late Oligocene warming event to the Oligocene–Miocene Transition whereas *Calamus*-types were not recorded past the Rupelian (Figure 15). Following

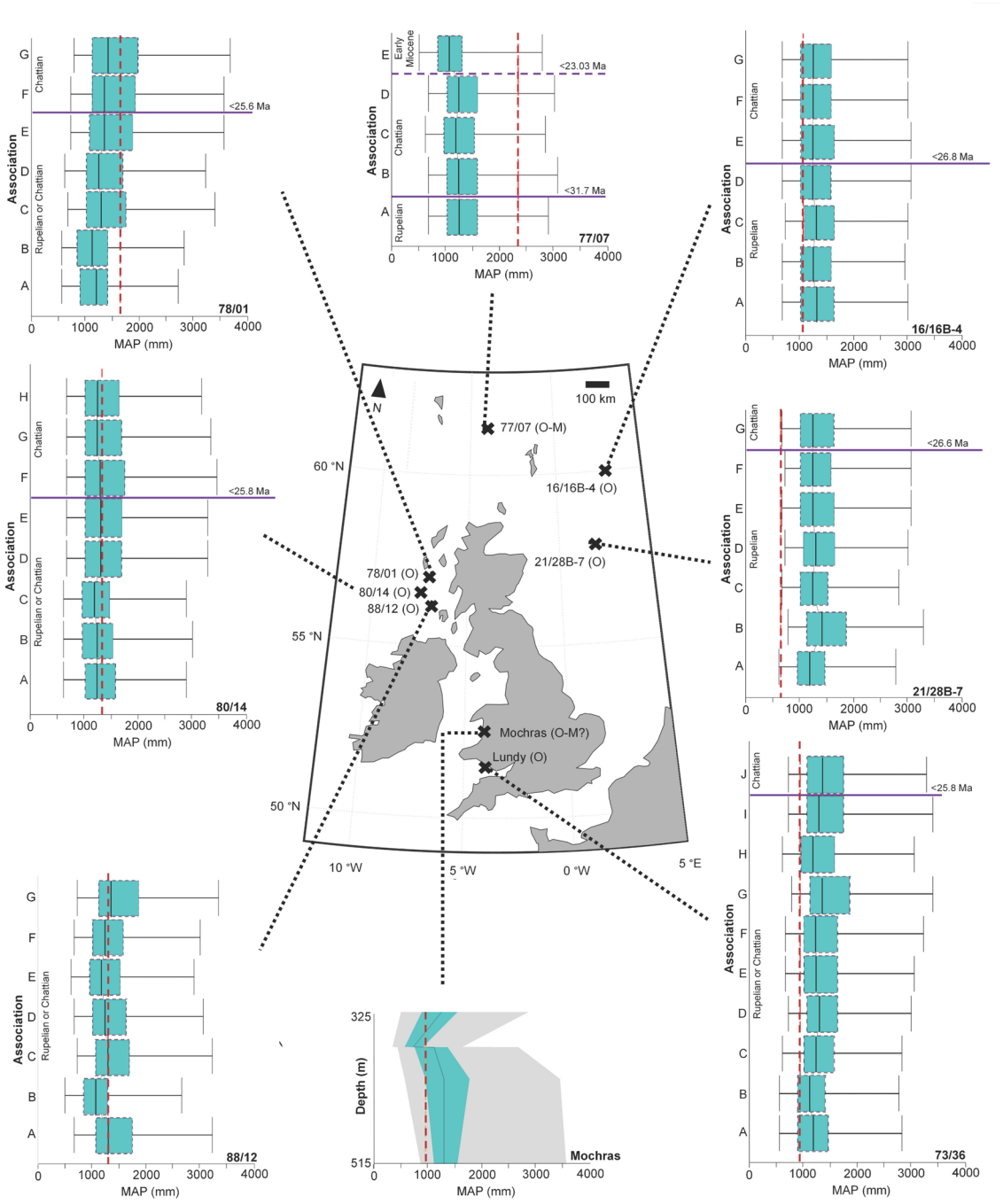

FIGURE 10. Mean Annual Precipitation (MAP) reconstructions from the sequential boreholes. The red dotted line shows the present-day MAP. Solid black lines show the value of the reconstructed optima. The grey dotted lines and grey solid lines show the respective uncertainty ranges of 50 % and 95 %. Oligocene and ?Miocene sites are labelled (O) and (M?), respectively. Purple solid lines and purple dotted lines separate Rupelian from Chattian, and Chattian from early Miocene associations, respectively, based on dinoflagellate cyst zonation. The uppermost/ lowermost ages of depicted boundaries between epochs, based on dinoflagellate cyst zonation, have been labelled where possible.

the LOWE, *Mangifera*-types were not recorded in the palaeovegetation record; Anacardiaceae, *Brownlowia*, and *Cupania*-types had an inferred relative abundance prior to the Oligocene–Miocene Transition (Figure 15). No tropical taxa were recorded in assemblages deposited throughout the early Miocene or post-Oligocene–Miocene Transition (>23.03 Ma) (Figure 15; Appendix 2).

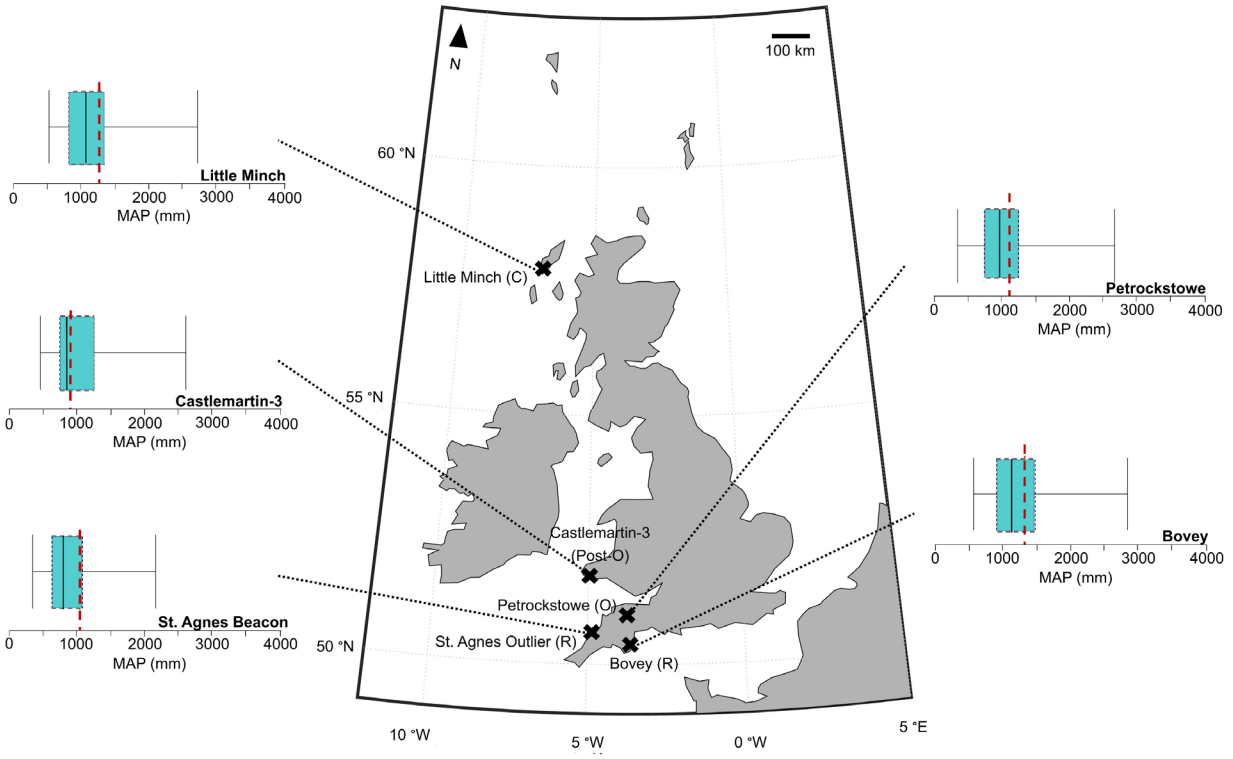

FIGURE 11. Mean Annual Precipitation (MAP) reconstructions, based on study sites where only one pollen assemblage was available. The red dotted line shows the present-day MAP. Solid black lines show the value of the reconstructed optima. The grey dotted lines and grey solid lines show the respective uncertainty ranges of 50 % and 95 %. Rupelian, Chattian, and Oligocene sites are labelled (R), (C), and (O), respectively.

Köppen-Geiger Classifications

Köppen-Geiger classifications were defined from CREST-modelled optimised value reconstructions and ranged from temperate wet and warm summer types *(Cfb)* to tropical rainforest types *(Af)* (Table 2; Figure 16A-B). This range of Köppen-Geiger classifications suggests the palaeoclimate of the early Oligocene (Rupelian) to early Miocene of the northwest margin of Europe ranged from subtropical with dry winters and warm summers to tropical. This is notably different from the present-day temperate climate, which has warm summers *(Cfb)* across the British Isles and cold summers *(Cfc)* with more consistent rainfall throughout the year in the North Sea Region (Peel et al., 2007; Beck et al., 2018). Köppen-Geiger classification assignments are listed in Table 2 and presented in Figure 16A–B.

References to assigned Köppen-Geiger types throughout this section, unless otherwise stated, refer to Table 2. The St. Agnes Beacon was the only Rupelian site to be assigned a subtropical-warm summer climate-type *(Cfb)*. Association C of the 73/36 borehole (33.9–31.8 Ma), and depths 515.42–408.43 m of the Mochras borehole are assigned a temperate climate signature, with dry winters and hot summers *(Cwa)*. The Petrockstowe Basin assemblage was assigned a temperate, dry-winter, warm-summer signal *(Cwb)*. A tropical rainforest signature *(Af)* was assigned to the Rupelian reconstruction of associations A–B of borehole 80/14 and association B of well 21/28B-7.

Tropical rainforest Köppen-Geiger signatures were assigned to Rupelian–Chattian associations E–G of 78/01 and G and J of 73/36 (Figure 16A). A subtropical warm summer climate-type was assigned to the assemblage from association B of borehole 88/12. All other Rupelian, Rupelian-Chattian, and Chattian assemblages were assigned a temperate climate-type with no dry season and hot summers *(Cfa)*. Tropical rainforest signatures were assigned to Chattian assemblages from associations E–G of 78/01, The Little Minch assemblage was assigned a temperate warm-summer *(Cfa)* Köppen-Geiger signature.

All early Miocene assemblages were assigned a temperate climate with warm-summers

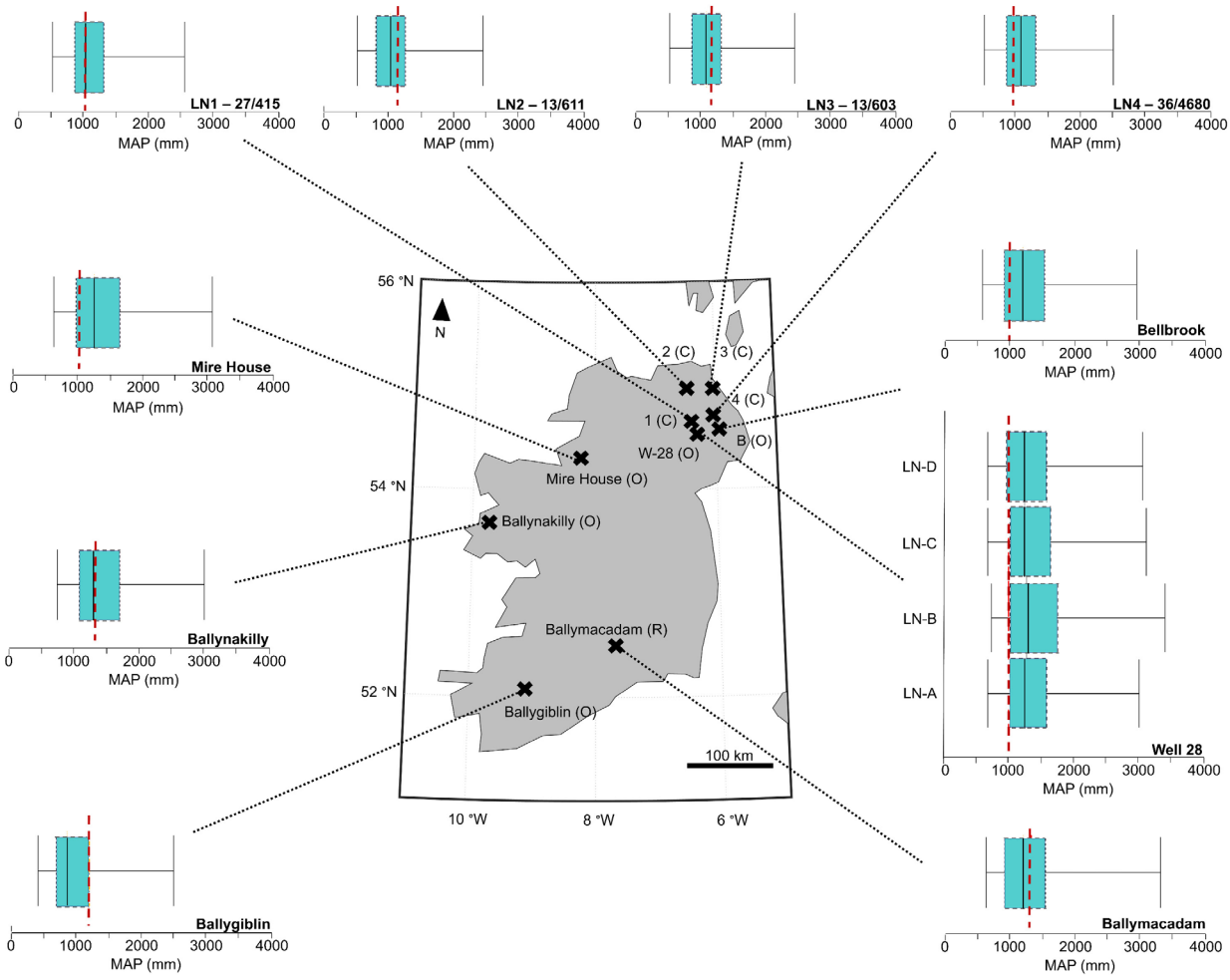

FIGURE 12. Mean Annual Precipitation (MAP) reconstructions based on pollen assemblages from Northern Ireland and the Republic of Ireland. The red dotted line shows the present-day MAP. Solid black lines show the value of the reconstructed optima. The grey dotted lines and grey solid lines show the respective uncertainty ranges of 50 % and 95 %. Rupelian, Chattian, and Oligocene sites are labelled (R), (C), and (O), respectively. "B" and "W-28" are abbreviated for "Bellbrook" and "Well-28", respectively.

signature. Depths of the Mochras borehole (i.e., 515.42–408.43 m, 368.80 m and 368.20–324.61 m) were assigned the respective Köppen-Geiger classifications of *Cwa, Cfa,* and *Cfb* (Table 2).

DISCUSSION

Our results show that the northwest margin of Europe was warmer throughout the Oligocene than palaeoclimates of Miocene (Figures 3–9 and 15–16). Most Rupelian and Chattian-dated reconstructions were assigned a Köppen-Geiger classification of either a temperate palaeoclimate with hot summers, and no dry season *(Cfa),* or a tropical rainforest Köppen-Geiger signature, with no outstanding dry season *(Af)* (Figure 16A–B). Selected Chattian, if not possibly younger, samples from the Little Minch Basin (Evans et al., 1991) reconstructed a temperate palaeoclimate with warm summers *(Cfb)* – comparable to the present-day climate of the British Isles (Table 2). Reductions in summer temperatures, resulted in alternating warm and hot summer-types *(Cfa–Cfb)* between associations B–H of 80/14 and from the samples taken from the same 80/14 borehole, from Evans et al (1991), see Table 2. These alternations between hot and warm summer reconstructions between the two studies be associated with the pulses of interglacials, due to low eccentricity forcing (Pälike et al., 2006; Levy et al., 2019).

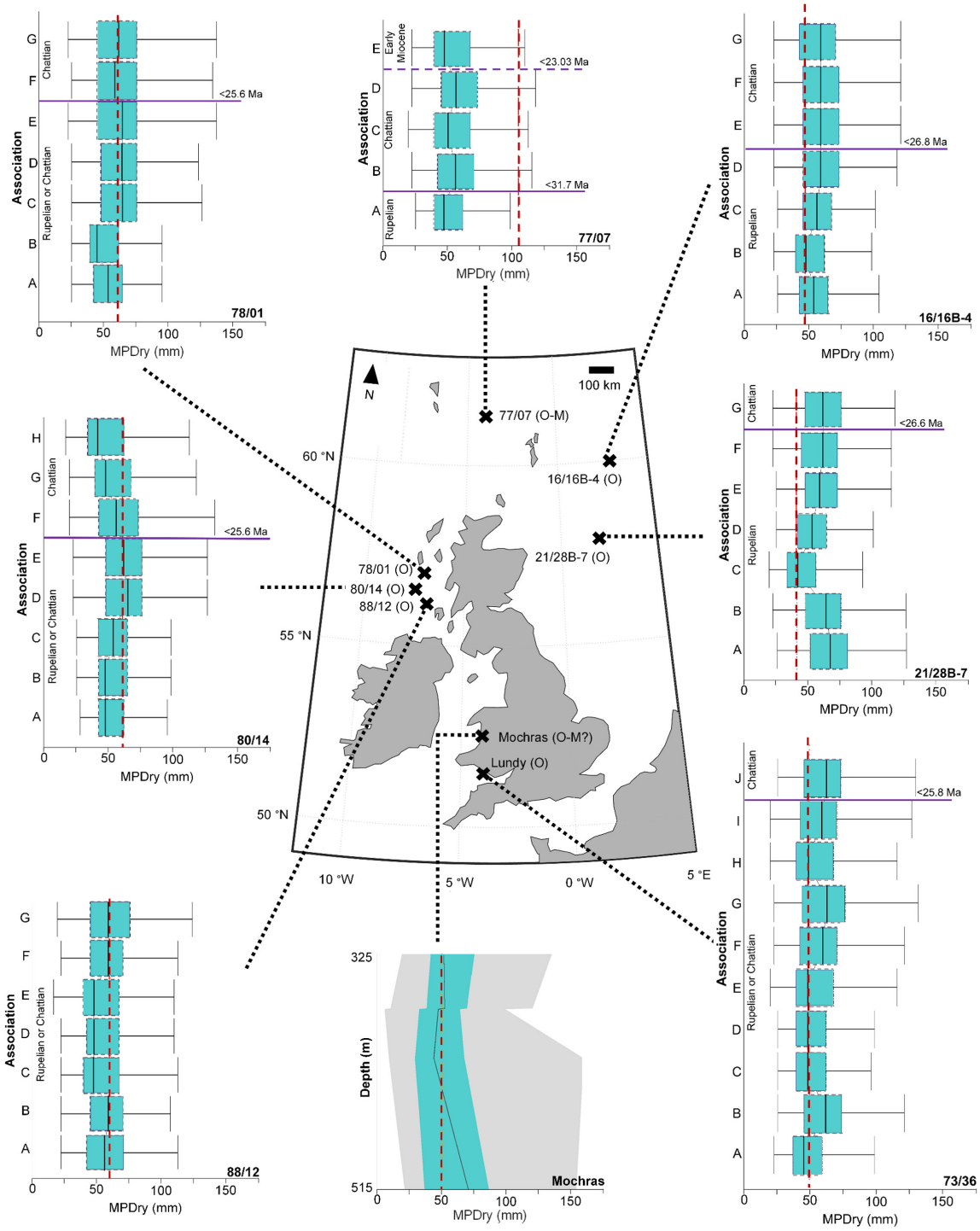

FIGURE 13. Mean Precipitation of the Driest Month (MPDry) reconstructions from the sequential boreholes. The red dotted line shows the present-day MPDry. Solid black lines show the value of the reconstructed optima. The grey dotted lines and grey solid lines show the respective uncertainty ranges of 50 % and 95 %. Oligocene and ?Miocene sites are labelled (O) and (M?), respectively. Purple solid lines and purple dotted lines separate Rupelian from Chattian, and Chattian from early Miocene associations, respectively, based on dinoflagellate cyst zonation. The uppermost/ lowermost ages of depicted boundaries between epochs, based on dinoflagellate cyst zonation, have been labelled where possible.

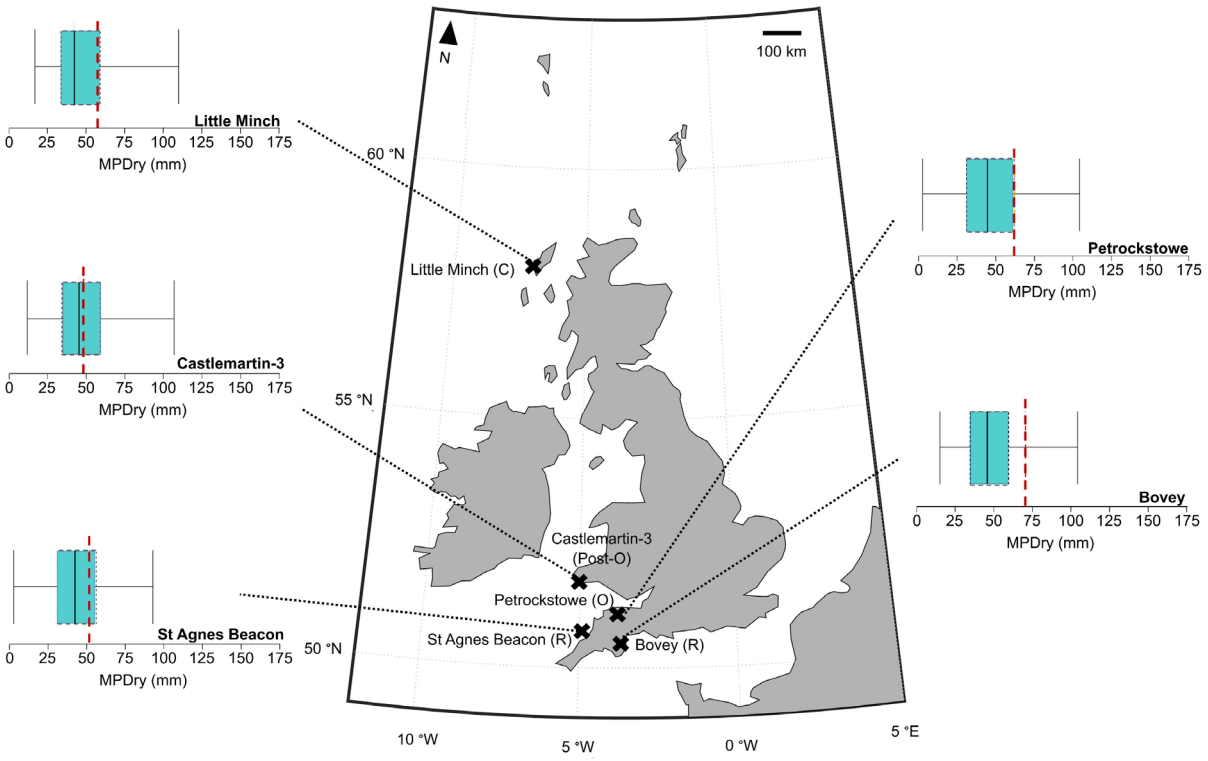

FIGURE 14. Mean Precipitation of the Driest Month (MPDry) reconstructions, based on study sites where only one pollen assemblage was available. The red dotted line shows the present-day MPDry. Solid black lines show the value of the reconstructed optima. The grey dotted lines and grey solid lines show the respective uncertainty ranges of 50 % and 95 %. Rupelian, Chattian and Oligocene sites are labelled (R), (C), and (O), respectively. Purple solid lines and purple dotted lines separate Rupelian from Chattian, and Chattian from early Miocene associations, respectively, based on dinoflagellate cyst zonation. The uppermost/ lowermost ages of depicted boundaries between epochs, based on dinoflagellate cyst zonation, have been labelled where possible.

Tropical Rainforest Signals at 57.77°N

Forests in the Rupelian, and maybe earlier. Tropical rainforest Köppen-Geiger classifications *(Af)* are assigned to the assemblages from association A of 80/14, which was dated to a minimum age of 31.8 Ma, based on the temporal zonation of recorded dinoflagellate cysts (Wilson, 1996; Egger et al., 2016; King et al., 2016; Table 2). Our reconstructions suggest tropical rainforests were present during the Rupelian, if not earlier, at 57.77°N (Table 2; Figure 16A–B). However, this disagrees with Rupelian biome reconstructions of temperate mixed forests and conifer forests (Pound and Salzmann 2017). Assigning a late Eocene age, rather than Wilson's (1996) previously assigned "Oligocene" age, for these assemblages, from association A of borehole 80/14, would allow our tropical reconstructions to be comparable with those from the Isle of Wight (latest Eocene) (Collinson and Hooker, 1987; Quicke, 1987; McCobb et al., 1998; Daley, 1989; Antropov et al., 2014; Krzemiński et al., 2019; Gorochov, 2019) amongst other tropical, western European Eocene reconstructions (Blondel, 2001). Warmer conditions are also correlative with high eustatic sea-levels in the Priabonian (Haq et al., 1987; Cande and Kent, 1995; Katz et al., 2008; Ladant et al., 2014).

A tropical rainforest-type is also reconstructed from the 21/28B-7 association A assemblage, the middle of which is dated to ~33–32.1 Ma (Egger et al., 2016; Figure 16; Table 2). Our reconstructions may suggest that the European tropical vegetation belt extended ~17.82° further north than previously proposed (Utescher et al., 2021). We suggest the possibility of the 21/28B-7 is likely older, given the middle of the assemblage was deposited within the timeframe of the Oi-2 cooling event, at 32.5 Ma, and so temperatures would have cooled, rather than have become more tropical (Wade and Pälike, 2004; Van Simaeys et al., 2005), furthermore, cor-

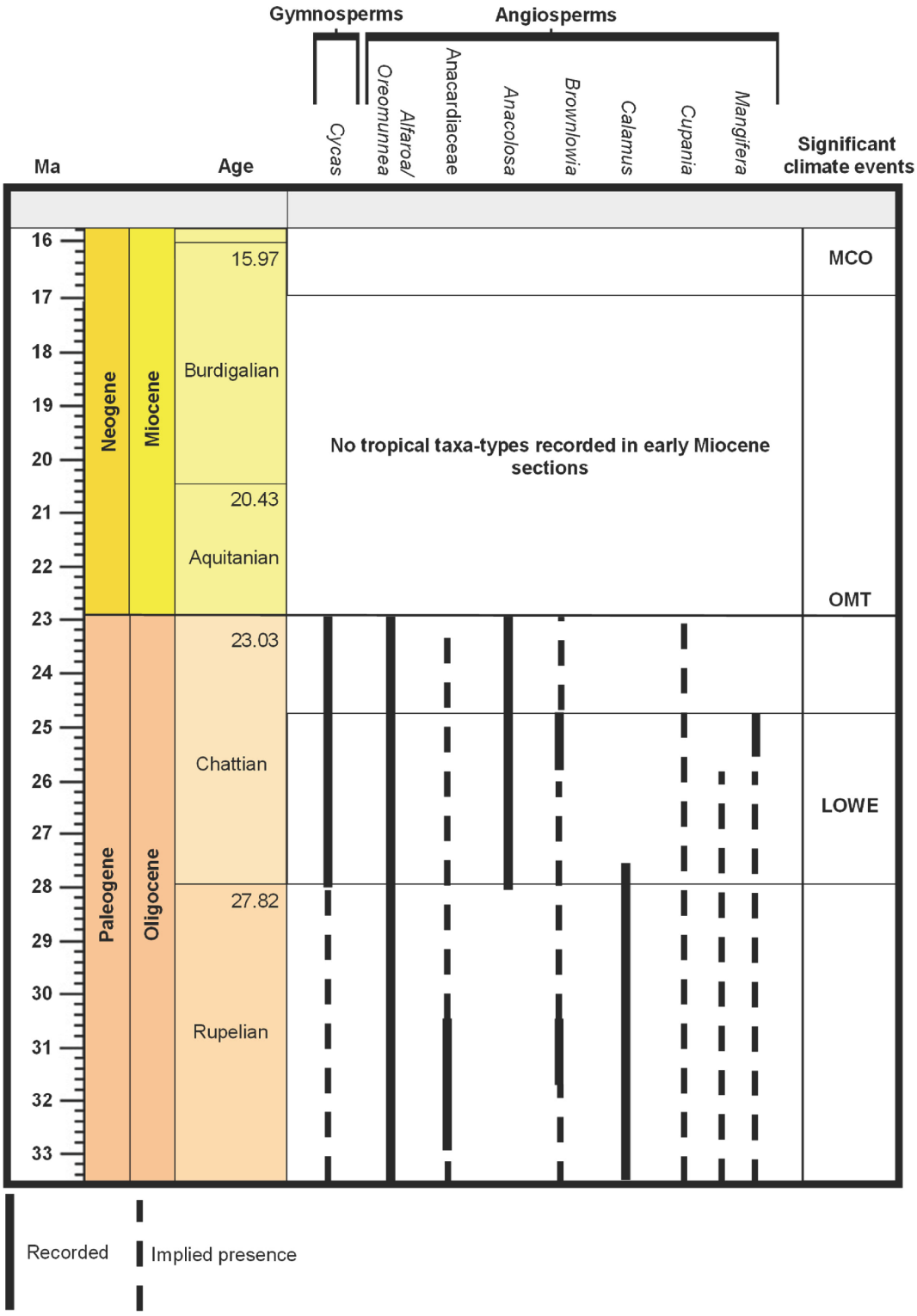

FIGURE 15. Stratigraphic age range and presence of tropical taxa-types in the pollen record, from the Oligocene-Miocene of the British Isles in correspondence with the possible age ranges of significant climate events. The Miocene Climatic Optimum (MCO), Oligocene-Miocene Transition (OMT), and Late Oligocene Warming Event (LOWE) are labelled.

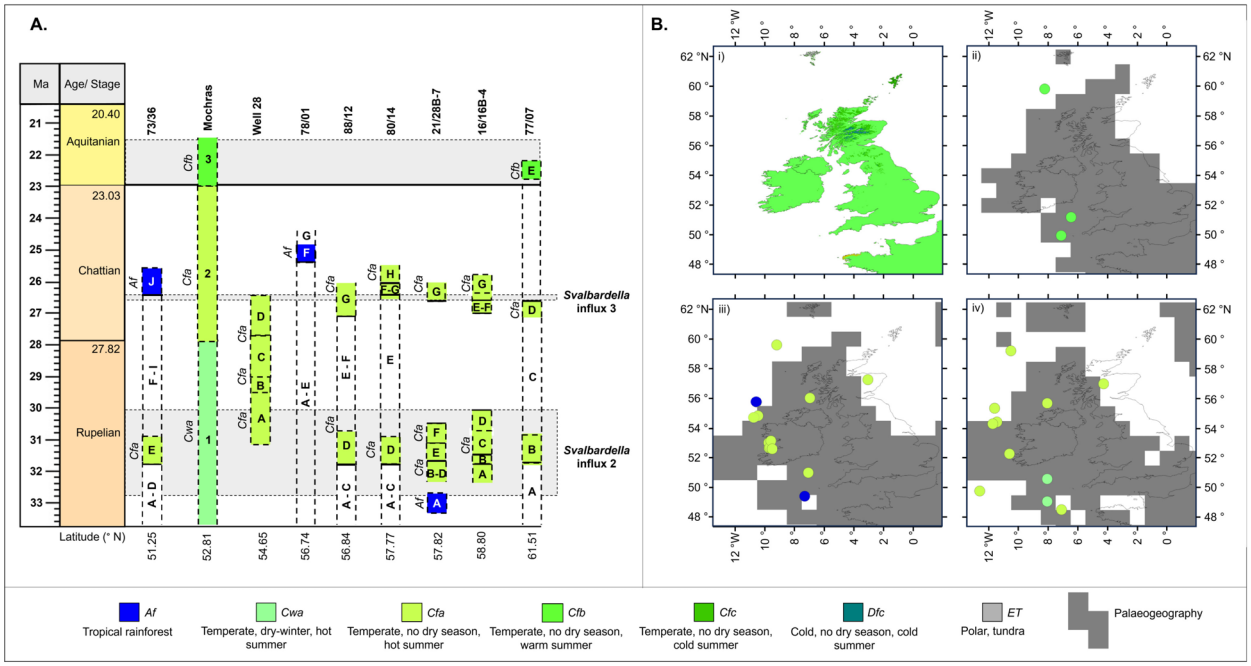

FIGURE 16. A. Köppen-Geiger signatures assigned to reconstructions of associations from Wilson (1996), and their likely age. The Mochras Basal Red Unit, the Transitional Unit and Lignite and Clay Units are labelled as 1-3, respectively. Age range of cooling *Svalbardella*-events 2 and 3, and their temporal overlaps with associations are labelled. Associations from Wilson (1996) are labelled alphabetically in accordance with original association assignment. Solid black lines in columns show a definitive age, based on dinoflagellate cyst stratigraphic age ranges. Dotted black lines in columns demonstrate an uncertain age range, based on dinoflagellate cysts stratigraphy. Dotted grey lines indicate possibility of age range regarding cooling events, i.e., *Svalbardella*-2, 3 and the early Miocene cooling. Latitude of boreholes are listed. B. Köppen-Geiger-based climate-type distributions across the British Isles, with key describing assigned climate types. Grey pixels show palaeolocations of British Isles (Scotese and Wright, 2018). Four stages are shown: i) Present-day Köppen-Geiger distribution of the British Isles (Beck et al., 2018); ii) Early Miocene; iii) Chattian; and iv) Rupelian.

responding pCO_2 levels were in decline (O'Brien et al., 2020; Zachos et al., 2001a). Should the assemblages from association B of 21/28B-7, note there was no overlap with the 50 % uncertainties between these depths, and so statistically significant changes occur outside the uncertainty, the transition from a tropical rainforest to a temperate hot-summer palaeoclimate, in later-deposited associations reconstructs a significant cooling event between possible Eocene and Oligocene horizons (Liu et al., 2009; Hutchinson et al., 2021).

Declines in MAT between associations A–C of 80/14 (3.01°C) and between associations B–C of 21/28B-7 (6.03°C), these reconstructed ranges fell outside of uncertainty ranges and so are consistent with ~4–6°C declines in annual air temperature reconstructions from the northwest margin of Europe at the Eocene–Oligocene Transition (Hren et al., 2013; Hutchinson et al., 2021; Table 2). These cores should be re-evaluated considering these palaeoclimate results may determine if a previously unknown sediment deposited throughout the Eocene–Oligocene Transition is present in the nearshore record of the British Isles.

Chattian rainforests. Chattian tropical rainforest *(Af)* Köppen-Geiger signatures are present in sequences 73/36 and 78/01 and are dated to 25.8–23.03 Ma, based on dinoflagellate cyst biostratigraphy (Wilson, 1996; Egger et al., 2016; King et al., 2016; Table 2). These reconstructions overlapped with the late Oligocene warming event (~26.3–23.7 Ma) in Europe (Liebrand et al., 2017; O'Brien et al., 2020; Brzelinski et al., 2023; Figure 16A). MTCQ optimal values increase above the Köppen-Geiger tropical threshold (Beck et al., 2018) in the Chattian associations F–G of borehole 73/36 (19.40 [±1.61]°C) and I–J (19.40 [±1.61]–21.01 [±1.61]°C) in a rhythmic pattern, resemblant of orbitally-induced forcing (Table 2). Increased MTCQ reconstructions coincide with peaks in the precession-cycle (~26 k.y.), and coeval warming events which occurred from 26.1–25.3 Ma (De Vleeschouwer et

al., 2017). Earth's position in perihelion during this time would have led to intense positive feedback associated with ablative regimes of sea-ice. This led to a reduced albedo effect, which enhanced deep water formation, leading to a warmer, more tropical, North Atlantic in the Chattian (Pälike et al., 2006; De Vleeschouwer et al., 2017; O'Brien et al., 2020).

High winter palaeotemperatures and tropical rainforest-type Northern Hemispheric palaeotemperature reconstructions throughout the Chattian are attributed to Earth being in eccentricity-driven perihelion from May through June (Zachos et al., 2001b; De Vleeschouwer et al., 2017). Large contrasts in winter temperature between higher and lower European latitudes can be attributed to a strengthening of the Hadley Cell (Mantsis et al., 2014). Under increased pCO_2 scenarios, dynamic coupling would lead to a narrowing of the Hadley Cell, and in turn would cool Northern Hemispheric climates (Chemke et al., 2019). However, during relatively low pCO_2 late Chattian (~300 ppm, O'Brien et al., 2020) periods, combined with periods of enhanced obliquity (41-k.y.) forcing (Xiao et al., 2010) more solar insolation would have been received at high Northern Hemisphere latitudes, causing a reverse in the meridional temperature gradient (Kang et al., 2019). We also note that sensitivity towards tropical climate types may also have been exacerbated by differences in orbital cycling, and subsequent eustatic sea-level fluctuations (Zachos et al., 2001a; Wade and Pälike, 2004), the opening and closing of seaways (Kennett, 1977; von der Heydt and Dijkstra, 2006), and aerosols (Bao et al., 2010), and therefore, further research is required.

This led to a reversal of the cross equatorial meridional transport gradient and contributed to increased heat transport to higher latitudes (Lobo and Bordoni, 2020) during winter, rather than in summer. Similar movement of heat occurred in low-obliquity model scenarios, which incorporated a present-day Earth system (Rind, 1998; Davis and Brewer, 2009; Mantsis et al., 2014).

Our tropical winter reconstructions highlight the possibility of an expansion of the Hadley Cell, and the establishment of tropical rainforests at 57°N, resulting from a reduction in temperature seasonality throughout northwest Europe. Tropical winter temperatures on the northwest margin of Europe were enhanced by advection from the tropical North Atlantic temperatures (25–26°C; O'Brien et al., 2020) resulting in a reduced latitudinal temperature gradient, compared to those reconstructed from Central Europe and the North Sea (Roth-Nebelsick et al., 2004; De Man and Van Simaeys, 2004). Our results reconstructed a decline in temperatures and precipitation seasonality, during a time prior to the latest Miocene, when cooling led to the development of before the Northern Hemispheric ice sheets (Herbert et al., 2016; Holbourn et al., 2018; Steinthorsdottir et al., 2021), and sea-ice, were established. Therefore, we suggest that in an Earth system without the Northern Hemispheric ice sheets, the northwest European palaeoclimate had amplified winter and mean annual temperatures (De Vleeschouwer et al., 2017). Such temperature change may be buffered by the existing Northern Hemispheric ice sheets in the present-day, reflected in modern temperatures.

Our results show the consistent preservation of the late Oligocene warming event and the correspondent relative abundance of tropical taxa-types (Figure 15) in the British palaeontological record.

Rupelian forests. We suggest that temperate palaeoclimate classifications, with hot summer signals *(Cfa)* reconstructed for later Rupelian associations B–F of 21/28B-7 and associations throughout 80/14, are more characteristic of the northwest European temperate palaeoclimates proposed by Pound and Salzmann (2017). Most of the northwestern European Rupelian reconstructions (associations A–B of 16/16B-4; associations C–F of 21/28B-7; association D of 88/12 and association E of 73/36 are most comparable to those taken from the Mittlerer Rupeleton Formation (Belgium), Mainz Basin, (Germany) and the Upper Rhine Graben (Germany) basins, for which a dominantly temperate, hot summer palaeoclimate with no dry season *(Cfa)* was reconstructed as well (Pross et al., 1998; Maxwell et al., 2016). All our new MATs, with various uncertainty ranges (8.14–19.40°C), are comparable to reconstructions from the Mittlerer Rupeleton Formation (16–18°C), if not cooler (Pross et al., 1998). These reductions in MAT reconstructions are attributable to the latitudinal difference between assemblages (Table 2).

Our new MAP reconstructions (Table 2; Appendix 4) are comparable to reconstruction ranges from the Mittlerer Rupeleton Formation, Mainz Basin, and the Upper Rhine Graben (1000–1300 mm and 1300–1700 mm) (Pross et al., 1998; Maxwell et al., 2016). These reconstructions suggest that the European palaeoclimatic record throughout the Rupelian was temperate–subtropical, and thus comparative to the biome reconstructions that show temperate mixed forests reaching

65.8°N (Pound and Salzmann, 2017; Utescher et al., 2021; Figure 16A–B).

Our results also show summer precipitation events, throughout the Rupelian, were slightly more intense on the northwest margin of Europe, in comparison to those in Central Europe (Table 2; Pross et al., 2001). This is demonstrated by our Rupelian temperate dry-winter Köppen-Geiger climate assignments *(Cwa),* at Association B of borehole 73/36 and at depths of 515.42–408.43 m of the Mochras borehole (Figure 16A), whereas central European Rupelian reconstructions, from the Mainz Basin (Germany) and Sava Basins (Slovenia) were assigned a no-dry-season *Cfa* Köppen-Geiger classification (Pross et al., 2001).

Rupelian Dry-Winter Palaeoclimates

Of all our studied intervals, Rupelian reconstructions suggested the largest ranges of seasonal precipitation differences and largest values in precipitation differences, being 4.58–27.30 mm (Table 2, uncertainties variable). Based on the reconstruction of dry-winter Köppen-Geiger types *(Cw-)* in the northwest European palaeoclimate record, we suggest that the British Isles had a slightly monsoonal-driven precipitation regime, during the Rupelian (Table 2). The Rupelian monsoonal palaeoclimate-type was determined from differences between the Precipitation of the Warmest Quarter and the Precipitation of the Coldest Quarter, and their comparison to the MAP, as adapted from Beck et al. (2018) (Table 2).

A shift in the precipitation regime, towards a temperate, dry-winter, hot-summer signal (Köppen Geiger signal of *Cwa*), as indicated by an increase in precipitation by 25.12–27.30 mm in summer, was assigned to Oligocene horizons 515.42 m and 408.43 m of the Mochras Basal Red Unit, and in Associations C of the 73/36 borehole (Figure 16A; Table 2; Appendix 4). Association C of the 73/36 borehole has a minimum age of 31.8 Ma, and so the associated assemblage was deposited either throughout the Rupelian age, or possibly Eocene (Table 2). Our Rupelian palaeoclimate dry-winter reconstructions are most like the dry-winter reconstructions from strata from the Upper Rhine Graben, Rauenberg, Germany dated to ~33.6 Ma (Kovar Eder, 2016). Our optima MAT reconstructions are comparable (19.40°C, uncertainty range variable) with those from Germany (19–24°C), though optima northwest European MTWQ reconstructions (24.62°C) were significantly cooler than German reconstructions (28–29°C) (Kovar Eder, 2016). Maximum northwest European MAP optima reconstructions are slightly lower, and thus were indicative of a drier palaeoclimate (1365 ±228 mm, Table 2) than highest MAP values reconstructed from Central European assemblages, of 1300–1700 mm (Kovar Eder, 2016) and 1500 mm (Mai, 1998), respectively. Like Central European signatures, *Cwa*-types on the northwest margin of Europe are characterised by slightly dry winters, where dry season precipitation does not fluctuate by more than 30 mm, suggesting monsoonal-types were most like *Cwa*-types in present-day North America near the Gulf of Mexico, presently 25–30°N (Köttek et al., 2006; Peel et al., 2007; Martinez et al., 2012). The northwest European monsoonal record was slightly drier, and cooler in comparison to Central European Rupelian moonsonal palaeoclimates (Kovar-Eder, 2016; Maxwell et al., 2016; Mai, 1995; 1998; Table 2). The temperate palaeoclimate with a dry-winter and hot-summer *(Cwa)* signal present at 31.8 Ma was not present throughout the remainder of the 73/36 associations (Table 2), and so its temporary appearance may have been the result of an orbitally forced pulse in the precipitation regime, given the Köppen-Geiger climate classification types vary between *Cfa* and *Af* in an alternating pattern (Table 2).

Northwest European dry-winter periods, throughout the Rupelian, are most consistent across the westernmost longitudes of the British Isles, highlighting that drier conditions are exacerbated by western processes, i.e., the contribution of the North Atlantic Sea to the terrestrial climate of northwest Europe (Figure 16A–B). Cooler and drier winter palaeoclimatic episodes in northernmost Rupelian Europe, compared to their slightly wetter, more southern European counterparts, suggest latitudinal differences in the winter precipitation regime that are like those driven by El Niño patterns in the present (Brönnimann, 2007; Koumoutsaris et al., 2008). Though, without concrete evidence regarding the timing of the establishment of the proto-El Niño's Southern Oscillation (ENSO), it is not possible to attribute pulses of enhanced, almost monsoonal-driven, winter drying episodes to an ENSO strengthening.

Dry-winter Rupelian episodes also coincided with a eustatic shallowing throughout the Chattian (Cande and Kent, 1995; Wilson, 1996). These shallowing events lead to reduced sea-level, advection, and moisture transport in the North Atlantic, resulting in dry phases. Expansion of the Hadley Cell would have forced trade winds to subside and migrate tropical temperatures to lower lat-

itudes, i.e., those in Central Europe (Gaemers and Van Hisbergh, 1978). Therefore, Europe's northwest margin became prone to drier, cloud-free winters with warm to hot summer conditions, with pronounced differences in cross-seasonal precipitation regimes (Chou et al., 2001; Seidel et al., 2008; Bordoni and Schneider, 2008; Velitzelos et al., 2014).

Our results show that in the context of an Earth system without extensive Northern Hemispheric ice sheets, an increase in sea-surface temperature (O'Brien et al., 2020) corresponds to a short-lived (regarding a geological time scale) summer-wet climate, particularly on the westernmost side of the northwest margin of Europe. Reductions in temperature change across seasons, and high MTCQ temperatures on the northwest margin of Europe resulted from high pCO_2 concentrations (~600–800 ppm, O'Brien et al., 2020). We suggest high pCO_2 concentrations contributed to a weakening of the meridional thermal advection gradient at mid-high latitudes during the cold season, and this led to a reduction in seasonality at higher latitudes (Screen and Simmonds, 2010; Dai et al., 2019; Dai and Deng, 2021).

East-moving jet streams from the tropics may have been induced by a weakened and poleward expansion of the Hadley Cell (Fu et al., 2006; Previdi and Liepert, 2007; Lu et al., 2007; Sharmila and Walsh, 2018), leading to an increase in MTCQ reconstructions at Northern Hemispheric latitudes (Table 2). Our results show that under an increased pCO_2 emission scenario, the northwest periphery of Europe may undergo a reduction in temperature seasonality due to increased winter temperatures (Dai and Deng, 2021).

Svalbardella-2 and 3 Events

Our results show that the *Svalbardella*-2 and 3 North Atlantic cooling events are present in the northwest European palaeorecord. *Svalbardella cooksoniae*-types were identified in association A of 73/36 (>31.8 Ma), overlapping with the *Svalbardella*-2 event (Wilson, 1996; Śliwińska and Heilmann-Clausen, 2011; Śliwińska et al., 2014; Appendix 2). Cooling phases throughout the Rupelian were reconstructed from reductions in MAT and MTWQ in 21/28B-7, 16/16B-4, 73/36, and 88/12 (Figures 5–8). We note that, based on 50% uncertainties, that MAT reductions from 21/28B-7 (Associations B–C) did not overlap (Appendix 4). Based on age re-assignment of associations A–B of 16/16B-4 and associations D–E of 80/14 to 32.8–30.2 Ma, declines in MAT (19.40 [±1.51]–17.89 [±1.51]°C, and 20.91 [±1.51]–19.40 [±1.51]°C, where 50 % uncertainty ranges overlap, respectively) may be associated with the *Svalbardella*-2 influx and cooling event in the North Atlantic (Pekar and Miller, 1996; Pekar et al., 2002; Śliwińska and Heilmann-Clausen, 2011; Figure, 16).

Furthermore, associations D–E and F–G of 16/16B-4 were dated as ~27.1–26.3 Ma based on dinoflagellate cyst biostratigraphy (Egger et al., 2016; Table 2). Reductions in MAT between these associations D–E, of 19.40 (±1.51)–17.89 (±1.51)°C, may correlate with the timings of the *Svalbardella*-3 cooling event and the Middle Oligocene Glacial Event, at the Rupelian-Chattian boundary (Śliwińska et al., 2010; Clausen et al., 2012; Śliwińska et al., 2014). Thus, not only do we demonstrate that the *Svalbardella*-2 and 3 events are preserved in the palaeontological record of the British Isles, but that the Rupelian-Chattian boundary may also be preserved. Furthermore, should late Eocene age strata have been preserved, in associations A–B of 80/14, we suggest the possibility that the *Svalbardella*-1 and corresponding Oi-1a cooling events are also preserved, and had more pronounced cooling, than that observed in *Svalbardella*-3 reconstructions (Oi-2b), contrary to Śliwińska and Heilmann-Clausen's (2011) proposal.

Our reconstructions, which overlap with the timing of the *Svalbardella* influx events, suggest that the palaeoclimate of the northwest margin of Europe may be susceptible to decreases in MAT during cooling phases in a climate scenario without extensive ice sheets in the Northern Hemisphere. Temperature declines, during *Svalbardella*-2 and 3, were not significant enough to cause changes in the Köppen-Geiger classification of a succession, based on reconstructed optimal values, or summer-type classification (Table 2; Figure 16A). However, our results show that despite the cooling phases present throughout the Oligocene–Miocene climate change much more sensitive, to increased winter temperatures (Table 2; Figure 16A–B).

The Early Miocene Palaeoclimate

Early Miocene conditions were cooler than those reconstructed for the Chattian. Whilst depths in the Lignite and Clay Unit of the Mochras borehole have been suggested to be early Miocene (Woodland, 1971; Herbert-Smith, 1979) we reconstruct reductions in MAT, MTCQ, and MAP, between depths 362.8–362.2 m (Table 2; Figures 5, 7 and 10). We attribute these reductions in

palaeoclimate variables to the Oligocene–Miocene cooling event at Mi-1, 23.03 Ma (Zachos et al., 1997; Table 2). Reductions in our Mochras (optima) MAT of <2°C, previously, are associated with the Oligocene–Miocene boundary, and subsequent time towards the Middle Miocene (Śliwińska et al., 2014; Greenop et al., 2014). This resulted in the removal of tropical taxa from the vegetation record of the British Isles (Figure 15). An Early Miocene age was assigned to association E of 77/07 (Figure 16A–B), based on the calibration of its pollen and dinoflagellate cyst assemblages with 16/16B-4 (Wilson, 1996). The uppermost depths of association F of 16/16B-4 and the association D of 77/07 are assigned an age of 26.6 Ma (King et al., 2016; Egger et al., 2016). Wilson (1996) suggested that associations E of 77/07 were likely younger, based on the 1.52 m hiatus between associations D–E. Association E was assigned an Early Miocene age, based on its assignment of a temperate warm-summer Köppen-Geiger signature with no dry season *(Cfb,* Table 2). We associate this summer cooling with the onset of the $\delta^{18}O$ maximum at the Oligocene-Miocene Transition, which leads to ice growth comparable, if not exceeding present-day volumes, and consequential cooling (Figure 16A–B; Liebrand et al., 2017; Miller et al., 2020; Steinthorsdottir et al., 2021).

This cooling phase was associated with long (400-k.y.) and short (100-k.y.) eccentricity cycling, before 16.9 Ma (Liebrand et al., 2016; Steinthorsdottir et al., 2021). Given the post-Oligocene-ages were assigned to the Castlemartin-3 assemblage, and to the Lignite and Clay Unit (368.8–368.2 m) of the Mochras borehole were also assigned a warm-summer signature *(Cfb),* we suggest these assemblages may also be early Miocene in age (Table 2; Woodland, 1971; McLean, 2002).

Given the Little Minch (Evans et al., 1991) assemblage, also reconstructed a *Cfb* signature, at depths 62.5–72 m, it is possible that these beds were deposited either throughout the Oligocene-Miocene Transition, or sometime throughout the *Svalbardella*-3 cooling phase. This is because our reconstructions, which overlapped with *Svalbardella*-3 (sequences Well 28, 88/12, 21/28B-7 and 16/16B-4), were used to reconstruct a temperate hot-summer climate with no dry season *(Cfa),* rather than a warm-summer *(Cfb)* Köppen-Geiger climate type. This warm-summer classification suggests the Little Minch (Evans et al., 1991) reconstructions are more likely early Miocene in age, given the consistency of *Cfb*-types in the Early Miocene age assemblages (Figure 16A). Sample 6 of Little Minch (Evans et al., 1991) was deposited above Association H of 80/14 (64.95–63.97 m), and so this core section is 25.5 Ma, at oldest (Wilson, 1996). Sample 6's assigned *Cfb* signature is comparable with the early Miocene signature from association E of 77/07. This suggests that sample 6 (Evans et al., 1991) is also likely Early Miocene in age. The disappearance of Arecaceae from the record of Evans et al. (1991), from ~72 m, further supports this early Miocene age assessment (Appendix 2; Figure 16A).

All our early Miocene temperature and precipitation palaeoclimate variable reconstructions are consistently lower than those reconstructed from the early Miocene Gröbern assemblage (Roth-Nebelsick et al., 2004). Our optimised early Miocene MAT reconstructions <11.86 (±1.51)°C were lower than the Gröbern (Germany) assemblage's MAT range, reconstructed using the co-existence approach, 14.1–20.8°C (Roth-Nebelsick et al., 2004). We show our optimised MTCQ reconstructions (4.92–6.53°C) overlap with the Gröbern Coldest Mean Month Temperature ranges of 4.7–13.3°C, as do our MAP reconstructions (853–1251 mm [variable uncertainty ranges]), with those reconstructed from Germany (897–1281 mm) (Roth-Nebelsick et al., 2004). However, our MTWQ reconstructions (17.59–21.81°C [variable uncertainty ranges]) are considerably cooler (25.7–28.1°C) than those from Gröbern (Roth-Nebelsick et al., 2004). CREST reconstructions are known to be cooler than co-existence approach reconstructions due to differences in input data and mathematical approach (Gibson et al., 2022). Furthermore, CREST and the co-existence approach use different modern climate databases, thus input data is different, resulting in inconsistencies between techniques (Mosbrugger and Utescher, 1997; Utescher et al., 2014; Grimm and Potts, 2016; Gibson et al., 2022). Our early Miocene assemblages reconstructed the smallest differences between summer and winter precipitation, of all studied intervals (-0.47–2.79 mm) (Table 2). The negligible, dry-summer seasonal difference in precipitation (<1 mm) suggests that following the Oligocene–Miocene Transition, there was a change in the precipitation regime. This likely resulted in the consistent, almost wholly equal precipitation distribution across our study sites (Table 2) up until the middle Miocene (Gibson et al., 2022). Our results reinforce the proposal that the precession (~26 k.y.) cycle had a bimodal impact on palaeoclimate (De Vleeschouwer et al., 2017), and so the northward (southward) migration of

monsoonal-climate and slightly dry-winters bands associated with decreased (increased) precessional cycling was balanced (Ding et al., 2021). This resulted in an alternating (but small) fluctuation between positive and negative seasonal differences in precipitation, suggestive of a pulse-like fluctuation between early Miocene Köppen-Geiger types with very slight dry-summers and dry-winter signals (Table 2).

CONCLUSIONS

The Oligocene and Miocene sedimentary archives from the British Isles record orbitally induced climate change. Tropical rainforest types were reconstructed in short-lived pulses during the Chattian and the Rupelian/Priabonian. During the Chattian, the reconstructed tropical rainforest Köppen-Geiger signatures are coeval with the late Oligocene warming event and these rainforest types could have been a response to obliquity maxima forcing. Dry-winter Köppen-Geiger reconstructions, during the Rupelian, may have been driven by eccentricity-modulated pulses in the precession cycle (~26 k.y.) that lead to strengthened feedback between oceanic-atmospheric interactions.

The *Svalbardella*-2 and 3 cooling events are apparent in the palaeontological record of the British Isles and are represented by respective reductions in MAT (24.22–22.61°C) and MTCQ (23.22–17.59°C). The Oligocene–Miocene Transition may have been preserved in the Mochras and 77/07 boreholes, with early Miocene reconstructions showing a MAT reduction from 24.22 to 11.36°C, and a MTWQ reduction from 24.62 to 16.18°C: the latter leading to a transition from hot to warm summer palaeoclimate types due to summer cooling. After the Oligocene–Miocene Transition, differences in seasonal precipitation were almost negligible perhaps because of the hemispheric-bimodal influence of the precession-cycle after the Oligocene–Miocene Transition. We suggest that under similar pCO_2 levels, the northwest edge of Europe may have wetter summers and possible tropical winter temperature because of anthropogenic climate change.

ACKNOWLEDGEMENTS

We would like to thank A.J. Suggitt for his help in resolving model errors in R. JM thanks NERC (NERC award identified NE/S007512/1) for funding ongoing research into the Cenozoic palynology of northwest Europe, through the ONEPlanet Doctoral Training Programme (OP 2170). MP, JO'K, and JM acknowledge funding from NSF/GeoNERC project “Fungi in a Warmer World (FiaWW)” (NSF award #2015813 to JO’K and NERC award identifier NE/V01501X/1 to MP). MP and JM thank The Royal Society (IECR2202086). The authors thank J. Hue, M. Hyžný and J. Rumford for facilitating the manuscript through *Palaeontologia Electronica.* We are grateful to two anonymous reviewers for their comments which helped greatly in the development of our manuscript.

REFERENCES

Antropov, A.V., Belokobylskij, S.A., Compton, S.G., Dlussky, G.M., Khalaim, A.I., Kolyada, V.A., Kozlov, M.A., Perfilieva, K.S., and Rasnitsyn, A.P. 2013. The wasps, bees and ants (insecta: Vespida Hymenoptera) from the insect limestone (late Eocene) of the Isle of Wight UK. Earth and Environmental Science Transactions of the Royal Society of Edinburgh, 104(3-4):335–446. https://doi.org/10.1017/S1755691014000103

Armstrong McKay, D.I., Staal, A., Abrams, J.F., Winkelmann, R., Sakschewski, B., Loriani, S., Fetzer, I., Cornell, S.E., Rockström, J., and Lenton, T.M. 2022. Exceeding 1.5°C global warming could trigger multiple climate tipping points. Science, 377(6611):1–10. https://doi.org/10.1126/science.abn7950

Bao, H., Yu, S., and Tong, D.Q. 2010. Massive volcanic SO2 oxidation and sulphate aerosol deposition in Cenozoic North America. Nature, 465(7300):909–912.

Beck, H.E., Zimmermann, N.E., McVicar, T.R., Vergopolan, N., Berg, A., and Wood, E.F. 2018. Present and future Köppen-Geiger climate classification maps at 1-km resolution. Scientific Data, 5(1):1–12. https://doi.org/10.1038/s41597-020-00616-w

Beddow, H.M., Liebrand, D., Sluijs, A., Wade, B.S., and Lourens, L.J. 2016. Global change across the Oligocene-Miocene transition high-resolution stable isotope records from IODP Site U1334 (equatorial Pacific Ocean). Paleoceanography, 31(1):81–97. https://doi.org/10.1002/2015PA002820

Bessedik, M. 1984. The early Aquitanian and upper Langhian-lower Serravallian environments in the northwestern Mediterranean region. Paléobiologie Continentale, 14(2):153–179.

Bhatia, H., Srivastava, G., Spicer, R.A., Farnsworth, A., Spicer, T.E., Mehrotra, R.C., Paudayal, K.N., and Valdes, P. 2021. Leaf physiognomy records the Miocene intensification of the South Asia Monsoon. Global and Planetary Change, 196:103365. https://doi.org/10.1016/j.gloplacha.2020.103365

Boers, N. and Rypdal, M. 2021. Critical slowing down suggests that the western Greenland ice sheet is close to a tipping point. Proceedings of the National Academy of Sciences, USA, 118(21):e2024192118. https://doi.org/10.1073/pnas.2024192118

Bordoni, S. and Schneider, T. 2008. Monsoons as eddy-mediated regime transitions of the Tropical Overturning Circulation. Nature Geoscience, 1(8):515–519. https://doi.org/10.1038/ngeo248

Bortenschlager, S. 1990. Aspects of pollen morphology in the Cupressaceae. Grana, 29(2):129–138.

Bouchal, J.M. and Denk, T. 2020. Low taxonomic resolution of papillate Cupressaceae pollen former Taxodiaceae impairs their applicability for palaeo-habitat reconstruction. Grana, 59(1):70–93.

Boulter, M.C. 1980. Irish Tertiary plant fossils in a European context. Journal of Earth Sciences:1–11.

Boulter, M.C. and Craig, D.L. 1979. A middle Oligocene pollen and spore assemblage from the Bristol Channel. Review of Palaeobotany and Palynology, 28(3-4):259–272. https://doi.org/10.1016/0034-6667(79)90028-9

Brönnimann, S. 2007. Impact of El Niño–Southern Oscillation on European climate. Reviews of Geophysics, 45(3):1–28. https://doi.org/10.1029/2006RG000199

Brzelinski, S., Bornemann, A., Liebrand, D., van Peer, T.E., Wilson, P.A., and Friedrich, O. 2023. Large obliquity-paced Antarctic ice-volume fluctuations suggest melting by atmospheric and ocean warming during late Oligocene. Communications Earth and Environment, 4(1):222. https://doi.org/10.1038/s43247-023-00864-9

Cande, S.C. and Kent, D.V. 1995. Revised calibration of the geomagnetic polarity timescale for the late Cretaceous and Cenozoic. Journal of Geophysical Research: Solid Earth, 100(B4):60936095. https://doi.org/10.1029/94JB03098

Chaanda, M.S. 2016. Cenozoic terrestrial palaeoenvironemtal change an investigation of the Petrockstowe and Bovey basins southwest United Kingdom. PhD Thesis, University of Plymouth, Plymouth, UK.

Chemke, R., Polvani, L.M., and Deser, C. 2019. The effect of Arctic Sea ice loss on the Hadley circulation. Geophysical Research Letters, 46(2):963–972. https://doi.org/10.1029/2018GL081110

Chevalier, M. 2019. Enabling possibilities to quantify past climate from fossil assemblages at a global scale. Global and Planetary Change, 175:27–35. https://doi.org/10.1016/j.gloplacha.2019.01.016

Chevalier, M. 2022. crestr: an R package to perform probabilistic climate reconstructions from palaeoecological datasets. Climate of the Past, 18(4):821–844. https://github.com/mchevalier2/crestr https://doi.org/10.5194/cp-18-821-2022

Chevalier, M., Cheddadi, R., and Chase, B.M. 2014. CREST (Climate REconstruction SofTware): a probability density function (PDF)-based quantitative climate reconstruction method. Climate of the Past, 10(6):2081–2098. https://doi.org/10.5194/cp-10-2081-2014

Chou, C., Neelin, J.D., and Su, H. 2001. Ocean-atmosphere-land feedbacks in an idealized monsoon. Quarterly Journal of the Royal Meteorological Society, 127(576):1869–1891. https://doi.org/10.1002/qj.49712757602

Clausen, O.R., Śliwińska, K.K., and Gołędowski, B. 2012. Oligocene climate changes controlling forced regression in the eastern North Sea. Marine and Petroleum Geology, 29(1):1–14. https://doi.org/10.1016/j.marpetgeo.2011.10.002

Collinson, M.E. and Hooker, J.J. 1987. Vegetational and mammalian faunal changes in the early Tertiary of southern England, p. 259–303. In Friis, E.M., Chaloner, W.G., and Crane, P.R. (eds.), The origins of angiosperms and their biological consequences. Cambridge University Press, Cambridge.

Coxall, H.K., Wilson, P.A., Pälike, H., Lear, C.H., and Backman, J. 2005. Rapid stepwise onset of Antarctic glaciation and deeper calcite compensation in the Pacific Ocean. Nature, 433(7021):53–57.

Crowley, T.J. and Berner, R.A. 2001. CO_2 and climate change. Science, 292(5518):870–872. https://doi.org/10.1126/science.1061664

Dai, A., Luo, D., Song, M., and Liu, J. 2019. Arctic amplification is caused by sea-ice loss under increasing CO_2. Nature Communications, 10(1):1–13. https://doi.org/10.1038/s41467-018-07954-9

Dai, A. and Deng, J. 2021. Arctic amplification weakens the variability of daily temperatures over northern middle-high latitudes. Journal of Climate, 34(7):2591–2609. https://doi.org/10.1175/JCLI-D-20-0514.1

Daley, B. 1989. Silica pseudomorphs from the Bembridge limestone (upper Eocene) of the Isle of Wight, southern England and their palaeoclimatic significance. Palaeogeography, Palaeoclimatology, Palaeoecology, 69:233–240. https://doi.org/10.1016/0031-0182(89)90166-1

Davis, B.A. and Brewer, S. 2009. Orbital forcing and role of the latitudinal insolation/temperature gradient. Climate Dynamics, 32:143–165. https://doi.org/10.1007/s00382-008-0480-9

De Man, E. and Van Simaeys, S. 2004. Late Oligocene warming event in the southern North Sea Basin benthic foraminifera as paleotemperature proxies. Netherlands Journal of Geosciences, 83(3):227–239. https://doi.org/10.1017/S0016774600020291

De Vleeschouwer, D., Vahlenkamp, M., Crucifix, M., and Pälike, H. 2017. Alternating Southern and Northern Hemisphere climate response to astronomical forcing during the past 35 my. Geology, 45(4):375–378. https://doi.org/10.1130/G38663.1

Denk, T., Grimm, G.W., Grímsson, F., and Zetter, R. 2013. Evidence from Köppen signatures of fossil plant assemblages for effective heat transport of Gulf Stream to subarctic North Atlantic during Miocene cooling. Biogeosciences, 10(12):7927–7942. https://doi.org/10.5194/bg-10-7927-2013

Ding, Z., Huang, G., Liu, F., Wu, R., and Wang, P. 2021. Responses of global monsoon and seasonal cycle of precipitation to precession and obliquity forcing. Climate Dynamics, 56:3733–3747. https://doi.org/10.1007/s00382-021-05663-6

Doppert, J.W.C. and Neele, N.G. 1983. Biostratigraphy of marine Paleogene deposits in the Netherlands and adjacent areas. Mededelingen Rijks Geologische Dienst, 37(2):–79.

Dupont-Nivet, G., Krijgsman, W., Langereis, C.G., Abels, H.A., Dai, S., and Fang, X. 2007. Tibetan plateau aridification linked to global cooling at the Eocene–Oligocene transition. Nature, 445(7128):635–638. https://doi.org/10.1038/nature05516

Egger, L.M., Śliwińska, K.K., Van Peer, T.E., Liebrand, D., Lippert, P.C., Friedrich, O., Wilson, P.A., Norris, R.D., and Pross, J. 2016. Magnetostratigraphically-calibrated dinoflagellate cyst bioevents for the uppermost Eocene to lowermost Miocene of the western North Atlantic (IODP Expedition 342, Paleogene Newfoundland sediment drifts). Review of Palaeobotany and Palynology, 234:159–185. https://doi.org/10.1016/j.revpalbo.2016.08.002

Ehrmann, W.U. and Mackensen, A. 1992. Sedimentological evidence for the formation of an east Antarctic ice sheet in Eocene/Oligocene time. Palaeogeography, Palaeoclimatology, Palaeoecology, 93(1-2):85–112. https://doi.org/10.1016/0031-0182(92)90185-8

Eldrett, J.S., Greenwood, D.R., Harding, I.C., and Huber, M. 2009. Increased seasonality through the Eocene to Oligocene transition in northern high latitudes. Nature, 459(7249):969–973. https://doi.org/10.1038/nature08069

Evans, D., Hallsworth, C., Jolley, D.W., and Morton, A.C. 1991. Late Oligocene terrestrial sediments from a small basin in the Little Minch. Scottish Journal of Geology, 27(1):33–40. https://doi.org/10.1144/sjg27010033

Farnsworth, A., Lunt, D.J., Robinson, S.A., Valdes, P.J., Roberts, W.H., Clift, P.D., Markwick, P., Su, T., Wrobel, N., Bragg, F., and Kelland, S.J. 2019. Past east Asian monsoon evolution controlled by paleogeography, not CO_2. Science Advances, 5(10):eaax1697. https://doi.org/10.1126/sciadv.aax1697

Fenero, R., Cotton, L., Molina, E., and Monechi, S. 2013. Micropalaeontological evidence for the late Oligocene Oi-2b global glaciation event at the Zarabanda section Spain. Palaeogeography, Palaeoclimatology, Palaeoecology, 369:1–13. https://doi.org/10.1016/j.palaeo.2012.08.020

Fick, S.E. and Hijmans, R.J. 2017. WorldClim 2 new 1-km spatial resolution climate surfaces for global land areas. International Journal of Climatology, 37(12):4302–4315. https://doi.org/10.1002/joc.5086

Fitzgerald, J.A. 1999. Pollen and spore assemblages from the Oligocene Lough Neagh Group Vol. 1, Published PhD Thesis, University of Sheffield, Sheffield, UK.

Figueiral, I., Mosbrugger, V., Rowe, N.P., Ashraf, A.R., Utescher, T., and Jones, T.P. 1999. The Miocene peat-forming vegetation of northwestern Germany an analysis of wood remains and comparison with previous palynological interpretations. Review of Palaeobotany and Palynology, 104(3-4):239–266. https://doi.org/10.1016/S0034-6667(98)00059-1

Fu, Q., Johanson, C.M., Wallace, J.M., and, Reichler, T. 2006. Enhanced mid-latitude tropospheric warming in satellite measurements. Science, 312(5777):1179. https://doi.org/10.1126/science.1125566

Gaemers, P.A. and van Hinsbergh, V.W.M. 1978. Rupelian middle Oligocene fish otoliths from the clay pit'De Vlijt'near Winterswijk the Netherlands. Scripta Geologica, 46:1–77.

Galeotti, S., DeConto, R., Naish, T., Stocchi, P., Florindo, F., Pagani, M., Barrett, P., Bohaty, S.M., Lanci, L., Pollard, D., and Sandroni, S. 2016. Antarctic ice sheet variability across the Eocene-Oligocene boundary climate transition. Science, 352(6281):76–80.

GBIF. 2020a. Cycadopsida occurrence data, downloaded 24 September 2020. GBIF Database. https://doi.org/10.15468/dl.sfjzxu

GBIF. 2020b. Gnetopsida occurrence data, downloaded 24 September 2020. GBIF Database. https://doi.org/10.15468/dl.h2kjnc

GBIF. 2020c. Liliopsida occurrence data, downloaded 24 September 2020. GBIF Database. https://doi.org/10.15468/dl.axv3yd

GBIF. 2020d. Lycopodiopsida occurrence data, downloaded 24 September 2020. GBIF Database. https://doi.org/10.15468/dl.ydhyhz

GBIF. 2020e. Magnoliopsida occurrence data, downloaded 24 September 2020. GBIF Database. https://doi.org/10.15468/dl.ra49dt

GBIF. 2020f. Pinopsida occurrence data, downloaded 24 September 2020. GBIF Database. https://doi.org/10.15468/dl.x2r7pa

GBIF. 2020g. Polypodiopsida occurrence data, downloaded 24 September 2020. GBIF Database. https://doi.org/10.15468/dl.87tbp6

Gorochov, A.V. 2019. Crickets and grasshoppers Orthoptera from the latest Eocene of the Isle of Wight southern England UK. Earth and Environmental Science Transactions of the Royal Society of Edinburgh, 110(3-4):317–329. https://doi.org/10.1017/S1755691018000889

Greenop, R., Foster, G.L., Wilson, P.A., and Lear, C.H. 2014. Middle Miocene climate instability associated with high-amplitude CO2 variability. Paleoceanography, 29(9):845–853. https://doi.org/10.1002/2014PA002653

Greenop, R., Sosdian, S.M., Henehan, M.J., Wilson, P.A., Lear, C.H., and Foster, G.L. 2019. Orbital forcing, ice volume, and CO2 across the Oligocene-Miocene transition. Paleoceanography and Paleoclimatology, 34(3):316–328. https://doi.org/10.1029/2018PA003420

Grimm, G.W. and Potts, A.J. 2016. Fallacies and fantasies the theoretical underpinnings of the coexistence approach for palaeoclimate reconstruction. Climate of the Past, 12(3):611–622. https://doi.org/10.1016/j.revpalbo.2016.07.001

Hall, R., Erdélyi, R., Hanna, E., Jones, J.M., and Scaife, A.A. 2015. Drivers of North Atlantic polar front jet stream variability. International Journal of Climatology, 35(8):1697–1720.

Han, F., Yang, T., Zhang, K., Hou, Y., and Song, B. 2020. Early Oligocene *Podocarpium* Leguminosae from Qaidam Basin and its paleoecological and biogeographical implications. Review of Palaeobotany and Palynology, 282:104309. https://doi.org/10.1016/j.revpalbo.2020.104309

Haq, B.U., Hardenbol, J., and Vail, P.R. 1987. Chronology of fluctuating sea levels since the Triassic. Science, 235(4793):1156–1167. https://doi.org/10.1002/joc.4121

Henrot, A.J., François, L., Favre, E., Butzin, M., Ouberdous, M., and Munhoven, G. 2010. Effects of CO2, continental distribution topography and vegetation changes on the climate at the middle Miocene a model study. Climate of the Past, 6(5):675–694. https://doi.org/10.5194/cp-6-675-2010

Herbert-Smith, M. 1971. The Palynology of the Mochras borehole. PhD Thesis, University College of Wales, Aberystwyth, UK.

Herbert-Smith, M. 1979. The Age of the Tertiary Deposits of the Llanbedr Mochras Farm borehole as determined from palynological studies, Institute of Geological Sciences Report 78/24:15–29.

Herbert, T.D., Lawrence, K.T., Tzanova, A., Peterson, L.C., Caballero-Gill, R., and Kelly, C.S. 2016. Late Miocene global cooling and the rise of modern ecosystems. Nature Geoscience, 9(11):843–847. https://doi.org/10.1038/ngeo2813

Holbourn, A.E., Kuhnt, W., Clemens, S.C., Kochhann, K.G., Jöhnck, J., Lübbers, J., and Andersen, N. 2018. Late Miocene climate cooling and intensification of southeast Asian winter monsoon. Nature Communications, 9(1):1584. https://doi.org/10.1038/s41467-018-03950-1

Hren, M.T., Sheldon, N.D., Grimes, S.T., Collinson, M.E., Hooker, J.J., Bugler, M., and Lohmann, K.C. 2013. Terrestrial cooling in Northern Europe during the Eocene–Oligocene transition. Proceedings of the National Academy of Sciences USA, 110(19):7562–7567. https://doi.org/10.1073/pnas.1210930110

Hugueney, M. and Truc, G. 1976. Decouvertes recentes de mammiferes et de mollusquesdans des formations d'age oligocene terminal et aquitanien du SE de la France comparaison avec les gisements deja connus dans la meme region. Geobios, 9(3):359–362. https://doi.org/10.1016/S0016-6995(76)80041-1

Hulme, M. and Barrow, E.M. 1997. Climates of the British Isles present, past and future. Psychology Press Routledge, London.

Hutchinson, D.K., Coxall, H.K., Lunt, D.J., Steinthorsdottir, M., De Boer, A.M., Baatsen, M., von der Heydt, A., Huber, M., Kennedy-Asser, A.T., Kunzmann, L., and Ladant, J.B. 2021. The Eocene–Oligocene transition: a review of marine and terrestrial proxy data, models and model–data comparisons. Climate of the Past, 17(1):269–315. https://doi.org/10.5194/cp-17-269-2021

Hyeong, K., Kuroda, J., Seo, I., and, Wilson, P.A. 2016. Response of the Pacific inter-tropical convergence zone to global cooling and initiation of Antarctic glaciation across the Eocene Oligocene Transition. Scientific Reports, 6(1):30647. https://doi.org/10.1038/srep30647

IPCC. 2022. Climate change 2022 impacts adaptation, and vulnerability. In Pörtner, H.-O., Roberts, D.C., Tignor, M., Poloczanska, E.S., Mintenbeck, K., Alegría, A., Craig, M., Langsdorf, S., Löschke, S., Möller, V., Okem, A., and Rama, B. (eds.), Contribution of working group II to the sixth assessment report of the Intergovernmental Panel on Climate Change. Cambridge University Press, Cambridge, UK and New York, USA. https://doi.org/10.1017/9781009325844

Ivany, L.C., Patterson, W.P., and Lohmann, K.C. 2000. Cooler winters as a possible cause of mass extinctions at the Eocene/ Oligocene boundary. Nature, 407(6806):887–890. https://doi.org/10.1038/35038044

Ivany, L.C., Van Simaeys, S., Domack, E.W., and Samson, S.D. 2006. Evidence for an earliest Oligocene ice sheet on the Antarctic Peninsula. Geology, 34(5):377–380. https://doi.org/10.1130/G22383.1

Jovane, L., Florindo, F., Sprovieri, M., and Pälike, H. 2006. Astronomic calibration of the late Eocene early Oligocene Massignano section central Italy. Geochemistry Geophysics Geosystems, 7(7). https://doi.org/10.1029/2005GC001195

Jowsey, N.L., Parkin, D.L., Slipper, I.J., Smith, A.P.C., and, Walsh, P.T. 1992. The geology and geomorphology of the Beacon Cottage Farm Outlier St Agnes Cornwall. Geological Magazine, 129(1):101–121. https://doi.org/10.1017/S0016756800008153

Kang, W., Cai, M., and Tziperman, E. 2019. Tropical and extratropical general circulation with a meridional reversed temperature gradient as expected in a high obliquity planet. Icarus, 330:142–154. https://doi.org/10.1016/j.icarus.2019.04.028

Katz, M.E., Miller, K.G., Wright, J.D., Wade, B.S., Browning, J.V., Cramer, B.S., and Rosenthal, Y. 2008. Stepwise transition from the Eocene greenhouse to the Oligocene icehouse. Nature Geoscience, 1(5):329–334. https://doi.org/10.1038/ngeo179

Kennett, J.P. 1977. Cenozoic evolution of Antarctic glaciation the circum-Antarctic Ocean and their impact on global paleoceanography. Journal of Geophysical Research, 82(27):3843–3860. https://doi.org/10.1029/jc082i027p03843

Kennett, J.P. and Shackleton, N.J. 1976. Oxygen isotopic evidence for the development of the psychrosphere 38 my ago, Nature, 260(513).

King, C. 1983. Cainozoic micropalaeontological biostratigraphy of the North Sea. Report Institute of Geological Sciences 82(7):1-40.

King, C. 1989. Cenozoic of the North Sea, p. 418–489. In Jenkins, D.G. and Murray, J.W. (eds.), Stratigraphical atlas of fossil foraminifera. British Micropalaeontological Society Series Ellis Horwood Limited, Chichester.

King, C., Gale, A.S., and Barry, T.L. 2016. A revised correlation of Tertiary rocks in the British Isles and adjacent areas of NW Europe, The Geological Society of London Special Reports No. 27, London. https://doi.org/10.1144/SR27

Koumoutsaris, S., Bey, I., Generoso, S., and Thouret, V. 2008. Influence of El Niño–Southern Oscillation on the interannual variability of tropospheric ozone in the northern midlatitudes. Journal of Geophysical Research Atmospheres, 113(D19). https://doi.org/10.1029/2007JD009753

Kovar-Eder, J. 2016. Early Oligocene plant diversity along the Upper Rhine Graben the fossil flora of Rauenberg Germany. Acta Palaeobotanica, 56(2):329–440. https://doi.org/10.1515/acpa-2016-0011

Krzemiński, W., Blagoderov, V., Azar, D., Lukashevich, E., Szadziewski, R., Wedmann, S., André, N.E.L., Collomb, F.M., Waller, A., and Nicholson, D.B. 2019. True flies insecta: Diptera from the late Eocene insect limestone Bembridge Marls of the Isle of Wight England UK. Earth and Environmental Science Transactions of the Royal Society of Edinburgh, 110(3-4):495–554. https://doi.org/10.1017/S1755691018000464

Ladant, J.B., Donnadieu, Y., Lefebvre, V., and Dumas, C. 2014. The respective role of atmospheric carbon dioxide and orbital parameters on ice sheet evolution at the Eocene-Oligocene transition. Paleoceanography, 29(8):810–823. https://doi.org/10.1002/2013PA002593

Lear, C.H., Elderfield, H., and Wilson, P.A. 2000. Cenozoic deep-sea temperatures and global ice volumes from Mg/Ca in benthic foraminiferal calcite. Science, 287(5451):269–272. https://doi.org/10.1126/science.287.5451.269

Lear, C.H., Rosenthal, Y., Coxall, H.K.. and, Wilson, P.A. 2004. Late Eocene to early Miocene ice sheet dynamics and the global carbon cycle. Paleoceanography, 19(4). https://doi.org/10.1029/2004PA001039

Levy, R.H., Meyers, S.R., Naish, T.R., Golledge, N.R., McKay, R.M., Crampton, J.S., DeConto, R.M., De Santis, L., Florindo, F., Gasson, E.G., and Harwood, D.M. 2019. Antarctic ice-sheet sensitivity to obliquity forcing enhanced through ocean connections. Nature Geoscience, 12(2):132–137. https://doi.org/10.1038/s41561-018-0284-4

Li, M., Wan, S., Colin, C., Jin, H., Zhao, D., Pei, W., Jiao, W., Tang, Y., Tan, Y., Shi, X., and Li, A. 2023. Expansion of C4 plants in South China and evolution of East Asian monsoon since 35 Ma black carbon records in the northern South China Sea. Global and Planetary Change, 223:104079. https://doi.org/10.1016/j.gloplacha.2023.104079

Liebrand, D., Beddow, H.M., Lourens, L.J., Pälike, H., Raffi, I., Bohaty, S.M., Hilgen, F.J., Saes, M.J., Wilson, P.A., Van Dijk, A.E., and Hodell, D.A. 2016. Cyclostratigraphy and eccentricity tuning of the early Oligocene through early Miocene 30.1–17.1 Ma *Cibicides mundulus* stable oxygen and carbon isotope records from Walvis Ridge Site 1264. Earth and Planetary Science Letters, 450:392–405. https://doi.org/10.1016/j.epsl.2016.06.007

Liebrand, D., de Bakker, A.T., Beddow, H.M., Wilson, P.A., Bohaty, S.M., Ruessink, G., Pälike, H., Batenburg, S.J., Hilgen, F.J., Hodell, D.A., and Huck, C.E. 2017. Evolution of the early Antarctic ice ages. Proceedings of the National Academy of Sciences USA, 114(15):3867–3872. https://doi.org/10.1073/pnas.1615440114

Lin, X., Wyrwoll, K.H., Chen, H., Zhang, X., Fu, K., Sun, M., Yu, X., and Shen, Z. 2015. An active east Asian monsoon at the Oligocene-Miocene boundary evidence from the Sikouzi Section, Northern China. The Journal of Geology, 123(4):355–367. https://doi.org/10.1086/682278

Ling, C.C., Ma, F.J., Dong, J.L., Zhou, G.H., Wang, Q.J., and Sun, B.N. 2021. A mid-altitude area in southwestern China experienced a humid subtropical climate with subtle monsoon signatures during the early Oligocene evidence from the Ningming flora of Guangxi. Palaeogeography, Palaeoclimatology, Palaeoecology, 579:110601. https://doi.org/10.1016/j.palaeo.2021.110601

Liu, Z., Pagani, M., Zinniker, D., DeConto, R., Huber, M., Brinkhuis, H., Shah, S.R., Leckie, R.M., and Pearson, A. 2009. Global cooling during the Eocene Oligocene climate transition. Science, 323(5918):1187–1190. https://doi.org/10.1126/science.1166368

Lobo, A.H. and Bordoni, S. 2020. Atmospheric dynamics in high obliquity planets. Icarus, 340:113592. https://doi.org/10.1016/j.icarus.2019.04.028

Lu, J., Vecchi, G.A., and Reichler, T. 2007. Expansion of the Hadley cell under global warming. Geophysical Research Letters, 34(6):L06805. https://doi.org/10.1029/2006GL028443

Mai, D.H. 1995. Tertiäre Vegetationgeschichte Europas. Fischer, Jena:691.

Mai, D.H. 1998. Contribution to the flora of the middle Oligocene Calau Beds in Brandenburg, Germany. Review of Palaeobotany and Palynology, 101(1-4):43–70. https://doi.org/10.1016/S0034-6667(97)00069-9

Mantsis, D.F., Lintner, B.R., Broccoli, A.J., Erb, M.P., Clement, A.C., and Park, H.S. 2014. The response of large-scale circulation to obliquity-induced changes in meridional heating gradients. Journal of Climate, 27(14): 5504–5516. https://doi.org/10.1175/JCLI-D-13-00526.1

Martinez, C.J., Maleski, J.J., and Miller, M.F. 2012. Trends in precipitation and temperature in Florida USA. Journal of Hydrology, 452:259–281. https://doi.org/10.1016/j.jhydrol.2012.05.066

Maxwell, E.E., Alexander, S., Bechly, G., Eck, K., Frey, E., Grimm, K., Kovar-Eder, J., Mayr, G., Micklich, N., Rasser, M., and Roth-Nebelsick, A. 2016. The Rauenberg fossil Lagerstätte Baden-Württemberg, Germany a window into early Oligocene marine and coastal

ecosystems of Central Europe. Palaeogeography, Palaeoclimatology, Palaeoecology, 463:238–260. https://doi.org/10.1016/j.palaeo.2016.10.002

Mayes, J.C. 1991. Regional airflow patterns in the British Isles. International Journal of Climatology, 11(5):473–491.

Mayes, J. 1996. Spatial and temporal fluctuations of monthly rainfall in the British Isles and variations in the mid-latitude westerly circulation, International Journal of Climatology A Journal of the Royal Meteorological Society, 16(5):585–596. https://doi.org/10.1002/(SICI)1097-0088(199605)16:5<585::AID-JOC24>3.0.CO;2-%23

McCobb, L.M.E., Duncan, I.J., Jarzembowski, E.A., Stankiewicz, B.A., Wills, M.A., and Briggs, D.E.G. 1998. Taphonomy of the insects from the insect bed Bembridge Marls late Eocene Isle of Wight England. Geological Magazine, 135(4):553–563. https://doi.org/10.1017/S0016756898001204

McLean, D. 2002. The nature age and origin of the Flimston Clay Pembrokeshire palynological and mineralogical analyses. Countyside Council for Wales Report No. 0019:1–26.

Methner, K., Campani, M., Fiebig, J., Löffler, N., Kempf, O., and Mulch, A. 2020. Middle Miocene long-term continental temperature change in and out of pace with marine climate records. Scientific Reports, 10(1):7989. https://doi.org/10.1038/s41598-020-64743-5

Miao, Y., Wu, F., Herrmann, M., Yan, X., and Meng, Q. 2013. Late early Oligocene east Asian summer monsoon in the NE Tibetan Plateau evidence from a palynological record from the Lanzhou Basin, China. Journal of Asian Earth Sciences, 75:46–57. https://doi.org/10.1016/j.jseaes.2013.07.003

Miller, K.G., Wright, J.D., and Fairbanks, R.G. 1991. Unlocking the icehouse Oligocene-Miocene oxygen isotopes eustasy and margin erosion. Journal of Geophysical Research: Solid Earth, 96(B4):6829–6848. https://doi.org/10.1029/90JB02015

Miller, K.G., Browning, J.V., Schmelz, W.J., Kopp, R.E., Mountain, G.S., and Wright, J.D. 2020. Cenozoic sea-level and cryospheric evolution from deep-sea geochemical and continental margin records. Science advances, 6(20):eaaz1346. https://doi.org/10.1126/sciadv.aaz1346

Moreno-Domínguez, R., Postigo-Mijarra, J.M., and Barrón, E. 2021. Palaeoclimatic reconstruction for the late Oligocene La Val fossil site Estadilla Huesca Spain based on CLAMP and LMA. Palaeogeography, Palaeoclimatology, Palaeoecology, 567: 110302. https://doi.org/10.1016/j.palaeo.2021.110302

Mosbrugger, V., Gee, C.T., Belz, G., and Ashraf, A.R. 1994. Three-dimensional reconstruction of an in-situ Miocene peat forest from the Lower Rhine Embayment northwestern Germany new methods in palaeovegetation analysis. Palaeogeography, Palaeoclimatology, Palaeoecology, 110(3-4):295–317. https://doi.org/10.1016/0031-0182(94)90089-2

Mosbrugger, V. and Utescher, T. 1997. The coexistence approach, a method for quantitative reconstructions of Tertiary terrestrial palaeoclimate data using plant fossils. Palaeogeography, Palaeoclimatology, Palaeoecology, 134(1-4):61–86. https://doi.org/10.1016/S0031-0182(96)00154-X

Murray, J.W. 1992. Palaeogene and Neogene. Geological Society, London, Memoirs, 13(1):141–147.

O'Brien, C.L., Huber, M., Thomas, E., Pagani, M., Super, J.R., Elder, L.E., and Hull, P.M. 2020. The enigma of Oligocene climate and global surface temperature evolution. Proceedings of the National Academy of Sciences USA, 117(41):25302–25309. https://doi.org/10.1073/pnas.2003914117

Pälike, H., Norris, R.D., Herrle, J.O., Wilson, P.A., Coxall, H.K., Lear, C.H., Shackleton, N.J., Tripati, A.K., and Wade, B.S. 2006. The heartbeat of the Oligocene climate system. Science, 314(5807):1894–1898. https://doi.org/10.1126/science.1133822

Pattyn, F., Ritz, C., Hanna, E., Asay-Davis, X., DeConto, R., Durand, G., Favier, L., Fettweis, X., Goelzer, H., Golledge, N.R., and Kuipers Munneke, P. 2018. The Greenland and Antarctic ice sheets under 1.5°C global warming. Nature Climate Change, 8(12):1053–1061. https://doi.org/10.1038/s41558-018-0305-8

Peel, M.C., Finlayson, B.L., and McMahon, T.A. 2007. Updated world map of the Köppen-Geiger climate classification. Hydrology and Earth System Sciences, 11(5):1633–1644. https://doi.org/10.5194/hess-11-1633-2007

Pekar, S. and Miller, K.G. 1996. New Jersey Oligocene icehouse sequences ODP Leg 150X correlated with global $\delta^{18}O$ and Exxon eustatic records. Geology, 24(6):567–570. https://doi.org/10.1130/0091-7613(1996)024<0567:NJOISO>2.3.CO;2

Pekar, S.F., Christie-Blick, N., Kominz, M.A., and Miller, K.G. 2002. Calibration between eustatic estimates from backstripping and oxygen isotopic records for the Oligocene. Geology, 30(10):903–906. https://doi.org/10.1130/0091-7613(2002)030<0903:CBEEFB>2.0.CO;2

Pope, J.O., Brown, K., Fung, F., Hanlon, H.M., Neal, R., Palin, E.J., and Reid, A. 2021. Investigation of future climate change over the British Isles using weather patterns. Climate Dynamics, 58(9-10):2405–2419. https://doi.org/10.1007/s00382-021-06031-0

Pound, M.J. and Riding, J.B. 2016. Palaeoenvironment, palaeoclimate and age of the Brassington Formation Miocene of Derbyshire UK. Journal of the Geological Society, 173(2):306–319. https://doi.org/10.1144/jgs2015-050

Pound, M.J. and Salzmann, U. 2017. Heterogeneity in global vegetation and terrestrial climate change during the late Eocene to early Oligocene transition. Scientific Reports, 7(1):43386. https://doi.org/10.1038/srep43386

Pound, M.J. and McCoy, J. 2021. Palaeoclimate reconstruction and age assessment of the Miocene flora from the Trwyn y Parc solution pipe complex of Anglesey Wales UK. Palynology, 45(4):697–703. https://doi.org/10.1080/01916122.2021.1916636

Previdi, M. and Liepert, B.G. 2007. Annular modes and Hadley cell expansion under global warming. Geophysical Research Letters, 34(22):L22701. https://doi.org/10.1029/2007GL031243

Pross, J., Bruch, A., and Kvaček, Z. 1998. Paläoklima-Rekonstruktion für den Mittleren Rupelton Unter-Oligozän des Mainzer Beckens auf der Basis mikro und makrobotanischer Befunde. Mainzer Geowissenschaftliche Mitteilungen., 27:79–92.

Pross, J., Bruch, A.A., Mosbrugger, V., and Kvacek, Z. 2001. Palaeogene pollen and spores as a tool for quantitative palaeoclimate reconstructions the Rupelian Oligocene of central Europe. Conference Proceedings of the IX International Palynological Congress, Houston, TX, USA, p. 299–310.

Quan, C., Liu, Y.S.C., Tang, H., and Utescher, T. 2014. Miocene shift of European atmospheric circulation from trade wind to westerlies. Scientific Reports, 4(1):1–6. https://doi.org/10.1038/srep05660

Quicke, D.L. 1987. The old-world genera of braconine wasps Hymenoptera: Braconidae. Journal of Natural History, 21(1):43–157. https://doi.org/10.1080/00222938700770031

Rind, D. 1998. Latitudinal temperature gradients and climate change. Journal of Geophysical Research: Atmospheres, 103(D6):5943–5971.

Roberts, D.G. 1975. Marine geology of the Rockall Plateau and Trough. Philosophical Transactions of the Royal Society of London Series A Mathematical and Physical Sciences, 278(1285):447–509. https://doi.org/10.1098/rsta.1975.0033

Roth-Nebelsick, A., Utescher, T., Mosbrugger, V., Diester-Haass, L., and Walther, H. 2004. Changes in atmospheric CO2 concentrations and climate from the late Eocene to early Miocene palaeobotanical reconstruction based on fossil floras from Saxony Germany. Palaeogeography, Palaeoclimatology, Palaeoecology, 205(1-2):43–67. https://doi.org/10.1016/j.palaeo.2003.11.014

Scheffer, M., Brovkin, V., and Cox, P.M. 2006. Positive feedback between global warming and atmospheric CO2 concentration inferred from past climate change. Geophysical research letters, 33(10):L10702. https://doi.org/10.1029/2005GL025044

Scotese, C. R. and Wright, N. 2018. PALEOMAP Paleodigital Elevation Models (PaleoDEMS) for the Phanerozoic PALEOMAP Project. Available at: https://www.earthbyte.org/paleodem-resourcescotese-and-wright-2018/

Screen, J.A. and Simmonds, I. 2010. The central role of diminishing sea ice in recent Arctic temperature amplification. Nature, 464(7293):1334–1337.
Seidel, D.J., Fu, Q., Randel, W.J., and Reichler, T.J. 2008. Widening of the tropical belt in a changing climate. Nature Geoscience, 1(1):21–24. https://doi.org/10.1038/ngeo.2007.38
Sharmila, S. and Walsh, K.J.E. 2018. Recent poleward shift of tropical cyclone formation linked to Hadley cell expansion. Nature Climate Change, 8(8):730–736. https://doi.org/10.1038/s41558-018-0227-5
Shukla, A., Mehrotra, R.C., Spicer, R.A., Spicer, T.E., and Kumar, M. 2014. Cool equatorial terrestrial temperatures and the South Asian Monsoon in the early Eocene evidence from the Gurha Mine Rajasthan India. Palaeogeography, Palaeoclimatology, Palaeoecology, 412:187–198. https://doi.org/10.1016/j.palaeo.2014.08.004
Simms, M.J. and Boulter, M.C. 2000. Oligocene cave sediments in County Cork implications for reconstructing the Tertiary landscape of southwest Ireland. Proceedings of the Geologists' Association, 111(4):363–372. https://doi.org/10.1016/S0016-7878(00)80092-9
Śliwińska, K.K., Clausen, O.R., and Heilmann-Clausen, C. 2010. A mid-Oligocene cooling Oi-2b reflected in the dinoflagellate record and in depositional sequence architecture an integrated study from the eastern North Sea Basin. Marine and Petroleum Geology, 27(7):1424–1430. https://doi.org/10.1016/j.marpetgeo.2010.03.008
Śliwińska, K.K. and Heilmann-Clausen, C. 2011. Early Oligocene cooling reflected by the dinoflagellate cyst *Svalbardella cooksoniae.* Palaeogeography, Palaeoclimatology, Palaeoecology, 305(1-4):138–149. https://doi.org/10.1016/j.palaeo.2011.02.027
Śliwińska, K.K., Dybkjær, K., Schoon, P.L., Beyer, C., King, C., Schouten, S., and Nielsen, O.B. 2014. Paleoclimatic and paleoenvironmental records of the Oligocene–Miocene transition central Jylland Denmark. Marine Geology, 350:1–15. https://doi.org/10.1016/j.margeo.2013.12.014
Srivastava, G., Spicer, R.A., Spicer, T.E., Yang, J., Kumar, M., Mehrotra, R., and Mehrotra, N. 2012. Megaflora and palaeoclimate of a late Oligocene tropical delta Makum Coalfield Assam evidence for the early development of the South Asia Monsoon. Palaeogeography, Palaeoclimatology, Palaeoecology, 342:130–142. https://doi.org/10.1016/j.palaeo.2012.05.002
Steinthorsdottir, M., Coxall, H.K., De Boer, A.M., Huber, M., Barbolini, N., Bradshaw, C.D., Burls, N.J., Feakins, S.J., Gasson, E., Henderiks, J., and Holbourn, A.E. 2021. The Miocene the future of the past. Paleoceanography and Paleoclimatology, 36(4):2020PA004037. https://doi.org/10.1029/2020PA004037
Straume, E.O., Nummelin, A., Gaina, C., and Nisancioglu, K.H. 2022. Climate transition at the Eocene–Oligocene influenced by bathymetric changes to the Atlantic–Arctic oceanic gateways. Proceedings of the National Academy of Sciences, USA, 119(17):e2115346119. https://doi.org/10.1073/pnas.2115346119
Stuchlik, L., Ziembińska-Tworzydło, M., Kohlman-Adamska, A., Grabowska, I., Ważyńska, B., Słodkowska, B., and Sadowska, A. 2001.Volume 1 – Spores. In Stuchlik, L. (ed.), Atlas of pollen and spores of the Polish Neogene, W. Szafer Institute of Botany, Polish Academy of Sciences, Kraków, Poland.
Stuchlik, L., Ziembińska-Tworzydło, M., Kohlman-Adamska, A., Grabowksa, I., Ważyńska, H., Słodkowska, B., and Sadowska, A. 2002. Volume 2 – Gymnosperms. In series: Stuchlik, L. (ed.) Atlas of pollen and spores of the Polish Neogene, W. Szafer Institute of Botany, Polish Academy of Sciences, Kraków, Poland.
Stuchlik, L., Ziembińska-Tworzydło, M., Kohlman-Adamska, A., Grabowska, I., Słodkowska, B., Ważyńska, H., and Sadowska, A. 2009. Volume 3 – Angiosperms (1). In Stuchlik, L. (ed.), Atlas of pollen and spores of the Polish Neogene, W. Szafer Institute of Botany, Polish Academy of Sciences, Kraków, Poland.
Stuchlik, L., Ziembińska-Tworzydło, M., Kohlman-Adamska, A., Grabowska, I., Słodkowska, B., Worobiec, E., and Durska, E. 2014. Volume 4 – Angiosperms (2) In Stuchlik, L. (ed.), Atlas of pollen and spores of the Polish Neogene, W. Szafer Institute of Botany, Polish Academy of Sciences, Kraków, Poland.

Tappin, D.R., Chadwick, R.A., Jackson, A.A., Wingfield, R.T.R., and Smith, N.J.P. 1994. The geology of Cardigan Bay and the Bristol Channel British Geological Survey. HMSO, London.
The Mathworks Inc. 2021. MATLAB version 9.10.1649659 (R2021a) Update 1, Mapping Toolbox Version 5.1The MathWorks Inc 2021, Natick, Massachusetts.
Torricelli, S., Menichetti, E., and Knezaurek, G. 2022. Climate-driven dinoflagellate cyst stratigraphy of the Oligocene-lower Miocene turbidite succession of the Lower Congo Basin offshore NW Angola. Journal of African Earth Sciences, 192:104536. https://doi.org/10.1016/j.jop.2022.03.004
Utescher, T., Bruch, A., and Mosbrugger, V. 2024. Documentation and Data (Version 2024), records accessed 2023. The Palaeoflora Database (Data set). Zenodo. https://doi.org/10.5281/zenodo.10881069
Utescher, T., Bruch, A.A., Erdei, B., François, L., Ivanov, D., Jacques, F.M.B., Kern, A.K., Mosbrugger, V., and Spicer, R.A. 2014. The coexistence approach theoretical background and practical considerations of using plant fossils for climate quantification. Palaeogeography, Palaeoclimatology, Palaeoecology, 410:58–73. https://doi.org/10.1016/j.palaeo.2014.05.031
Utescher, T., Bondarenko, O.V., and Mosbrugger, V. 2015. The Cenozoic coolingcontinental signals from the Atlantic and Pacific side of Eurasia. Earth and Planetary Science Letters, 415:121–133. https://doi.org/10.1016/j.epsl.2015.01.019
Utescher, T., Erdei, B., François, L., Henrot, A.J., Mosbrugger, V., and Popova, S. 2021. Oligocene vegetation of Europe and western Asia diversity change and continental patterns reflected by plant functional types. Geological Journal, 56(2):628–649. https://doi.org/10.1002/gj.3830
Van Simaeys, S. 2004. The Rupelian-Chattian boundary in the North Sea Basin and its calibration to the international timescale. Netherlands Journal of Geosciences, 83(3):241–248. https://doi.org/10.1017/S0016774600020308
Van Simaeys, S., Munsterman, D., and Brinkhuis, H. 2005. Oligocene dinoflagellate cyst biostratigraphy of the southern North Sea Basin. Review of Palaeobotany and Palynology, 134(1-2):105–128. https://doi.org/10.1016/j.revpalbo.2004.12.003
Velitzelos, D., Bouchal, J.M., and Denk, T. 2014. Review of the Cenozoic floras and vegetation of Greece. Review of Palaeobotany and Palynology, 204:56–117. https://doi.org/10.1016/j.revpalbo.2014.02.006
Via, R.K. and Thomas, D.J. 2006. Evolution of Atlantic thermohaline circulation early Oligocene onset of deep-water production in the North Atlantic. Geology, 34(6):441–444. https://doi.org/10.1130/G22545.1
Von der Heydt, A. and Dijkstra, H.A. 2006. Effect of ocean gateways on the global ocean circulation in the late Oligocene and early Miocene. Paleoceanography, 21(1):PA1011. https://doi.org/10.1029/2005PA001149
Wade, B.S. and Pälike, H. 2004. Oligocene climate dynamics. Paleoceanography, 19(4): PA4019. https://doi.org/10.1029/2004PA001042
Wade, B.S., Houben, A.J., Quaijtaal, W., Schouten, S., Rosenthal, Y., Miller, K.G., Katz, M.E., Wright, J.D., and Brinkhuis, H. 2012. Multiproxy record of abrupt sea-surface cooling across the Eocene-Oligocene transition in the Gulf of Mexico. Geology, 40(2):159–162. https://doi.org/10.1130/G32577.1
Walsh, P. 2001. The Palaeogeography of the southern half of the British Isles and adjacent Continental Shelf at the Palaeogene/Neogene (g/n) boundary and its subsequent modification: a reconsideration, PhD thesis, Wydawnictwo Uniwersytetu Śląskiego, Katowice, Poland.
Walsh, P.T., Atkinson, K., Boulter, M.C., and Shakesby, R.A. 1987. The Oligocene and Miocene outliers of west Cornwall and their bearing on the geomorphological evolution of Oldland Britain. Philosophical Transactions of the Royal Society of London Series A Mathematical and Physical Sciences:211–245.
Watts, W.A. 1962. Early Tertiary pollen deposits in Ireland. Nature, 193(4815):600.
Wilkinson, G.C. and Boulter, M.C. 1980. Oligocene pollen and spores form the western part of the British Isles. Palaeontographica Abteilung B, 175B(1-3):27–83.

Wilkinson, G.C., Bazley, R.A.B., and Boulter, M.C. 1980. The geology and palynology of the Oligocene Lough Neagh clays Northern Ireland. Journal of the Geological Society, 137(1):65–75. https://doi.org/10.1144/gsjgs.137.1.0065

Wilson, G.S., Pekar, S.F., Naish, T.R., Passchier, S., and DeConto, R. 2008. The Oligocene Miocene boundary Antarctic climate response to orbital forcing. Developments in Earth and Environmental Sciences, 8:369–400. https://doi.org/10.1016/S1571-9197(08)00009-8

Wilson, S.J. 1996. High resolution comparative palynostratigraphy and palaeoecology of Oligocene sequences in the terrestrial basins of the western British Isles and the marine North Sea Basin. PhD thesis, University of Sheffield, Sheffield, UK.

Woodland, A.W. 1971. The Llanbedr (Mochras Farm) borehole – Report 71/18, Institute of Geological Sciences, HMSO, London.

Woods, M.A., Vandenbroucke, T.R.A., Williams, M., Riding, J.B., De Schepper, S., and Saabe, K. 2014. Complex response of dinoflagellate cyst distribution patterns to cooler early Oligocene oceans. Earth-Science Reviews, 138:215–230. https://doi.org/10.1016/j.earscirev.2014.02.004

Xiao, G.Q., Abels, H.A., Yao, Z.Q., Dupont-Nivet, G., and Hilgen, F.J. 2010. Asian aridification linked to the first step of the Eocene-Oligocene climate Transition (EOT) in obliquity-dominated terrestrial records Xining Basin China. Climate of the Past, 6(4):501–513. https://doi.org/10.5194/cp-6-501-2010

Zachos, J.C., Flower, B.P., and Paul, H. 1997. Orbitally paced climate oscillations across the Oligocene /Miocene boundary. Nature, 388(6642):567–570. https://doi.org/10.1038/41528

Zachos, J.C., Pagani, M., Sloan, L., Thomas, E., and Billups, K. 2001a. Trends, rhythms, and aberrations in global climate 65 Ma to present. Science, 292(5517):686–693. https://doi.org/10.1126/science.1059412

Zachos, J.C., Shackleton, N.J., Revenaugh, J.S., Palike, H., and Flower, B.P. 2001b. Climate response to orbital forcing across the Oligocene-Miocene boundary. Science, 292(5515):274–278. https://doi.org/10.1126/science.1058288

Zachos, J.C. and Kump, L.R. 2005. Carbon cycle feedbacks and the initiation of Antarctic glaciation in the earliest Oligocene. Global and Planetary Change, 47(1):51–66. https://doi.org/10.1016/j.gloplacha.2005.01.001

Zanazzi, A., Kohn, M.J., MacFadden, B.J., and Terry, D.O. 2007. Large temperature drop across the Eocene–Oligocene transition in central North America. Nature, 445(7128):639–642. https://doi.org/10.1038/nature05551

TABLE 1. List of recorded taxa types and their associated Nearest Living Relatives. Fossil taxa with unknown Nearest Living Relatives are also listed. Available as a spreadsheet at https://palaeo-electronica.org/content/2024/5275-mid-cenozoic-palaeoclimates-northwest-europe. Tables 1 and 2 are available for download with Appendix tables at: https://palaeo-electronica.org/content/2024/5275-mid-cenozoic-palaeoclimates-northwest-europe.

Type	Division	Family	Taxa	NLR	Removed from MPDry reconstructions? (Y, N or N/A)
Spores and ferns	Unknown	Unknown	*Stereisporites*	Sphagnaceae/ *Sphagnum*?	N
	Unknown	Unknown	*Stereisporites granisteroides*	Sphagnaceae/ *Sphagnum*?	N
	Unknown	Unknown	*Stereisporites microzonales*	Sphagnaceae/ *Sphagnum*?	N
	Unknown	Unknown	*Stereisporites minimoides*	Sphagnaceae/ *Sphagnum*?	N
	Unknown	Unknown	*Stereisporites minor microsteresis*	Sphagnaceae/ *Sphagnum*?	N
	Unknown	Unknown	*Stereisporites semigranulus*	Sphagnaceae/ *Sphagnum*?	N
	Unknown	Unknown	*Stereisporites steroides*	Sphagnaceae/ *Sphagnum*?	N
	Unknown	Unknown	*Corrugatisporites*	*Lygodium*	N
	Unknown	Unknown	*Corrugatisporites multivallatus*	*Lygodium*	N
	Filicophyta	Unknown	*Triplanosporites*	Unknown	N
	Filicophyta	Unknown	*Triplanosporites microsinuosus*	Unknown	N
	Filicophyta	Unknown	*Triplanosporites sinomaxoides*	Unknown	N
	Filicophyta	Unknown	*Triplanosporites sinuosus*	Unknown	N
	Lycophyta	Lycopodiaceae	*Camarozonosporites*	*Lycopodiella*	N
	Lycophyta	Lycopodiaceae	*Camarozonosporites heskemensis*	*Lycopodiella*	N
	Lycophyta	Lycopodiaceae	*Lycopodium inundatum*	*Lycopodium*	N
	Lycophyta	Lycopodiaceae	*Lycopodium clavatum*	*Lycopodium*	N
	Lycophyta	Selaginellaceae	*Cingulatisporites*	Selaginellaceae	N
	Lycophyta	Selaginellaceae	*Echinatisporis*	Selaginellaceae	N
	Lycophyta	Selaginellaceae	*Echinatisporis echinoides*	Selaginellaceae	N
	Lycophyta	Selaginellaceae	*Echinatisporis embryonalis*	Selaginellaceae	N
	Lycophyta	Selaginellaceae	*Echinatisporis longechimus*	Selaginellaceae	N
	Lycophyta	Selaginellaceae	*Echinosporis echinatus*	Selaginellaceae	N
	Lycophyta	Selaginellaceae	*Echinosporis miocenicus*	Selaginellaceae	N
	Lycophyta	Selaginellaceae	*Muerrigerisporis*	Selaginellaceae	N
	Lycophyta	Selaginellaceae	*Muerrigerisporis monstrans*	Selaginellaceae	N
	Polypodiophyta	Anemiaceae	*Cicatricosisporites*	*Anemia*	N
	Polypodiophyta	Anemiaceae	*Cicatricosisporites chattensis*	*Anemia*	N
	Polypodiophyta	Anemiaceae	*Cicatricosisporites paradorogensis*	*Anemia*	N
	Polypodiophyta	Davalliaceae?	*Radialisporis*	Davalliaceae, Dryopteridaceae, Polypodiaceae	N
	Polypodiophyta	Davalliaceae?	*Radialisporis radiatus*	Davalliaceae, Dryopteridaceae, Polypodiaceae	N
	Polypodiophyta	Dennstaedtiaceae	*Verrucatosporites alienus*	Dennstaedtiaceae, *Paesia*	N
	Polypodiophyta	Dennstaedtiaceae	*Verrucatosporites clatriformis*	Dennstaedtiaceae, *Paesia*	N

Type	Division	Family	Taxa	NLR	Removed from MPDry reconstructions? (Y, N or N/A)
Spores and ferns	Polypodiophyta	Dennstaedtiaceae	*Verrucatopsorites favus* subsp. *pseudosecundus*	Dennstaedtiaceae, *Paesia*	N
	Polypodiophyta	Dennstaedtiaceae	*Verrucatosporites favus*	Histiopteris	N
	Polypodiophyta	Dennstaedtiaceae	*Verrucatosporites favus*	Histiopteris	N
	Polypodiophyta	Dennstaedtiaceae	*Verrucatosporites histiopteroides*	Histiopteris	N
	Polypodiophyta	Dennstaedtiaceae	*Verrucatosporites histiopteroides histiopteroides*	Histiopteris	N
	Polypodiophyta	Gleicheniaceae	*Verrucingulatisporites undulatus*	*Gleichenia*	N
	Polypodiophyta	Gleicheniaceae	*Verrucingulatisporites treplinensis*	*Gleichenia*	N
	Polypodiophyta	Gleicheniaceae	*Gleicheniidites*	Gleicheniaceae	N
	Polypodiophyta	Gleicheniaceae	*Gleicheniidites senonicus*	Gleicheniaceae	N
	Polypodiophyta	Gleicheniaceae	*Undulatisporites*	Gleicheniaceae	N
	Polypodiophyta	Gleicheniaceae	*Undulatisporites sculpturis*	Gleicheniaceae	N
	Polypodiophyta	Lygodiaceae	*Leiotriletes*	*Lygodium*	N
	Polypodiophyta	Lygodiaceae	*Leiotriletes triangulus*	*Lygodium*	N
	Polypodiophyta	Lygodiaceae	*Leioltriletes woffi*	*Lygodium*	N
	Polypodiophyta	Osmundaceae	*Baculatisporites*	*Osmunda*	N
	Polypodiophyta	Osmundaceae	*Baculatisporites nanus*	*Osmunda*	N
	Polypodiophyta	Osmundaceae	*Baculatisporites primarius*	*Osmunda*	N
	Polypodiophyta	Osmundaceae	*Osmundacidites*	*Osmunda*	N
	Polypodiophyta	Osmundaceae	*Osmundacidites lignitum*	*Osmunda*	N
	Polypodiophyta	Osmundaceae	*Stratiotes*	*Osmunda*	N
	Polypodiophyta	Osmundaceae	*Stratiotes websteri*	*Osmunda*	N
	Polypodiophyta	Polypodiaceae	*Laevigatosporites*	Various, Polypodiaceae?	N
	Polypodiophyta	Polypodiaceae	*Laevigatosporites discordatus*	Various, Polypodiaceae?	N
	Polypodiophyta	Polypodiaceae	*Laevigatosporites haardti*	Various, Polypodiaceae?	N
	Polypodiophyta	Polypodiaceae	*Polypodiaceoisporites*	*Polypodium*	N
	Polypodiophyta	Polypodiaceae	*Polypodiaceoisporites marxheimensis*	*Polypodium*	N
	Polypodiophyta	Schizaeaceae	*Triletes*	Schizaeaceae	N
	Polypodiophyta	Schizaeaceae	*Triletes corruvallatus*	Schizaeaceae	N
	Polypodiophyta	Schizaeaceae	*Triletes multivallatus*	Schizaeaceae	N
	Polypodiophyta	Schizaeaceae	*Triletes sp. 1*	Schizaeaceae	N
	Polypodiophyta	Schizaeaceae	*Trilites*	Schizaeaceae	N
	Polypodiophyta	Schizaeaceae	*Trilites corruvallatus*	Schizaeaceae	N
	Polypodiophyta	Schizaeaceae	*Trilites multivallatus*	Schizaeaceae	N
	Polypodiophyta	Schizaeaceae	*Trilites sp.1*	Schizaeaceae	N

Type	Division	Family	Taxa	NLR	Removed from MPDry reconstructions? (Y, N or N/A)
Gymnosperms	Cycadophyta	Cycadaceae	*Cycadopites*	*Cycas*	N
	Gnetophyta	Ephedraceae	*Ephedripites*	*Ephedra*	N
	Pinophyta	Cupressaceae	Cupressaceae	Cupressaceae	N
	Pinophyta	Cupressaceae	*Inaperturopollenites*	Cupressaceae	N
	Pinophyta	Cupressaceae	*Inaperturopollenites dubius*	Cupressaceae	N
	Pinophyta	Cupressaceae	*Inaperturopollenites distichiforme*	Cupressaceae	N
	Pinophyta	Cupressaceae	*Inaperturopollenites hiatus*	Cupressaceae	N
	Pinophyta	Cupressaceae	*Inaperturopollenites magnus*	Cupressaceae	N
	Pinophyta	Cupressaceae	*Sequoiapollenites*	Cupressaceae	N
	Pinophyta	Cupressaceae	*Sequoiapollenites polyformosus*	Cupressaceae	N
	Pinophyta	Cupressaceae	*Taxodium*	Cupressaceae	N
	Pinophyta	Pinaceae	*Abiespollenites*	*Abies*	N
	Pinophyta	Pinaceae	*Abietineaepollenites microalatus*	*Abies*	N
	Pinophyta	Pinaceae	*Cathayapollenites*	*Cathaya*	N/A
	Pinophyta	Pinaceae	*Cedripites*	*Cedrus*	N
	Pinophyta	Pinaceae	*Piceaepollis*	*Picea*	N
	Pinophyta	Pinaceae	*Piceaepollis alatus*	*Picea*	N
	Pinophyta	Pinaceae	*Pinuspollenites*	*Pinus*	N
	Pinophyta	Pinaceae	*Pinuspollenites labdacus*	*Pinus*	N
	Pinophyta	Pinaceae	*Pityosporites*	*Pinus*	N
	Pinophyta	Pinaceae	*Pityosporites antarcticus*	*Pinus*	N
	Pinophyta	Pinaceae	*Pityosporites cedroides*	*Cedrus*	N
	Pinophyta	Podocarpaceae	*Podocarpidites*	*Podocarpus*	N
	Pinophyta	Sciadopityaceae	*Sciadopityspollenites*	*Sciadopitys*	N/A
	Pinophyta	Sciadopityaceae	*Sciadopityspollenites serratus*	*Sciadopitys*	N/A
Angiosperms	Angiospermae	Altingiaceae	*Periporopollenites*	*Liquidambar*	N
	Angiospermae	Altingiaceae	*Periporopollenites stigmosus*	*Liquidambar*	N
	Angiospermae	Anacardiaceae	*Tricolpopollenites pseudocingulum*	Anacardiaceae	Y
	Angiospermae	Anacardiaceae	*Tricolporopollenites mangiferoides*	Mangifera	N
	Angiospermae	Aquifoliaceae	*Ilexpollenites*	*Ilex*	N
	Angiospermae	Aquifoliaceae	*Ilexpollenites iliacus*	*Ilex*	N
	Angiospermae	Aquifoliaceae	*Ilexpollenites margaritatus*	*Ilex*	N
	Angiospermae	Aquifoliaceae	*Ilexpollenites microiliacus*	*Ilex*	N
	Angiospermae	Arecaceae	*Arecipites*	Arecaceae, Calamoideae	N
	Angiospermae	Arecaceae	*Calamus*	*Calamus*	N
	Angiospermae	Arecaceae	*Calamus daemonorops*	*Calamus*	N
	Angiospermae	Arecaceae	*Dicolpopollis*	Arecaceae, Calamoideae	N

Type	Division	Family	Taxa	NLR	Removed from MPDry reconstructions? (Y, N or N/A)
	Angiospermae	Arecaceae	*Dicolpopollis kockeli*	Arecaceae, Calamoideae	N
	Angiospermae	Arecaceae	*Monocolpopollenites*	Arecaceae, Calamoideae	N
	Angiospermae	Arecaceae	*Monocolpopollenites tranquillus*	Arecaceae, Calamoideae	N
	Angiospermae	Asteraceae	*Artemisiaepollenites*	*Artemisia*	N
	Angiospermae	Asteraceae	*Compositioipollenites*	Asteraceae	Y
	Angiospermae	Asteraceae	*Compositioipollenites rizophorus*	Asteraceae	Y
	Angiospermae	Asteraceae	*Echitricolporites*	Asteraceae	Y
	Angiospermae	Asteraceae	*Echitricolporites spinosus*	Asteraceae	Y
	Angiospermae	Asteraceae	*Taraxacum*	*Taraxacum*	N
	Angiospermae	Betulaceae	*Alnipollenites*	*Alnus*	N
	Angiospermae	Betulaceae	*Alnipollenites verus*	*Alnus*	N
	Angiospermae	Betulaceae	*Betulaepollenites*	*Betula*	N
	Angiospermae	Betulaceae	*Betulaepollenites betuloides*	*Betula*	N
	Angiospermae	Betulaceae	*Carpinites*	*Carpinus*	N
	Angiospermae	Betulaceae	*Carpinites carpinoides*	*Carpinus*	N
	Angiospermae	Betulaceae	*Triatriopollenites coryloides*	*Corylus*	N
	Angiospermae	Brassicaceae	*Brassicaceae*	Brassicaceae	N
	Angiospermae	Cambombaceae	*Brasenia*	*Brasenia*	N
Angiosperms	Angiospermae	Cambombaceae	*Brasenia ovula*	*Brasenia*	N
	Angiospermae	Caprifoliaceae	*Caprifoliipites*	Caprifoliaceae	Y
	Angiospermae	Caprifoliaceae	*Caprifoliipites viburnoides*	Caprifoliaceae	Y
	Angiospermae	Caryophyllaceae	Caryophyllaceae	Caryophyllaceae	N
	Angiospermae	Chenopodiaceae	Chenopodiaceae	Chenopodiaceae	N
	Angiospermae	Cyperaceae	*Cyperaceaepollis*	Cyperaceae	Y
	Angiospermae	Cyperaceae	*Cyperaceaepollis neogenicus*	Cyperaceae	Y
	Angiospermae	Cyrillaceae/ Clethraceae	*Cyrillaceaepollenites*	Cyrillaceae-Clethraceae	N
	Angiospermae	Cyrillaceae/ Clethraceae	*Cyrillaceaepollenites megaexactus*	Cyrillaceae-Clethraceae	N
	Angiospermae	Elaeagnaceae	*Boehlensipollis*	Elaeagnaceae, Lythraceae	Lythraceae only
	Angiospermae	Elaeagnaceae	*Boehlensipollis hohli*	Elaeagnaceae, Lythraceae	Lythraceae only
	Angiospermae	Ericaceae	*Ericipites*	Ericaceae	N
	Angiospermae	Ericaceae	*Ericipites callidus*	Ericaceae	N
	Angiospermae	Fagaceae	*Cupuliferoipollenites*	Castanea	N
	Angiospermae	Fagaceae	*Cupuliferoipollenites cingulum*	Castanea	N
	Angiospermae	Fagaceae	*Cupuliferoipollenites fusus*	Castanea	N
	Angiospermae	Fagaceae	*Cupuliferoipollenites oviformis*	Castanea	N
	Angiospermae	Fagaceae	*Cupuliferoipollenites pusillus*	Castanea	N
	Angiospermae	Fagaceae	*Tricolporopollenites*	Fagaceae	N

Type	Division	Family	Taxa	NLR	Removed from MPDry reconstructions? (Y, N or N/A)
	Angiospermae	Fagaceae	*Faguspollenites*	*Fagus*	N
	Angiospermae	Fagaceae	*Tricolpopollenites*	*Quercus*	N
	Angiospermae	Fagaceae	*Quercoidites*	*Quercus*	N
	Angiospermae	Fagaceae	*Quercoidites henrici*	*Quercus*	N
	Angiospermae	Fagaceae	*Quercoidites microhenrici*	*Quercus*	N
	Angiospermae	Juglandaceae	*Caryapollenites*	*Carya*	N
	Angiospermae	Juglandaceae	*Caryapollenites circulus*	*Carya*	N
	Angiospermae	Juglandaceae	*Caryapollenites imparilis*	*Carya*	N
	Angiospermae	Juglandaceae	*Caryapollenites simplex*	*Carya*	N
	Angiospermae	Juglandaceae	*Caryapollenites veripites*	*Carya*	N
	Angiospermae	Juglandaceae	*Plicatopollis*	Juglandaceae	N
	Angiospermae	Juglandaceae	*Plicatopollis plicatus*	Juglandaceae	N
	Angiospermae	Juglandaceae	*Plicatopollis pseudopollenites*	Juglandaceae	N
	Angiospermae	Juglandaceae	*Subtriporopollenites*	*Juglans*	N
	Angiospermae	Juglandaceae	*Momipites*	*Alfaroa, Oreomunnea*	N
	Angiospermae	Juglandaceae	*Momipites anellus*	*Alfaroa, Oreomunnea*	N
	Angiospermae	Juglandaceae	*Momipites coryloides*	*Alfaroa, Oreomunnea*	N
	Angiospermae	Juglandaceae	*Momipites quietus*	*Alfaroa, Oreomunnea*	N
	Angiospermae	Juglandaceae	*Momipites tenuipolus*	*Engelhardia*	N
	Angiospermae	Juglandaceae	*Juglanspollenites*	*Juglans*	N
	Angiospermae	Juglandaceae	*Multiporopollenites*	*Juglans*	N
	Angiospermae	Juglandaceae	*Platycaryapollenites*	*Juglans*	N
	Angiospermae	Juglandaceae	*Polyatriopollenites*	*Platycarya*	N
	Angiospermae	Juglandaceae	*Polyatriopollenites stellatus*	*Platycarya*	N
	Angiospermae	Juglandaceae	*Pterocaryapollenites*	*Platycarya*	N
	Angiospermae	Loranthaceae	*Gothanipollis*	*Loranthus*	N
	Angiospermae	Loranthaceae	*Gothanipollis gothanii*	*Loranthus*	N
	Angiospermae	Malvaceae	*Intratriporopollenites*	Brownlowoideae, *Brownlowia, Diplodiscus,* Malvaceae	Malvaceae only
	Angiospermae	Malvaceae	*Intratriporopollenites cecilensis*	Brownlowoideae, *Brownlowia, Diplodiscus,* Malvaceae	Malvaceae only
	Angiospermae	Malvaceae	*Intratriporopollenites indubitabilis*	Brownlowoideae, *Brownlowia, Diplodiscus,* Malvaceae	Malvaceae only
	Angiospermae	Malvaceae	*Intratriporopollenites instructus*	Brownlowoideae, *Brownlowia, Diplodiscus,* Malvaceae	Malvaceae only
	Angiospermae	Malvaceae	*Intratriporopollenites microreticulatus*	Brownlowoideae, *Brownlowia, Diplodiscus,* Malvaceae	Malvaceae only
	Angiospermae	Malvaceae	*Intratriporopollenites pseudoinstructus*	Brownlowoideae, *Brownlowia, Diplodiscus,* Malvaceae	Malvaceae only
	Angiospermae	Malvaceae	*Reevesiapollis*	Malvaceae	Y
	Angiospermae	Malvaceae	*Reevesiapollis triangulus*	Malvaceae	Y
	Angiospermae	Malvaceae	*Intratriporopollenites instructus*	*Tilia*	N
	Angiospermae	Myricaceae	*Myricipites*	*Myrica*	N
	Angiospermae	Myricaceae	*Myricipites bituitus*	*Myrica*	N
Angiosperms					

Type	Division	Family	Taxa	NLR	Removed from MPDry reconstructions? (Y, N or N/A)
	Angiospermae	Myricaceae	*Myricipites robustus*	*Myrica*	N
	Angiospermae	Myricaceae	*Myricipites microcoryphaeus*	*Myrica*	N
	Angiospermae	Myricaceae	*Triatriopollenites*	Myricaceae	N
	Angiospermae	Myricaceae	*Triatriopollenites aroboratus*	Myricaceae	N
	Angiospermae	Myricaceae	*Triatriopollenites roboratus*	Myricaceae	N
	Angiospermae	Myricaceae	*Triatriopollenites rurensis*	Myricaceae	N
	Angiospermae	Myricaceae	*Triatriopollenites subtriangulus*	Myricaceae	N
	Angiospermae	Myrtaceae	*Myrtaceidites*	Myrtaceae	N
	Angiospermae	Nymphaeaceae	*Nymphaeacidites*	*Nymphaea*	N
	Angiospermae	Nyssaceae	*Nyssapollenites*	*Nyssa*	N
	Angiospermae	Nyssaceae	*Nyssapollenites analepticus*	*Nyssa*	N
	Angiospermae	Nyssaceae	*Nyssapollenites instructus*	*Nyssa*	N
	Angiospermae	Nyssaceae	*Nyssapollenites kruschi*	*Nyssa*	N
	Angiospermae	Nyssaceae	*Nyssapollenites pseudocruciatus*	*Nyssa*	N
	Angiospermae	Nyssaceae	*Nyssapollenites pseudolaesus*	*Nyssa*	N
	Angiospermae	Nyssaceae	*Nyssapollenites rodderensis*	*Nyssa*	N
	Angiospermae	Nyssaceae	*Nyssapollenites satzveyensis*	*Nyssa*	N
Angiosperms	Angiospermae	Onagraceae	*Corsinipollenites*	Onagraceae	N
	Angiospermae	Onagraceae	*Corsinipollenites oculusnoctis*	Onagraceae	N
	Angiospermae	Poaceae	*Graminidites*	Poaceae	Y
	Angiospermae	Poaceae	*Graminidites annulatus*	Poaceae	Y
	Angiospermae	Poaceae	*Graminidites laevigatus*	Poaceae	Y
	Angiospermae	Poaceae	*Graminidites medius*	Poaceae	Y
	Angiospermae	Restionaceae	*Milfordia*	*Milfordia*	N
	Angiospermae	Restionaceae	*Milfordia incerta*	*Milfordia*	N
	Angiospermae	Salicaceae	*Retitricolpites*	*Salix*	N
	Angiospermae	Salicaceae	*Retitricolpites anguloluminosus*	*Salix*	N
	Angiospermae	Salicaceae	*Salixipollenites*	*Salix*	N
	Angiospermae	Salicaceae	*Salixipollenites gracilis*	*Salix*	N
	Angiospermae	Santalaceae	*Mediocolpopollis*	Santalaceae	N
	Angiospermae	Santalaceae	*Mediocolpopollis compactus*	Santalaceae	N
	Angiospermae	Sapindaceae	*Cupaneidites*	*Cupania*	N
	Angiospermae	Sapindaceae	*Cupaneidites eucalyptoides*	*Cupania*	N
	Angiospermae	Sapotaceae	*Tetracolporopollenites*	Sapotaceae	N
	Angiospermae	Sapotaceae	*Tetracolporopollenites sapotoides*	Sapotaceae	N
	Angiospermae	Symplocaceae	*Symplocospollenites*	*Symplocos*	N
	Angiospermae	Symplocaceae	*Symplocospollenites anglica*	*Symplocos*	N
	Angiospermae	Symplocaceae	*Symplocospollenites hidasensis*	*Symplocos*	N
	Angiospermae	Symplocaceae	*Symplocospollenites latisporis*	*Symplocos*	N

Type	Division	Family	Taxa	NLR	Removed from MPDry reconstructions? (Y, N or N/A)
Angiosperms	Angiospermae	Symplocaceae	*Symplocospollenites verus*	*Symplocos*	N
	Angiospermae	Symplocaceae	*Symplocospollenites vestibulum*	*Symplocos*	N
	Angiospermae	Thymelaeaceae	*Daphnogene*	Thymelaeaceae?	N
	Angiospermae	Trapaceae	*Trapaceae*	Trapaceae	N
	Angiospermae	Typhaceae	*Sparganiaceaepollenites*	*Spargania*	N
	Angiospermae	Typhaceae	*Sparganiaceaepollenites polygonalis*	*Spargania*	N
	Angiospermae	Ulmaceae	*Zelkovaepollenites*	*Ulmus*	N
	Angiospermae	Urticaceae	*Triporopollenites urticoides*	*Urtica*	N
	Angiospermae	Vitaceae	*Parthenocissus*	*Parthenocissus*	N
	Angiospermae	Vitaceae	*Parthenocissus britannica*	*Parthenocissus*	N
	Angiospermae	Vitaceae	*Vitispollenites*	*Vitis*	N
	Angiospermae	Vitaceae	*Vitispollenites stipitata*	*Vitis*	N
Unknown	Unknown	Unknown	*Corrusporis*	Unknown	N/A
	Unknown	Unknown	*Corrusporis chattensis*	Unknown	N/A
	Unknown	Unknown	*Corrusporis globoverrucatus*	Unknown	N/A
	Unknown	Unknown	*Corrusporis granotuberculatus*	Unknown	N/A
	Unknown	Unknown	*Corrusporis tuberculatus*	Unknown	N/A
	Unknown	Unknown	*Tricolpopollenites hians*	Unknown	N/A
	Unknown	Unknown	*Tricolpopollenites verrucatus*	Unknown	N/A
	Unknown	Unknown	*Tricolpopollenites hastus*	Unknown	N/A
	Unknown	Unknown	*Tricolpopollenites baculoferus*	Unknown	N/A
	Unknown	Unknown	*Tricolporopollenites spinoreticulatus*	Unknown	N/A
	Unknown	Unknown	*Tricolporopollenites spinus*	Unknown	N/A
	Unknown	Unknown	*Tricolporopollenites verrucatus*	Unknown	N/A
	Unknown	Unknown	*Areoligera semicirculata*	Unknown	N/A
	Unknown	Unknown	*Callialasporites*	Unknown	N/A
	Unknown	Unknown	*Carpolithes lividus*	Unknown	N/A
	Unknown	Unknown	*Carpolithes vinaceus*	Unknown	N/A
	Unknown	Unknown	*Cerebropollenites*	Unknown	N/A
	Unknown	Unknown	*Classopollis*	Unknown	N/A
	Unknown	Unknown	*Dewalquea*	Unknown	N/A
	Unknown	Unknown	*Diporicellaesporites*	Unknown	N/A
	Unknown	Unknown	*Dryandroides*	Unknown	N/A
	Unknown	Unknown	*Dryandroides bankslaefolia*	Unknown	N/A
	Unknown	Unknown	*Dryandroides hakeaeafolia*	Unknown	N/A
	Unknown	Unknown	*Dryandroides laevigata*	Unknown	N/A
	Unknown	Unknown	*Echitonium sophiae*	Unknown	N/A
	Unknown	Unknown	*Fusiformisporites*	Unknown	N/A

Type	Division	Family	Taxa	NLR	Removed from MPDry reconstructions? (Y, N or N/A)
Unknown	Unknown	Unknown	*Holkopollenites*	Unknown	N/A
	Unknown	Unknown	*Holkopollenites chemardensis*	Unknown	N/A
	Unknown	Unknown	*Ichyosporites*	Unknown	N/A
	Unknown	Unknown	*Ichyosporites foveasolidus*	Unknown	N/A
	Unknown	Unknown	*Intrapunctosporis*	Unknown	N/A
	Unknown	Unknown	*Intrapunctosporis lusaticus*	Unknown	N/A
	Unknown	Unknown	*Intrapunctosporis pliocaenicus*	Unknown	N/A
	Unknown	Unknown	*Toroisporis*	Unknown	N/A
	Unknown	Unknown	*Triporopollenites aroboratus*	Unknown	N/A
	Unknown	Unknown	*Microfoveolatisporis apheloides*	Unknown	N/A
	Unknown	Unknown	*Microfoveolatisporis tuemmlitzensis*	Unknown	N/A
	Unknown	Unknown	*Minorpollis*	Unknown	N/A
	Unknown	Unknown	*Pompeckjoidaepollenites*	Unknown	N/A
	Unknown	Unknown	*Pompeckjoidaepollenites subhercynicus*	Unknown	N/A
	Unknown	Unknown	*Monolites*	Unknown	N/A
	Unknown	Unknown	*Nudopollis*	Unknown	N/A
	Unknown	Unknown	*Oligopollis*	Unknown	N/A
	Unknown	Unknown	*Obtusisporis*	Unknown	N/A
	Unknown	Unknown	*Tricolporopollenites baculoferus*	Unknown	N/A
	Unknown	Unknown	*Tricolporopollenites spinus*	Unknown	N/A
	Unknown	Unknown	*Tricolporopollenites verrucatus*	Unknown	N/A
	Unknown	Unknown	*Schizosporis*	Unknown	N/A

TABLE 2A. Study site details, including modern and palaeo-location coordinates. Geological ages of core sections are listed (in Ma), alongside key sources of pollen assemblages. Present-day climate variables were taken from WorldClim 2.1 (Fick and Hijmans, 2017). The reconstructed optima of climate variables are listed under the palaeo-variable section. Available as a spreadsheet at https://palaeo-electronica.org/content/2024/5275-mid-cenozoic-palaeoclimates-northwest-europe.

Site	Modern location lat (°)	lon (°)	no. of levels	stage	maximum age (Ma)	minimum age (Ma)	dating technique	assemblage references
Washing Bay	54.54	-6.60	1	?Oligocene	33.9	23	Pollen	Wilkinson and Boulter (1980)
Bovey	50.57	-3.92	1	Rupelian	33.9	27.82	Pollen	Wilkinson and Boulter (1980)
Ballynakilly	53.56	-9.96	1	?Oligocene	33.9	23	Pollen	Wilkinson et al. (1980)
Bellbrook	54.61	-6.25	1	?Oligocene	33.9	23	Pollen	Wilkinson et al. (1980)
Mire House	54.55	-6.75	1	?Oligocene	33.9	23	Pollen	Wilkinson et al. (1980)
Petrockstowe	51.00	-4.13	1	Oligocene	33.9	23	Pollen	Chaanda (2016)
Little Minch (80/14) ALL	58.06	-5.97	6	Rupelian-Chattian*	27.82	23.03	Pollen	Evans et al. (1991)
Little Minch - 1 (62.5 m)	58.06	-5.97	1	Chattian*	25.5	Indeterminate	Pollen, comparison with 80/14 (Wilson, 1996), above 80/14-H	Evans et al. (1991)
Little Minch - 2 (66-67 m)	58.06	-5.97	1	Chattian	25.8	25.5	Pollen, comparison with 80/14 (Wilson, 1996), with 80/14-G	Evans et al. (1991)
Little Minch - 3 (70-72 m)	58.06	-5.97	1	Rupelian or Chattian	31.8	Indeterminate	Pollen, comparison with 80/14 (Wilson, 1996), with 80/14-E	Evans et al. (1991)
Little Minch - 4 (72-73 m)	58.06	-5.97	1	Rupelian	31.8	Indeterminate	Pollen, comparison with 80/14 (Wilson, 1996), with 80/14 - D	Evans et al. (1991)
Little Minch - 5 (73-74 m)	58.06	-5.97	1	Rupelian	31.8	Indeterminate	Pollen, comparison with 80/14 (Wilson, 1996), with 80/14 - D	Evans et al. (1991)
Little Minch - 6 (78 m)	58.06	-5.97	1	Rupelian*	Indeterminate	31.8	Pollen, comparison with 80/14 (Wilson, 1996), with 80/14 - B	Evans et al. (1991)
St. Agnes Beacon	50.31	-5.23	1	Rupelian	33.9	27.82	Pollen	Jowsey et al. (1992); Walsh et al. (1987)
73/35	51.19	-4.59	1	Chattian	27.82	23.03	Pollen	Boulter and Craig (1979)
73/58	51.19	-4.41	1	Chattian	27.82	23.03	Pollen	Boulter and Craig (1979)
Ballygiblin	52.22	-8.52	1	Oligocene	33.9	23	Pollen	Simms and Boulter (2000)
Ballymacadam	52.24	-9.43	1	Oligocene	33.9	23	Pollen	Boulter (1980); Watts (1962)
16/16B-A	58.80	1.23	1	Rupelian	>32.1	<32.1	Pollen, dinoflagellate cyst	Wilson (1996)
16/16B-B	58.80	1.23	1	Rupelian	Indeterminate	31.7	Pollen, dinoflagellate cyst	Wilson (1996)
16/16B-C	58.80	1.23	1	Rupelian	31.5	Indeterminate	Pollen, dinoflagellate cyst	Wilson (1996)
16/16-D	58.80	1.23	1	Rupelian	Indeterminate	31.05	Pollen, dinoflagellate cyst	Wilson (1996)

Site	Modern location lat (°)	lon (°)	no. of levels	stage	maximum age (Ma)	minimum age (Ma)	dating technique	assemblage references
16/16-E	58.80	1.23	1	Chattian	26.8	Indeterminate	Pollen, dinoflagellate cyst	Wilson (1996)
16/16-F	58.80	1.23	1	Chattian		26.6	Pollen, dinoflagellate cyst	Wilson (1996)
16/16-G	58.80	1.23	1	Chattian	>26.3	<26.3	Pollen, dinoflagellate cyst	Wilson (1996)
21/28-A	57.82	-3.10	1	Rupelian	~33	~33	Pollen, dinoflagellate cyst	Wilson (1996)
21/28-B	57.82	-3.10	1	Rupelian	>32.1	<32.1	Pollen, dinoflagellate cyst	Wilson (1996)
21/28-C	57.82	-3.10	1	Rupelian	32		Pollen, dinoflagellate cyst	Wilson (1996)
21/28-D	57.82	-3.10	1	Rupelian		31.8	Pollen, dinoflagellate cyst	Wilson (1996)
21/28-E	57.82	-3.10	1	Rupelian		31.05	Pollen, dinoflagellate cyst	Wilson (1996)
21/28-F	57.82	-3.10	1	Rupelian		30.5	Pollen, dinoflagellate cyst	Wilson (1996)
21/28-G	57.82	-3.10	1	Chattian	26.6	Indeterminate	Pollen, dinoflagellate cyst	Wilson (1996)
80/14-A	57.77	-6.92	1	Rupelian*		31.8	Pollen	Wilson (1996)
80/14-B	57.77	-6.92	1	Rupelian*		31.8	Pollen	Wilson (1996)
80/14-C	57.77	-6.92	1	Rupelian*		31.8	Pollen	Wilson (1996)
80/14-D	57.77	-6.92	1	Rupelian	31.8	Indeterminate	Pollen	Wilson (1996)
80/14-E	57.77	-6.92	1	Rupelian or Chattian	31.8	25.8	Pollen	Wilson (1996)
80/14-F	57.77	-6.92	1	Chattian	25.8	25.5	Pollen	Wilson (1996)
80/14-G	57.77	-6.92	1	Chattian	25.8	25.5	Pollen	Wilson (1996)
80/14-H	57.77	-6.92	1	Chattian	25.5	Indeterminate	Pollen	Wilson (1996)
88/12-A	56.84	-6.99	1	Rupelian*	Indeterminate	31.8	Pollen	Wilson (1996)
88/12-B	56.84	-6.99	1	Rupelian*	Indeterminate	31.8	Pollen	Wilson (1996)
88/12-C	56.84	-6.99	1	Rupelian*	Indeterminate	31.8	Pollen	Wilson (1996)
88/12-D	56.84	-6.99	1	Rupelian	31.8	Indeterminate	Pollen	Wilson (1996)
88/12-E	56.84	-6.99	1	Rupelian or Chattian	31.8	Indeterminate	Pollen	Wilson (1996)
88/12-F	56.84	-6.99	1	Rupelian or Chattian	31.8	Indeterminate	Pollen	Wilson (1996)
88/12-G	56.84	-6.99	1	Chattian	27.05	Indeterminate	Pollen	Wilson (1996)
78/01-A	56.74	-7.32	1	Rupelian or Chattian	33.9	25.6	Pollen	Wilson (1996)
78/01-B	56.74	-7.32	1	Rupelian or Chattian	33.9	25.6	Pollen	Wilson (1996)
78/01-C	56.74	-7.32	1	Rupelian or Chattian	33.9	25.6	Pollen	Wilson (1996)
78/01-D	56.74	-7.32	1	Rupelian or Chattian	33.9	25.6	Pollen	Wilson (1996)

Site	Modern location lat (°)	lon (°)	no. of levels	stage	maximum age (Ma)	minimum age (Ma)	dating technique	assemblage references
78/01-E	56.74	-7.32	1	Rupelian or Chattian	33.9	25.6	Pollen	Wilson (1996)
78/01-F	56.74	-7.32	1	Chattian	25.6	24.8	Pollen	Wilson (1996)
78/01-G	56.74	-7.32	1	Chattian*	24.8	Indeterminate	Pollen	Wilson (1996)
77/07-A	61.51	-4.61	1	Rupelian*	Indeterminate	31.7	Pollen	Wilson (1996)
77/07-B	61.51	-4.61	1	Rupelian	31.7	Indeterminate	Pollen	Wilson (1996)
77/07-C	61.51	-4.61	1	Rupelian or Chattian	31.7	26.8	Pollen	Wilson (1996)
77/07-D	61.51	-4.61	1	Rupelian or Chattian	31.7	26.8	Pollen	Wilson (1996)
77/07-E	61.51	-4.61	1	Early Miocene	23.03	Indeterminate	Pollen	Wilson (1996)
73/36-A	51.25	-4.65	1	Rupelian*	33.9	31.8	Pollen, dinoflagellate cyst	Wilson (1996)
73/36-B	51.25	-4.65	1	Rupelian*	33.9	31.8	Pollen, dinoflagellate cyst	Wilson (1996)
73/36-C	51.25	-4.65	1	Rupelian*	33.9	31.8	Pollen, dinoflagellate cyst	Wilson (1996)
73/36-D	51.25	-4.65	1	Rupelian*	33.9	31.8	Pollen, dinoflagellate cyst	Wilson (1996)
73/36-E	51.25	-4.65	1	Rupelian	31.8	Indeterminate	Pollen, dinoflagellate cyst	Wilson (1996)
73/36-F	51.25	-4.65	1	Rupelian or Chattian	31.8	25.8	Pollen, dinoflagellate cyst	Wilson (1996)
73/36-G	51.25	-4.65	1	Rupelian or Chattian	31.8	25.8	Pollen, dinoflagellate cyst	Wilson (1996)
73/36-H	51.25	-4.65	1	Rupelian or Chattian	31.8	25.8	Pollen, dinoflagellate cyst	Wilson (1996)
73/36-I	51.25	-4.65	1	Rupelian or Chattian	31.8	25.8	Pollen, dinoflagellate cyst	Wilson (1996)
73/36-J	51.25	-4.65	1	Chattian*	25.8	Indeterminate	Pollen, dinoflagellate cyst	Wilson (1996)
LNA	54.65	-6.62	1	Rupelian or Chattian	31.65	25.8	Pollen	Wilson (1996)
LNB	54.65	-6.62	1	Rupelian or Chattian	31.65	25.8	Pollen	Wilson (1996)
LNC	54.65	-6.62	1	Rupelian or Chattian	31.65	25.8	Pollen	Wilson (1996)
LND	54.65	-6.62	1	Rupelian or Chattian	31.65	25.8	Pollen	Wilson (1996)
Castlemartin	51.61	-4.99	1	Early Miocene	23	15.97	Pollen, dinoflagellate cyst	McLean (2002)
LN_13611	54.99	-6.58	1	?Chattian	27.82	23.03	Pollen	Fitzgerald (1999)
LN_27415	54.68	-6.55	1	?Chattian	27.82	23.03	Pollen	Fitzgerald (1999)
LN_603	55.11	-6.40	1	?Chattian	27.82	23.03	Pollen	Fitzgerald (1999)
LN_36_4680	54.56	-6.40	1	?Chattian	27.82	23.03	Pollen	Fitzgerald (1999)
Mochras borehole								
Mochras (1)	52.81	-4.14	2	Oligocene	33.9	23	Pollen	Herbert-Smith (1971)

Site	Modern location lat (°)	lon (°)	no. of levels	stage	maximum age (Ma)	minimum age (Ma)	dating technique	assemblage references
Mochras (2)	52.81	-4.14	3	Oligocene-Early Miocene	33.9	15.97	Pollen	Herbert-Smith (1971)
Depths (m)								
515.42	52.81	-4.14	1	Oligocene, if not older	33.9	23	Pollen	Herbert-Smith (1971)
408.43	52.81	-4.14	1	Oligocene, if not older	33.9	23	Pollen	Herbert-Smith (1971)
368.8	52.81	-4.14	1	Oligocene-Early Miocene	33.9	15.97	Pollen	Herbert-Smith (1971)
368.2	52.81	-4.14	1	Oligocene-Early Miocene	33.9	15.97	Pollen	Herbert-Smith (1971)
324.61	52.81	-4.14	1	Oligocene-Early Miocene, if not younger	33.9	Indeterminate	Pollen	Herbert-Smith (1971)

*Rupelian	If not older, i.e.: Eocene
*Chattian	If not younger, i.e.: Miocene

*Rupelian If not older, i.e.: Eocene
*Chattian If not younger, i.e.: Miocene

TABLE 2B (continued)..

Site	Present-day climate variables							
	MAT (°C)	Warmest Quarter Mean (°C)	Coldest Quarter Mean (°C)	MAP (mm)	Wettest month (mm)	Driest month (mm)	Precipitation seasonality (%)	Köppen-Geiger
Washing Bay	9.58	14.75	5.02	898	93	57	18.24	Cfb
Bovey	8.9	14.02	4.42	1326	159	70	28.2	Cfb
Ballynakilly	9.65	13.9	5.97	1324	147	71	25.52	Cfb
Bellbrook	9.32	14.53	4.68	989	104	59	19.36	Cfb
Mire House	9.23	14.4	4.68	1022	105	64	18.7	Cfb
Petrockstowe	10.08	15.2	5.62	1106	128	62	26.63	Cfb
Little Minch (80/14) ALL	8.35	12.46	4.88	1272	151	57	32.34	Cfb
Little Minch - 1 (62.5 m)	8.35	12.46	4.88	1272	151	57	32.34	Cfb
Little Minch - 2 (66-67 m)	8.35	12.46	4.88	1272	151	57	32.34	Cfb
Little Minch - 3 (70-72 m)	8.35	12.46	4.88	1272	151	57	32.34	Cfb
Little Minch - 4 (72-73 m)	8.35	12.46	4.88	1272	151	57	32.34	Cfb
Little Minch - 5 (73-74 m)	8.35	12.46	4.88	1272	151	57	32.34	Cfb
Little Minch - 6 (78 m)	8.35	12.46	4.88	1272	151	57	32.34	Cfb
St. Agnes Beacon	10.61	15.12	6.82	1040	126	52	39.1	Cfb
73/35	10.65	15.18	6.7	932	113	48	28.15	Cfb
73/58	10.5	15.38	6.3	996	121	52	29.05	Cfb
Ballygiblin	9.77	14.47	5.65	1195	142	66	29.57	Cfb
Ballymacadam	10.15	14.6	6.25	1317	161	70	30.26	Cfb
16/16B-A	7.88	11.65	4.65	1070	131	47	33.18	Cfc
16/16B-B	7.88	11.65	4.65	1070	131	47	33.18	Cfc
16/16B-C	7.88	11.65	4.65	1070	131	47	33.18	Cfc
16/16-D	7.88	11.65	4.65	1070	131	47	33.18	Cfc
16/16-E	7.88	11.65	4.65	1070	131	47	33.18	Cfc
16/16-F	7.88	11.65	4.65	1070	131	47	33.18	Cfc
16/16-G	7.88	11.65	4.65	1070	131	47	33.18	Cfc
21/28-A	8.37	13.45	3.92	660	66	41	15.53	Cfb
21/28-B	8.37	13.45	3.92	660	66	41	15.53	Cfb
21/28-C	8.37	13.45	3.92	660	66	41	15.53	Cfb
21/28-D	8.37	13.45	3.92	660	66	41	15.53	Cfb
21/28-E	8.37	13.45	3.92	660	66	41	15.53	Cfb
21/28-F	8.37	13.45	3.92	660	66	41	15.53	Cfb
21/28-G	8.37	13.45	3.92	660	66	41	15.53	Cfb
80/14-A	8.96	12.73	5.75	1337	156	61	30.26	Cfb
80/14-B	8.96	12.73	5.75	1337	156	61	30.26	Cfb
80/14-C	8.96	12.73	5.75	1337	156	61	30.26	Cfb
80/14-D	8.96	12.73	5.75	1337	156	61	30.26	Cfb
80/14-E	8.96	12.73	5.75	1337	156	61	30.26	Cfb
80/14-F	8.96	12.73	5.75	1337	156	61	30.26	Cfb
80/14-G	8.96	12.73	5.75	1337	156	61	30.26	Cfb
80/14-H	8.96	12.73	5.75	1337	156	61	30.26	Cfb
88/12-A	8.89	12.58	5.75	1312	153	60	29.91	Cfb

Site	Present-day climate variables							
	MAT (°C)	Warmest Quarter Mean (°C)	Coldest Quarter Mean (°C)	MAP (mm)	Wettest month (mm)	Driest month (mm)	Precipitation seasonality (%)	Köppen-Geiger
88/12-B	8.89	12.58	5.75	1312	153	60	29.91	Cfb
88/12-C	8.89	12.58	5.75	1312	153	60	29.91	Cfb
88/12-D	8.89	12.58	5.75	1312	153	60	29.91	Cfb
88/12-E	8.89	12.58	5.75	1312	153	60	29.91	Cfb
88/12-F	8.89	12.58	5.75	1312	153	60	29.91	Cfb
88/12-G	8.89	12.58	5.75	1312	153	60	29.91	Cfb
78/01-A	9.35	13.33	5.97	1419	163	61	32.19	Cfb
78/01-B	9.35	13.33	5.97	1419	163	61	32.19	Cfb
78/01-C	9.35	13.33	5.97	1419	163	61	32.19	Cfb
78/01-D	9.35	13.33	5.97	1419	163	61	32.19	Cfb
78/01-E	9.35	13.33	5.97	1419	163	61	32.19	Cfb
78/01-F	9.35	13.33	5.97	1419	163	61	32.19	Cfb
78/01-G	9.35	13.33	5.97	1419	163	61	32.19	Cfb
77/07-A	6.74	9.98	4.1	2345	277	105	33.38	Cfc
77/07-B	6.74	9.98	4.1	2345	277	105	33.38	Cfc
77/07-C	6.74	9.98	4.1	2345	277	105	33.38	Cfc
77/07-D	6.74	9.98	4.1	2345	277	105	33.38	Cfc
77/07-E	6.74	9.98	4.1	2345	277	105	33.38	Cfc
73/36-A	10.54	15.1	6.62	957	116	49	28.64	Cfb
73/36-B	10.54	15.1	6.62	957	116	49	28.64	Cfb
73/36-C	10.54	15.1	6.62	957	116	49	28.64	Cfb
73/36-D	10.54	15.1	6.62	957	116	49	28.64	Cfb
73/36-E	10.54	15.1	6.62	957	116	49	28.64	Cfb
73/36-F	10.54	15.1	6.62	957	116	49	28.64	Cfb
73/36-G	10.54	15.1	6.62	957	116	49	28.64	Cfb
73/36-H	10.54	15.1	6.62	957	116	49	28.64	Cfb
73/36-I	10.54	15.1	6.62	957	116	49	28.64	Cfb
73/36-J	10.54	15.1	6.62	957	116	49	28.64	Cfb
LNA	9.41	14.52	4.92	1004	105	62	19.33	Cfb
LNB	9.41	14.52	4.92	1004	105	62	19.33	Cfb
LNC	9.41	14.52	4.92	1004	105	62	19.33	Cfb
LND	9.41	14.52	4.92	1004	105	62	19.33	Cfb
Castlemartin	10.6	15.25	6.57	904	108	48	26.9	Cfb
LN_13611	9.47	14.33	5.1	1131	120	63	22.4	Cfb
LN_27415	9.4	14.4	4.97	1017	106	61	20.04	Cfb
LN_603	9.16	13.9	4.9	1157	127	61	24.57	Cfb
LN_36_4680	9.59	14.62	5.18	959	103	58	19.71	Cfb
Mochras borehole								
Mochras (1)	10.14	15.1	5.72	955	112	51	25.04	Cfb
Mochras (2)	10.14	15.1	5.72	955	112	51	25.04	Cfb
Depths (m)								
515.42	10.14	15.1	5.72	955	112	51	25.04	Cfb

Site	Present-day climate variables							
	MAT (°C)	Warmest Quarter Mean (°C)	Coldest Quarter Mean (°C)	MAP (mm)	Wettest month (mm)	Driest month (mm)	Precipitation seasonality (%)	Köppen-Geiger
408.43	10.14	15.1	5.72	955	112	51	25.04	Cfb
368.8	10.14	15.1	5.72	955	112	51	25.04	Cfb
368.2	10.14	15.1	5.72	955	112	51	25.04	Cfb
324.61	10.14	15.1	5.72	955	112	51	25.04	Cfb

*Rupelian
*Chattian

TABLE 2C (continued).

Site	Palaeoclimate variables												
	MAT bio1	Temp Wet bio8	Warmest Quarter Mean bio10	Coldest Quarter Mean bio11	seasonality diff.	MAP bio12	Wettest month bio13	Driest month bio14	Seasonality bio15	Pdry bio17	Pwarm bio18	Pcold bio19	Köppen-Geiger
Washing Bay	13.37	22.61	17.59	9.75	7.84	1308	282	45	25.63	151	298	201	Cfb
Bovey	13.37	22.61	23.22	6.53	16.68	1138	184	45	20.50	151	298	201	Cfa
Ballynakilly	13.37	22.61	23.22	8.14	15.08	1308	282	48	23.92	159	298	221	Cfa
Bellbrook	13.37	22.61	17.59	8.14	9.45	1195	233	45	23.92	151	298	201	Cfb
Mire House	13.37	22.61	23.22	8.14	15.08	1251	270	45	23.92	151	298	221	Cfa
Petrockstowe	12.13	22.61	21.52	5.02	16.51	967	110	45	17.72	143	298	181	Cwb
Little Minch (80/14) ALL	11.27	12.96	17.99	5.33	12.66	1066	108	42	17.03	151	271	201	Cfb
Little Minch - 1 (62.5 m)	10.35	11.36	17.59	4.92	12.66	1081	110	42	17.09	159	271	261	Cfb
Little Minch - 2 (66-67 m)	10.35	11.36	17.59	4.92	12.66	1081	110	42	17.09	159	271	261	Cfb
Little Minch - 3 (70-72 m)	10.35	11.36	17.59	4.92	12.66	1081	110	42	17.09	159	271	261	Cfb
Little Minch - 4 (72-73 m)	11.86	22.61	23.22	4.92	18.29	1081	110	42	17.09	159	271	261	Cfa
Little Minch - 5 (73-74 m)	11.86	22.61	23.22	6.53	16.68	1138	110	42	18.79	159	271	261	Cfa
Little Minch - 6 (78 m)	11.86	22.61	23.22	6.53	16.68	1138	110	42	18.79	159	271	261	Cfa
St. Agnes Beacon	10.35	12.96	17.59	4.92	12.66	796	98	42	17.09	143	217	181	Cfb
73/35	14.87	22.61	23.22	9.75	13.47	1251	257	42	23.92	151	326	201	Cfa
73/58	11.86	22.61	23.22	6.53	16.68	1081	135	42	20.50	143	271	181	Cfa
Ballygiblin	10.83	12.96	17.60	6.53	11.06	853	110	45	18.40	159	217	201	Cfb
Ballymacadam	16.38	22.61	23.22	12.96	10.25	1195	233	42	22.21	143	298	201	Cfa
16/16B-A	19.40	22.61	24.62	16.18	8.44	1308	245	53	30.75	183	326	221	Cfa
16/16B-B	17.89	22.61	24.62	16.18	8.44	1251	196	48	29.05	167	298	221	Cfa
16/16B-C	19.40	22.61	24.62	16.18	8.44	1308	245	56	30.75	191	326	221	Cfa
16/16-D	19.40	22.61	24.62	16.18	8.44	1251	184	59	20.50	214	298	241	Cfa
16/16-E	17.89	22.61	24.62	16.18	8.44	1251	184	59	20.50	206	298	241	Cfa
16/16-F	19.40	22.61	24.62	17.79	6.83	1251	245	59	20.50	214	298	241	Cfa
16/16-G	19.40	22.61	24.62	16.18	8.44	1251	196	59	20.50	198	298	241	Cfa
21/28-A	20.96	23.29	24.97	20.08	4.89	1180	112	67	17.03	234	281	265	Af
21/28-B	20.90	22.61	24.62	19.40	5.23	1422	270	65	22.21	230	326	261	Cfa
21/28-C	14.87	22.61	23.22	8.14	15.08	1251	208	42	32.46	151	326	221	Cfa
21/28-D	17.89	22.61	24.62	16.18	8.44	1308	233	53	30.75	183	326	221	Cfa
21/28-E	19.40	22.61	24.62	16.18	8.44	1251	208	59	20.50	206	298	241	Cfa
21/28-F	17.89	22.61	24.62	17.79	6.83	1251	245	62	20.50	214	298	241	Cfa
21/28-G	17.89	22.61	24.62	16.18	8.44	1251	196	62	20.50	222	298	241	Cfa
80/14-A	22.41	24.22	24.62	21.01	3.62	1251	123	48	51.26	167	326	221	Af
80/14-B	19.40	24.22	24.62	19.40	5.23	1251	123	48	34.17	167	326	221	Cfa

	Palaeoclimate variables												
Site	MAT bio1	Temp Wet bio8	Warmest Quarter Mean bio10	Coldest Quarter Mean bio11	seasonality diff.	MAP bio12	Wettest month bio13	Driest month bio14	Seasonality bio15	Pdry bio17	Pwarm bio18	Pcold bio19	Köppen-Geiger
80/14-C	19.40	24.22	24.62	17.79	6.83	1195	123	53	30.75	167	298	221	Cfa
80/14-D	20.90	24.22	24.62	17.79	6.83	1308	245	65	20.50	230	326	261	Cfa
80/14-E	19.40	24.22	24.62	17.79	6.83	1308	257	62	20.50	222	298	241	Cfa
80/14-F	20.90	24.22	24.62	19.40	5.23	1308	257	56	22.21	175	298	241	Cfa
80/14-G	16.38	22.61	24.62	11.36	13.27	1251	257	48	22.21	167	298	241	Cfa
80/14-H	13.37	22.61	23.22	8.14	15.08	1251	257	42	27.34	151	298	241	Cfa
88/12-A	14.87	22.61	23.22	9.75	13.47	1308	270	56	22.21	175	326	241	Cfa
88/12-B	11.86	22.61	23.22	4.92	18.29	1081	110	59	17.09	175	298	241	Cfa
88/12-C	13.37	22.61	23.22	8.14	15.08	1308	270	48	23.92	167	326	261	Cfa
88/12-D	13.37	22.61	23.22	8.14	15.08	1251	257	48	20.50	167	298	241	Cfa
88/12-E	11.86	22.61	17.59	6.53	11.06	1195	257	48	20.50	167	298	241	Cfb
88/12-F	13.37	22.61	23.22	8.14	15.08	1251	257	59	22.21	198	326	241	Cfa
88/12-G	14.87	22.61	23.22	9.75	13.47	1365	282	59	25.63	214	326	261	Cfa
78/01-A	17.89	22.61	24.62	16.18	8.44	1138	110	53	29.05	175	298	221	Cfa
78/01-B	19.40	22.61	24.62	16.18	8.44	1138	110	45	30.75	159	298	201	Cfa
78/01-C	20.90	24.22	24.62	19.40	5.23	1308	257	65	22.21	230	298	261	Cfa
78/01-D	20.90	24.22	24.62	19.40	5.23	1195	110	65	17.09	230	298	241	Cfa
78/01-E	22.41	24.22	24.62	21.01	3.62	1365	270	65	22.21	230	326	261	Af
78/01-F	20.90	24.22	24.62	21.01	3.62	1365	270	59	22.21	230	326	261	Af
78/01-G	22.41	24.22	24.62	21.01	3.62	1422	282	62	22.21	230	326	261	Af
77/07-A	17.89	22.61	24.62	16.18	8.44	1251	245	48	32.46	167	326	221	Cfa
77/07-B	17.89	22.61	24.62	16.18	8.44	1251	196	56	22.21	183	298	221	Cfa
77/07-C	17.89	22.61	24.62	14.57	10.05	1195	172	51	22.21	175	298	221	Cfa
77/07-D	17.89	22.61	24.62	16.18	8.44	1251	184	56	22.21	214	298	241	Cfa
77/07-E	11.86	21.01	21.81	4.92	16.88	1081	110	48	18.79	167	271	241	Cfb
73/36-A	17.89	22.61	24.62	14.57	10.05	1195	110	45	30.75	159	298	201	Cfa
73/36-B	20.90	24.22	24.62	17.79	6.83	1138	110	62	17.09	222	298	241	Cfa
73/36-C	19.40	22.61	24.62	17.79	6.83	1251	123	48	34.17	167	543	201	Cwa
73/36-D	17.89	22.61	24.62	16.18	8.44	1308	233	48	30.75	167	326	221	Cfa
73/36-E	17.89	22.61	24.62	16.18	8.44	1251	221	48	23.92	167	298	241	Cfa
73/36-F	20.90	22.61	24.62	19.40	5.23	1251	257	59	22.21	214	298	241	Cfa
73/36-G	20.96	23.29	24.41	20.08	4.33	1384	269	63	22.48	222	314	261	Af
73/36-H	17.89	22.61	24.62	16.18	8.44	1195	172	48	20.50	167	298	241	Cfa
73/36-I	22.41	24.22	24.62	19.40	5.23	1308	257	59	22.21	214	298	261	Cfa
73/36-J	22.41	24.22	24.62	21.01	3.62	1195	110	62	17.09	222	298	221	Af
LNA	17.89	22.61	24.62	16.18	8.44	1251	233	53	23.92	183	298	241	Cfa
LNB	22.41	24.22	24.62	19.40	5.23	1308	257	59	20.50	214	298	261	Cfa
LNC	17.89	22.61	24.62	16.18	8.44	1251	184	56	20.50	206	298	241	Cfa
LND	14.87	22.61	23.22	9.75	13.47	1251	245	48	22.21	167	298	241	Cfa
Castlemartin	11.86	22.61	17.59	4.92	12.66	853	110	45	25.63	151	217	221	Cfb
LN_13611	14.87	22.61	23.22	9.75	13.47	1024	110	45	18.79	151	298	201	Cfa
LN_27415	13.37	22.61	24.62	4.92	19.70	1024	110	48	18.79	159	298	221	Cfa

	Palaeoclimate variables												
Site	MAT bio1	Temp Wet bio8	Warmest Quarter Mean bio10	Coldest Quarter Mean bio11	seasonality diff.	MAP bio12	Wettest month bio13	Driest month bio14	Seasonality bio15	Pdry bio17	Pwarm bio18	Pcold bio19	Köppen-Geiger
LN_603	13.37	22.61	24.62	6.53	18.09	1081	110	48	17.09	159	298	221	Cfa
LN_36_4680	13.37	22.61	24.62	6.53	18.09	1081	110	48	17.09	159	298	221	Cfa
Mochras borehole													
Mochras (1)	17.89	22.61	26.03	9.75	16.28	1308	147	73	15.38	246	570	241	Cwa
Mochras (2)	16.38	24.22	24.62	8.14	16.48	1138	123	42	17.09	143	298	181	Cfa
Depths (m)													
515.42	17.89	22.61	26.03	9.75	16.28	1308	147	73	15.38	246	570	241	Cwa
408.43	23.92	24.22	26.03	9.75	16.28	1308	270	45	17.09	151	543	201	Cwa
368.8	14.87	24.22	24.62	6.53	18.09	1138	110	45	15.38	151	298	201	Cfa
368.2	8.84	11.36	16.18	3.32	12.86	739	86	42	17.09	135	190	181	Cfb
324.61	11.86	11.36	17.59	6.53	11.06	1251	135	53	17.09	175	298	302	Cfb

APPENDIX 1.

Geological setting of sediments dated to the Oligocene and Miocene of the northwest edge of Europe

Details concerning previous palynological investigations of exclusively Rupelian (section 1); exclusively Chattian (section 2), Oligocene (section 3), early Miocene (section 4) and sequences containing various ages (section 5) of the northwest edge of Europe have been described below. Descriptions of cores, boreholes and wells taken from sites, and their corresponding lithologies are listed. Dating methods applied to assemblages, proposed depositional settings, palaeoenvironmental reconstructions and palaeoclimate variable reconstructions, where possible, are described below for each study site.

APPENDIX 1.1.

Rupelian sites

Ballymacadam, Co. Tipperary, Republic of Ireland. The Ballymacadam assemblage was taken from pre-Quaternary sediment preserved in a 10 m-thick karstic infill, overlying 80 m of Carboniferous limestone, located in County Tipperary, Republic of Ireland (Wynne, 1857; Boulter, 1980; Coxon and Coxon, 1997; Coxon and McCarron, 2009). The sedimentology of the infill consisted of clays and biogenic material (Coxon and McCarron, 2009). The assemblage was used to reconstruct a well-drained, mixed woodland palaeoenvironment (Boulter, 1980). An Oligocene age was initially assigned to the site, based on the relative abundances of subtropical-tropical elements (*Engelhardia* and Arecaceae); this assignment was further refined to the Rupelian, based on the relative abundance of Rupelian-marker *Boehlensipollis hohli* (King et al., 2016).

Beacon Cottage Farm Outlier at St. Agnes Beacon, Cornwall. The St. Agnes Beacon (Beacon Cottage Farm Outlier) consists of two members including the lowermost, basal, and pebbly sand unit, the Basal Sand Unit and the overlying Candle Clay Unit (Davies and Kitto, 1878; Ussher, 1879; Jowsey et al., 1992). Lignite sample MR 10401, taken from the Candle Clay Member's grey unctuous, laminated clays yielded microfloral remains (Atkinson et al., 1975; Walsh et al., 1987; Jowsey et al., 1992). The assemblage reconstructed a fern dominated assemblage, which thrived in a lacustrine subtropical palaeoenvironment (Walsh et al., 1987; Jowsey et al., 1992). Relative abundance of palms suggested winters were frost-free; mean annual lowland temperatures were reconstructed to 12°C (Walsh et al., 1987) This assignment was based on comparisons with assemblages of similar ages, taken from Bovey and Lough Neagh, from present-day and extinct comparisons of leaf physiognomic qualities of palms (Wolfe, 1978, 1979; Hubbard and Boulter, 1983; Walsh et al., 1987).

Bovey Basin. Bovey Basin contains <1200 m of post-Rupelian sequences of kaolinitic clays, sands and lignites which overlie Eocene flint gravels and Albian-Cenomanian shallow marine sands (Edwards, 1969, 1976). Rootlets were recovered from grey and brown silty clays near the Southacre Clay Pit from borehole 855754 (Edwards, 1976). Descriptions of floral remains from the Blue Water Mine deposits are listed by Heer (1862a-b), Reid and Reid (1910), Chandler (1957) and Wilkinson and Boulter (1980). The palynofloral assemblages reconstructed a frost-free palaeoenvironment with tropical to sub-tropical elements (Chaanda, 2016). Heer (1862a–b) retrieved samples from unnamed sections of the Bovey Tracey formation, though based on lithological descriptions of light-coloured quartzose sand and white clay beds and underlying brown clay sand lignite beds suggest samples were taken from the Blatchford Sands and the underlying Southacre Clay and Lignite (Vincent, 1974; Edwards, 1976; Huggett and Knox, 2006; Chaanda, 2016). White clay units were dominated by riparian elements and reconstructed a cold-peat moor (Heer, 1862a–b). Vegetation reconstructed around basins is dominated by marshlands and tree-covered slopes (Chandler, 1957). Bovey Basin was previously assigned a Chattian, based on the relative abundance of *Boehlensipollis hohli,* which has since been revised to a Rupelian age (Wilkinson et al., 1980; King et al., 2016). The "Tertiary" Bovey floral types were taken from the Heathfield, Brimley, Stover, Twinyeo, Southacre and Abbrook sections of the basin (Wilkinson and Boulter, 1980).

APPENDIX 1.2.

Chattian sites

Lough Neagh, Well 28 and the Lough Neagh Group. The post-Eocene Antrim Lava Group consists of basalts and rhyolites; the overlying Lough Neagh Group is relatively abundant with clays and lignite (McCann, 1991). The Oligocene deposits at Lough Neagh, Northern Ireland, were formed over the Palaeocene Antrim Lava Group (Parnell and Meighan, 1989). Deposits were made in a series of isolated sub-basins, which developed in regions influenced by subaerial volcanism, constrained by NE-SW strike-slip fault movements and by extensional (NNW-SSE) fault regimes (Parnell and Meighan, 1989). Furthermore, mudstones were retrieved from a claypit at Ballynakilly, Co. Tyrone; clays were found to contain many intrastratal microfaults, suggesting the Lough Neagh sediment was deposited under a syndepositional extensional regime (Parnell et al., 1989).

The Lough Neagh Group consists of four main lithologies: conglomerates; sandstones; mudrocks and lignites (Parnell et al., 1989). Conglomerate-types are found primarily in the sequence base; they contain basaltic clasts, including in situ regolithic basalt, chalk fragments and Carboniferous pebbles (Parnell et al., 1989; Fitzgerald, 1999). The Lough Neagh sandstones are both poorly and well-sorted; both types display crossing, low-angle laminations (Parnell et al., 1989; Fitzgerald, 1999). Poorly sorted sandstones contain fine-coarse grains with an angular texture within an abundant clay matrix, whereas well-sorted sandstones contain higher abundances of rounded and quartzose grains (Parnell et al., 1989). The mudstone and siltstone lithologies (mudrocks) are present in a variety of hues (inc. green, brown, black and grey) and contain plant root and biota remains (Parnell et al., 1989). Preserved gastropods – *Viviparus lentus*; *Bernicia* sp. and *Unio* sp. – are indicative of freshwater palaeoenvironments (Parnell et al., 1989). Lignite stratifications are interbedded within the lithologies; they are categorised into woody and non-woody types with woody-types containing <75% organic carbon (Parnell et al., 1989). Clays are dominantly pale-grey and bluish grey with sandy fractions, and high illite and kaolinite fractions – indicative of a non-marine sedimentary palaeoenvironment (Fitzgerald, 1999).

Pollen fossils retrieved from the Lough Neagh lignites suggest Lough Neagh's Chattian palaeoenvironment contained a variety of ferns, palms, swamp cypress-types and conifers – indicative of warm-temperate autochthonous lake-margin swamps with frost-free palaeoenvironments (Wilkinson et al., 1980; Parnell et al., 1989; Parnell and Meighan 1989). Open lake deposits were also reconstructed for Lough Neagh, based on autochthonous assemblages (Parnell and Meighan 1989).

Boreholes taken from the edge of the Lough Neagh (see following sections) were assigned a Chattian age based on the assumption they were taken from the Chattian-dated Lough Neagh Clays (Fitzgerald, 1999). A Chattian was initially assigned to boreholes taken from the Lough Neagh Group, and the surrounding boreholes, being 13/611, 27/415, 13/603 and 36/4680 and Well 28 (Parnell et al., 1989; Hubbard and Boulter, 1980; Wilson, 1996; Fitzgerald, 1999; King et al., 2016). Sediment taken from Well 28 was deposited in a lacustrine depositional setting; lignitic sections were deposited in mudflat palaeoenvironments (Portlock, 1834; Parnell et al., 1989; Wilson, 1996).

Landagivey-1 (BH 13/611). The 13/611 borehole was taken from Landagivey (Lann Áth Geimhe) from County Londonderry, Northern Ireland. Fitzgerald (1999) took 31 samples from the Landagivey borehole at depths 265.65-47.00 m (13/611). The uppermost depths of the borehole contained thick bands of brown and black lignites, intermixed with clayey, fine-grained light to medium grey clays (Fitzgerald, 1999). Lignitic horizons contained <1 mm diameter white clasts (Fitzgerald, 1999). Depths 47.00-166.00 m were dominant in light bluish, grey, olive, and dark yellow clays (Fitzgerald, 1999). Lowermost depths of the 13/611 borehole (261.00-265.65 m) contained greenish-grey clays.

Ballymoney-1 (BH 13/603). Borehole 13/603 was taken from the Tow Valley Fault Line, and 16 samples were taken from depths 290.00-48.00 m (Fitzgerald, 1999). Its uppermost depths (48.00-161.19 m) were characterised by light grey and brownish clay lithologies and with occasional black and brown lignitic fragments (Fitzgerald, 1999). The Ballymoney basin lignites have a high V/Cr ratio, representative of low Cr concentrations, suggesting inorganic matter in the Ballymoney lignites was sourced from the weathering products of the corresponding basalt (Parnell et al., 1989).

Deerpark-2 (BH 36/4680). The Deerpark-2 borehole was sampled at 19 depths along the depths from 72.05-265.13 m (Fitzgerald, 1999). The uppermost clay sections of the Deerpark-2 borehole were described as dominantly yellow and

brown with fine sandy clays. Black woody lignitic fragments were present at depths 103.62 m, and occasional olive colouring of clays was observed (Fitzgerald, 1999). The middle-most layers (233.18-250.00 m) contained brown to black lignitic and organic clays; some showed a notable bright lustrous shine. Layers up to depth 250.00 m contained patches of stiff, brown, and yellow clays. Lowermost depths (250.00-265.13 m) contained greenish, olive, and bluish-hued clays (Fitzgerald, 1999).

Upper Mullan-1 (BH 27/415). The Upper Mullan-1 borehole (27/415) is one of four boreholes (27/416; 27/417; 27/418) taken from the Coagh region, Northern Ireland (Parnell et al., 1989). The Coagh deposit lies on the top of the Antrim Lava Group, based on seismic surveys (Griffith et al., 1987; Fitzgerald, 1999). All four of the Coagh boreholes contain pollen-productive lithologies. In lignitic regions (<1 km-deep) contain many tricolpates and trilete-types (Parnell et al., 1989; Fawcett and Grimshaw, 1989). The Coagh boreholes are relatively uniform in their lithologies; lowermost layers contain mudrock and conglomerates, which are overlain by green mudrocks – which are plentiful in alete spores but limited in bisaccate pollen-types; uppermost green mudrocks contain the vice-versa in assemblage recovery (Parnell et al., 1989). Based on the report of *Sequoia*-types in the Coagh boreholes, the transition towards a drier-climate towards the later Chattian was proposed (Parnell et al., 1989).

APPENDIX 1.3.

Oligocene sites

Petrockstowe Basin, Devon. The Petrockstowe Basin overlies the Culm Measures, Devon, and is composed of sharply based red clays beds which contain spherulitic siderites (Bristow et al., 1992). The palaeobotanical remains found in the uppermost layers are comparable to the Bovey Basin assemblages, thus an Oligocene was assigned to the basin (Vincent 1974; Echlin 2009). Consistent with a post-Eocene assigned from carbon isotope excursions between depths 120-240 m (Chaanda, 2016). Examples of determinant genera *include Arecipites, Monocolpopollenites, Inaperturopollenites, Pompeckjoidaepollenites* (Chaanda, 2016). Petrockstowe Basin's assemblage reconstructed a subtropical-tropical wetland palaeoenvironment (Turner, 1979; Chaanda, 2016).

Stanley Bank Basin. The Stanley Bank Basin is a half-graben adjacent to the Sticklepath-Lustleigh Fault Zone composed of three units with Palaeozoic bedrock, based on seismic survey and borehole results (Tappin et al., 1994). Stanley Bank Basin's middle unit's seismic character is represented by parallel reflectors and is composed of two main facies (King et al., 2016). The lower facies of the middle unit consist of a matrix of colour-mottled clay intermixed with carbonaceous debris (King et al., 2016). The upper facies of the middle unit contain lignitic beds (<5 m-thick), clay and laminations of interbedded silt (King et al., 2016). The Stanley Bank Basin was deposited on a coastal plain, with lignitic sections deposited on Rupelian alluvial floodplains and swamps; marine influence is evident but limited in sections, based on the relative abundance of microplankton (King et al., 2016). Both facies were assigned an Oligocene age, based on the diatoms found, the *Alnipollenites* verus-*Symplocos vestibulum* ratios (Chattian) and *Boehlensipollis* sp. (Rupelian) relative abundance in BGS borehole 73/36 (Boulter and Craig, 1979; Tappin et al., 1994; Evans et al., 1991). Relative abundances of microplankton *Areoligera semicirculata* imply a Rupelian-early Chattian age (Wilson, 1996; King et al., 2016). Facies age is assumed Rupelian at its lowest boundary, given similarities in lignite observed with the proximal Bovey Formation (Wilson, 1996; King et al., 2016).

Washing Bay. The Washing Bay Borehole (<600 m-thick) contains three distinct layers: the Upper Clay and Sand Unit (245 m-thick); the Middle Shales (38 m-thick) and the Lower Clays and Sands (58 m-thick) – which contains lignitic layers up to 2 m-thick, and dark fossiliferous material (Wilkinson et al., 1980). Macrofossil, dicotyledon leaf (*Dewalquea*-types), and freshwater mollusc remains (*Unio* and *Viviparus*-types) were recovered, but due to the poor condition of remains, palaeoenvironmental reconstructions attempts have been unreliable (Johnson and Gilmour, 1921, 1922; Wright, 1924; Johnson, 1941). Wilkinson et al. (1980) suggested sediment was deposited proximal to river deltas, and shallow lake systems (Manning et al., 1970; Watts, 1970). An Oligocene age is assigned to the Washing Bay borehole, based on the borehole's proximity to other Oligo-

cene basins taken from the Lough Neagh Group (Wilkinson et al., 1980; King et al., 2016).

Ballynakilly. The Ballynakilly borehole (31/1091) contains 31 m of Oligocene-dated light grey kaolinite-dominated, silty clays, which were taken from a site near Coalisland (Bain et al., 1976; Wilkinson et al., 1980). Where plant debris was present, clays were darker; ironstone nodules were reported in proximal clay pits (Wilkinson et al., 1980). The Ballynakilly assemblage reconstructed a woodland-wetland palaeoenvironment with very minor subtropical-tropical elements (Bain et al., 1976; Wilkinson et al., 1980). A broad "Oligocene-age" was assigned to the assemblage, based on the basin's proximity to the Lough Neagh Group (King et al., 2016).

Ballygiblin, County Cork. The Ballygiblin assemblage, retrieved from a poorly productive red and grey clay deposit, was assigned an ?Oligocene age based on the relative abundance of *Cicatricosisporites*-type and the assemblage's proximity to the Chattian Lough Neagh basin (Simms and Boulter, 2000; King et al., 2016). Based on the abundances of mosses and ferns, a humid, heavily vegetated palaeoenvironment, with proximity to a lowland stream, was reconstructed (Simms and Boulter, 2000).

Mire House. The Mire House borehole, Northern Ireland, penetrated the edge of the Oligocene Lough Neagh Clays, and it yielded a very limited assemblage (Fowler and Robbie 1961; Watts, 1962; McCann, 1991). The Mire House lignite bands were assigned an Oligocene-age, based on the borehole's proximity to the Lough Neagh Group (Watts 1962; King et al., 2016).

Bellbrook. The Bellbrook borehole was taken from the east edge of the Lough Neagh Clays, and consists of thin, sandy horizons, representative of a low energy palaeoenvironment (Wilkinson et al., 1980). Whilst Bellbrook samples had limited pollen recovery, the Oligocene dominantly autochthonous assemblage reconstructed a woodland palaeoenvironment, with a forest-floor heathland population (Wilkinson et al., 1980; McCabe et al., 1987). A ?Chattian age was proposed for sediment (King et al., 2016).

APPENDIX 1.4.

Early Miocene sites

Castlemartin-3 borehole, Flimston Bay, Pembrokeshire. The Castlemartin-3 borehole was abundant in varicoloured mottled clays of white, red and brown hues (King et al., 2016). Palynological analysis of the Flimston Bay borehole yielded a limited assemblage; post-late Oligocene dating (estimated age 23.03-15.97 Ma) was assigned based on the relative abundance of *Taraxacum* sp. and a lack of *Cicatricosisporites*-types (Jenkins et al., 1995; McLean, 2002; King et al., 2016). The assemblage reconstructed a brackish-freshwater lake environment with a fluctuating lake margin, which was periodically colonised by low-level aquatic plants (McLean, 2002).

APPENDIX 1.5.

Sequences

Mochras. The Mochras borehole was drilled 3 km west of Llanbedr, North Wales, and was taken from a southeast-dipping half-graben (Boomer and Whatley, 1992; Holford et al., 2005). The lowermost depths of the post-Jurassic sediment (77.47-601.78 m) contain lignite, clays and silts dated to the Oligocene, with possible Miocene horizons at the uppermost layers (Woodland, 1971; Herbert-Smith, 1979; Dobson and Whittington, 1987; Tappin et al., 1994). The lowermost unit of the Cenozoic sequence was termed the Basal Red Group (441.0-601.78 m) and is defined by striking-red and structureless layers of silt, which had undergone extensive bioturbation regimes (Woodland, 1971; Herbert-Smith, 1979; Tappin et al., 1994). Silts are slickensided at a 70° angle, and iron banding throughout the member varies in length (Woodland, 1971; Herbert-Smith, 1979). The overlying unit, the Transitional Series (326.8-441.0 m) contains upwards fining sediment beds with clays and silts most prominent towards the upper layer sections (Herbert-Smith, 1971; Woodland, 1971). We do not consider the uppermost Lignite and Clay Unit, as its age is post-early Miocene (Herbert-Smith, 1971; Woodland, 1971; Tappin et al., 1994 King et al., 2016). Previous palynological work form the Mochras Borehole used 66 pollen samples to reconstruct a subtropical to warm-temperate palaeoenvironment with no dominance between moist or arid conditions inferred (Herbert-Smith, 1971). The relative abundances of *Triatriopollenites rurensis* and *Triatriopollenites microcoryphaeus* were used to assign a Rupelian-middle Miocene age to depths (Herbert-Smith, 1971).

Marine boreholes, North Sea. The associations in the marine sequences (16/16B-4 and 21/28B-7) were dated using the relative abundances of listed microplankton, dinoflagellate cyst and pollen-based biomarkers (Wilson, 1996; King et al., 2016). Ages were proposed for listed associations, based on the sea-level curve; proposed ages are listed in Table 2 and Figure 2 (Haq et al., 1987; Cande and Kent, 1995; Wilson, 1996).

Well 16/16B-4. Core 16/16B-4 was taken from the southern section of the South Viking Graben of the North Sea (Wilson, 1996). The 16/16B-4 sequence is comprised of ten associations; Associations A–C were dated to the Rupelian (>28.28 Ma), Associations D–F were dated to the Chattian (28.28-24.23 Ma) and an early Miocene age was proposed for Association G (Wilson, 1996). Oligocene sections contain micaceous, sandy-clayey siltstones, grey-brown claystones and calcareous sands. Brittle sections of lignite were dark brown to black in hue (Wilson, 1996). 7 assemblages were taken and labelled as Associations A–G. Associations were assigned to the Oligocene, based on the relative abundance of pollen-types, including *Tricolpopollenites*-types; *Nyssa*-types; *Sciadopitys*-types, amongst others (Wilkinson and Boulter, 1980; Wilson, 1996). Assemblages Associations A–C reconstructed an open marine palaeoenvironment (Wilson, 1996). A Rupelian assignment on the listed associations was based on the relative abundances of *Aerosphaeridium arcuatum, A. actinocoronatum, Deflandrea phosphoritica, Distatodinium ellipticum,* the top occurrence of *Dicolpopollis kockeli* (Association C), *Pompeckjoidaepollenites subhercynicus, Phthanoperidinium alectrelophum, Retitricolpites angululuminosus, Sparganiaceoepollenites polygonalis, Svalbardella cooksoniae, Wetzeliella gochtii, W. symmetrica* and undefined species listed as *Microdinium* sp.1 (Châteauneuf, 1980) and *Spiniferites* sp.1 (Manum et al., 1989; Wilson, 1996).

Associations D–G were dated based on the first appearances of relative abundances of selected taxa, including but not limited to – *Quercoidites microhenrici, Corrusporis tuberculatus, Corsinipollenites paradorogensis* and *Cicatricosisporites*-types (Wilson, 1996). No changes in relative abundances of taxa were observed between the latest Oligocene and early Miocene sections (Wilson, 1996). An early Miocene age was assigned to Association G, based on the relative abundances of selected taxa, such as – *Momipites*-types, and increases in the relative abundance of *Cupuliferoipollenites*-types and *Trivestibulopollenites*-types (Wilson, 1996). Microplankton associations in the Chattian assemblages, taken from Associations D-F reconstructed shallower marine conditions, with a dominantly brackish palaeoenvironment (Châteauneuf, 1980; Brinkhuis, 1994; Wilson, 1996).

Well 21/28B-7. Core 21/28B-7 was taken from the Outer Moray Firth from the North Sea basin, and Oligocene sediment was present between depths 2770–3200 ft (Wilson, 1996). 7 assemblages were taken and were assigned to sections labelled as “associations” from 21/28B-7 Association A–G (Wilson, 1996). Oligocene layers contained grey and green layers of calcareous claystones and

brown, sandy siltstones with micaceous, sandy patches (Wilson, 1996). Associations A–D were assigned a Rupelian age (>28.28 Ma), whereas Associations E–G were assigned a Chattian age (27.03–25.50 Ma) (Wilson, 1996). A hiatus was recorded after the top of Association D (Wilson, 1996).

Assemblages from Associations A–C reconstructed an open marine palaeoenvironment (Wilson, 1996). Marine biomarkers *Apteodinium spiridoides, Areosphaeridium arcuatum, Areoligera semicirculata, Chiropteridium mespilanum, C. lobospinosum, C. partispinosum, Dapsilidinium simplex, Phthanoperidinium amoenum, P.comatum, P. filigranum, Rhombodinium draco Systematophora placacantha, Thalassiphora pelagica* and *Wetzeliella symmetrica* were used to assign a Rupelian age to Associations A-C (Wilson, 1996). Unspecified species, *Spiniferites* sp. 1 (Manum et al., 1989) and *Microdinium* sp.1 (Châteauneuf, 1980) were also used to date Associations to the Rupelian (Wilson, 1996). Pollen-types *Camerozonosporites haskemsis; Cicatricosisporites chattensis; Micrhystridium fragile; Porocolpopollenites vestibulum; Retitricolpites retiformis; Stereisporites (Stereisporites) stereoides* and *Tricolporopollenites spinus* were used to support a Rupelian assignment (Wilson, 1996). The assemblages from Associations E-G reconstructed a marine palaeoenvironment with proxies deposited in a shallow, near-shore basin (Islam, 1983; Brinkhuis, 1994; Wilson, 1996). A Chattian age was assigned to Associations E–G, based on the relative abundances of *Verrucatosporites alienus*, *V. balticus* and *Echinosporis echinatus*-types and comparisons with the sea-level curve (Haq et al., 1987; Cande and Kent, 1995; Wilson, 1996).

Borehole 80/14, Little Minch Basin, Isle of Skye (57.77°N, 6.92°W). Borehole 80/14 was taken from the west section of the Minch Fault, and it penetrated through 34.6 m and 44.4 m of Quaternary and Oligocene sediments, respectively (Wilson, 1996). The 80/14 borehole was split into 8 associations- Associations A-C were assigned to the Rupelian, Associations D–H were assigned to the Chattian (<28.28 Ma) (Wilson, 1996).

The Little Minch Basin is a small half-graben which lies along the Minch Fault in Scotland (Fyfe et al., 1993; King et al., 2016; Fyfe et al., 2021). The basin's lithology contains plant debris (in core 80/14), poorly sorted interbedded sandstone layers and kaolinitic and carbonaceous clays with occasional allochthonous lignite layers (O'Sullivan, 1979; Wilson, 1996; King et al., 2016). The borehole's lithology is dominated by grey, fossiliferous claystones and carbonaceous fragments (Wilson 1996). Lignite bands (0.1–1 m-think) were present throughout depths 60–80 m; layers of conglomerates and grit were recorded at respective depths 71.6 m and 75.5 m (Wilson, 1996).

The Rupelian-dated associations of the 80/14 borehole (depths 78.93–77.00 m, Associations A–C) are dominantly comprised of layers of grey claystone (Wilson, 1996). A Rupelian age was assigned to Associations A–C, based on the base occurrence of *Verrucatosporites alienus* and *V. histiopteroides* (Wilson, 1996). A Chattian age was assigned to Associations D–E, based on the relative abundance of *Cicatricosisporites chattensis* and *Cyrillaceaepollenites megaexactus*, respectively (Wilkinson and Boulter, 1980; Vinken, 1988; Wilson, 1996). The Little Minch assemblage from borehole 80/14 was dated to the Chattian, based on the relative abundances of *Alnipollenites verus* and *Symplocos vestibulum*, but this was further refined with reference to more stratigraphic taxa-types, as assemblages from Association F–H were comparable with Chattian assemblages from core 16/16B-4, thus were also assigned to the Chattian (Wilson, 1996). Material was deposited in a non-marine, alluvial floodplain palaeoenvironment (Evans et al., 1991). The Little Minch pollen records reconstructed a freshwater fen palaeoenvironment, based on the relative abundance of *Alnipollenites verus* and *Verrucatosporites histiopteroides*, and a proximal conifer-surrounded wetland (Evans et al., 1991; Wilson, 1996).

Borehole 88/12 (57.78°N, 7.00°W). The Oligocene section of the 88/12 borehole consists of conglomerates, interbedded laminations of siltstones and mudstones, alongside sections of lignite (Wilson, 1996). The 88/12 sequence was split into 7 associations; a Rupelian age was assigned to Associations A–C (>28.28 Ma), and a Chattian age was assigned to Associations D–H (28.28–24.23 Ma).

Rupelian-dated associations of the 88/12 borehole (depths 48.50–41.70 m) contains sands with conglomerates at lowermost depths, and sands with pebble clasts (Wilson, 1996). Uppermost Rupelian layers contain thin bands of lignite, held within layers of sands and conglomerates (Wilson, 1996). Rupelian-dating of Associations A–C was based on the relative abundance of *Laevigatosporites discordatus* and one algae-type (sp.1); assemblages were comparable to those described in the Rupelian-dated Association B in borehole 21/28B-7 (Wilson, 1996). The recovered palynological assemblage was limited, but Associ-

ations D–G were assigned to the Chattian, based on the relative abundance of *Trivestibulopollenites betuloides; Cupuliferoipollenites cingulum*-types; the top appearance of *Arecipites*-types (Wilson, 1996).

Borehole 78/01, Canna Basin (57.14°N, 6.75°W). The 78/01 borehole was taken from Canna Basin, which overlies the Little Minch Trough, located in the Sea of Hebrides (Smythe and Kenolty, 1975; Evans et al., 1979; Wilson, 1996). The Canna Basin (<20 km in length) infills a downwarped section of Paleocene basalts (Smythe and Kenolty, 1975; Evans et al., 1979; Fyfe et al., 1993). Its Oligocene section (where depths < 1091.18 m) is comprised of dark-green and lignite-containing layers of brown claystones; layers of coarse sand, grit and pebbled beds are present in the uppermost sections (Wilson, 1996; King et al., 2016). Samples were taken from 7 sections, split into Associations; Associations A–B and Associations C–G were assigned to the Rupelian and Chattian, respectively (Wilson, 1996). Sediment was deposited in non-marine, lacustrine to brackish palaeoenvironmetal settings (Evans et al., 1979; Wilson, 1996; King et al., 2016).

Rupelian-dated depths in the 78/01 borehole (141.20–139.57 m) are comprised of green-brown claystone layers (Wilson, 1996). A Rupelian age-assignment to borehole 78/01 was based on the relative abundance of biomarkers *Cicatricosisporites chattensis; Cupuliferoipollenites cingulum* subsp. *pusillus* and the base occurrence of *Favitricolporites microreticulatus* (Wilson, 1996). Associations C–G were assigned to the Chattian, based on the assemblage comparisons with Chattian-associations of cores 16/16B-4, 77/07 and 88/12, where *Quercoidites microhenrici, Verrucatosporites megabalticus* and *Graminidites*-types were present (Wilkinson and Boulter, 1980; Wilson, 1996).

Borehole 77/07, Solan Bank High, Rona Basin (59.34°N, 4.95°W). Borehole 77/07 was taken from the northwest edge of the Solan Bank High, from its Oligocene-Miocene post-rift drape, which overlies subsided sections of Jurassic-Paleocene infills (Evans et al., 1991; Wilson, 1996). The 77/07 was sampled in five different sections, and assemblages were labelled to have been derived from Associations A–E, respectively (Wilson, 1996). Association A, Association B–D and Association E were dated to Rupelian, Chattian and an early Miocene age, respectively (Wilson, 1996). Hiatuses were recorded in Associations B and D (Wilson, 1996).

The Rupelian-dated association of the 77/07 borehole is dominantly comprised of fine-grained sand, containing vertical rootlets (Wilson, 1996). Assemblages were taken from 5 Associations from borehole 77/07. Association A was dated to the Rupelian, and Associations B–D were assigned to the Chattian; Association E was assigned an early Miocene age (Wilson, 1996). Association A was assigned a “Middle-Oligocene”/ Rupelian, based on the base occurrences of *Triatriopollenites rurensis, Tricolporopollenites pseudocingulum* and similarities in assemblages with those established by 21/28B-7 (Association D), 88/12 (Association B) and those listed by Wilkinson and Boulter (1980); Vinken (1988) (Wilson, 1996). The Mudstone Unit (110.2–112.2 m) was dated to the Oligocene, based on the relative abundance of Chattian markers, including *Favitricolporites microreticulatus, Polyatriopollenites carpinoides, Graminidites annulatus, Gothanipollis gothanii* and *Quercoidites microhenrici* (Châteauneuf, 1980; Vinken, 1988; Wilson 1996). Assemblages were comparable with the Chattian units in 16/16B-4, 21/28B-7 and 80/14 (Wilson, 1996). The Mudstone Unit contained fossiliferous layers of siltstones and dark carbonaceous claystones (Wilson, 1996). The overlying Carbonaceous Unit (112.5–125.3 m) contains highly carbonaceous sandstones and sulphurous, yellow layers of lignite (Wilson, 1996). Association E was dated with an early Miocene age, based on the relative abundance of Aa1 biozone dinoflagellate cyst markers *(Spiniferites ramosus, Systematophora placacantha* and *Paralecaniella indentata)* (Powell, 1992; Wilson, 1996), although based on the presence of the listed dinocyst-types, its true age could overlap with the southern North Sea Miocene zones 1–9, being latest-Chattian to earliest Tortonian (Munsterman and Brinkhuis, 2004). Early Miocene sections contained fossiliferous dark-green, sandy siltstones and layers of mudstone and sandstone (Wilson, 1996). The layers between Oligocene-Miocene-dated sediment are composed of silty, buff mudstone (Wilson, 1996).

Stanley Bank Basin (73/36). The Stanley Bank Basin is a half-graben adjacent to the Sticklepath-Lustleigh Fault Zone composed of three units with Palaeozoic bedrock, based on seismic survey and borehole results (Tappin et al., 1994). Stanley Bank Basin’s middle unit’s seismic character is represented by parallel reflectors and is composed of two main facies (King et al., 2016). The lower facies of the middle unit consist of a matrix of colour-mottled clay intermixed with carbonaceous

debris (King et al., 2016). The upper facies of the middle unit contain lignitic beds (<5 m-thick), clay and laminations of interbedded silt (King et al., 2016). Wilson (1996) dated 10 sections/ associations of the 73/36 borehole, with Associations A–D and Associations E–J, being Rupelian and Chattian, respectively (Wilson, 1996). A hiatus was recorded between Associations D and E (Wilson, 1996).

Rupelian-dated associations A-D (depths 33.10-20.09 m) of the 73/36 borehole contains brown, laminated claystones, sandy siltstones and grey sands at lowermost depths (Wilson, 1996). Uppermost layers contain a frequently varying sedimentology. Layers contain laminated, waxy claystones, red sandstones, orange siltstones and occasional rootlets (Wilson, 1996). Associations A-D were dated to the Rupelian based on the relative abundances of *Dicolpopollis kockeli* (Association A); *Corrusporis tuberculatus; C. granotuberculatus; Reevesiapollis triangulus; Trivestibulopollenites betuloides; Verrucatosporites balticus; V. favus; V. histiopteris* (Wilson, 1996). Rupelian ages were also assigned based on the base occurrences of *Camerozonosporites heskemensis; Graminidites*-types; *Tricolporopollenites pseudocingulum* and *Triletes multivallatus* and the first appearances of *Tricolporopollenites baculoferus* in the pollen records (Wilson, 1996).

The Stanley Bank Basin was deposited on a coastal plain, with lignitic sections deposited on Rupelian alluvial floodplains and swamps; marine influence is evident but limited in sections, based on the relative abundance of microplankton (King et al., 2016). Relative abundances of microplankton *Areoligera semicirculata* imply a Rupelian-early Chattian age (Wilson, 1996; King et al., 2016). Facies age is assumed Rupelian at its lowest boundary, given similarities in lignite observed with the proximal Bovey Formation (Wilson, 1996; King et al., 2016).

REFERENCES

Atkinson, K., Boulter, M.C., Freshney, E.C., Walsh, P.T., and Wilson, A.C. 1975. A revision of the geology of the St Agnes Outlier, Cornwall. Proceedings of the Ussher Society, 3: 86.

Bain, J.A., Stacey, F.R., and Morgan, D.J. 1976. Composition, properties and potential uses of Lough Neagh Clays, Ballynakilly, Northern Ireland. Geological Survey of Northern Ireland. Open file report 58.

Boomer, I. and Whatley, R. 1992. Ostracoda and Dysaerobia in the Lower Jurassic of Wales: the reconstruction of past oxygen levels. Palaeogeography, Palaeoclimatology, Palaeoecology, 99(3–4): 373–379. https://doi.org/10.1016/0031-0182(92)90024-Y

Boulter, M.C. 1980. Irish Tertiary plant fossils in a European context. Journal of Earth Sciences, 3(1), 1–11.

Boulter, M.C. and Craig, D.L. 1979. A middle Oligocene pollen and spore assemblage from the Bristol Channel. Review of Palaeobotany and Palynology, 28(3-4): 259–272. https://doi.org/10.1016/0034-6667(79)90028-9

Brinkhuis, H. 1994. Late Eocene to early Oligocene dinoflagellate cysts from the Priabonian type-area (Northeast Italy): biostratigraphy and paleoenvironmental interpretation. Palaeogeography, Palaeoclimatology, Palaeoecology, 107(1-2): 121–163.

Bristow, C.M., Palmer, Q.G., and Pirrie, D. 1992. Palaeogene basin development: new evidence from the southern Petrockstow Basin, Devon, Proceedings-Ussher Society, 8: 19.

Cande, S.C. and Kent, D.V. 1995. Revised calibration of the geomagnetic polarity timescale for the late Cretaceous and Cenozoic. Journal of Geophysical Research: Solid Earth, 100(B4): 60936095. https://doi.org/10.1029/94JB03098

Chaanda, M.S. 2016. Cenozoic terrestrial palaeoenvironemtal change: an investigation of the Petrockstowe and Bovey basins, south west United Kingdom. PhD Thesis, University of Plymouth, UK.

Chandler, M.E.J. 1957. The Oligocene flora of the Bovey Tracey lake basin, Devonshire. British Museum (Natural History) Geology.

Châteauneuf, J.J. 1980. Palynostratigraphie et paléoclimatologie de l'Eocène supérieur et de l'Oligocène du Bassin de Paris (France).

Coxon, P. and Coxon, C. 1997. A pre-Pliocene or Pliocene land surface in County Galway, Ireland. Geological Society, London, Special Publications, 120(1): 37–55. https://doi.org/10.1144/GSL.SP.1997.120.01.04
Davies, A. and Kitto, B. 1878. On some beds of sand and clay in the parish of St Agnes Cornwall. Transactions of the Royal Geological Society of Cornwall, 9: 196–203.
Dobson, M.R. and Whittington, R.J. 1987. The geology of Cardigan Bay. Proceedings of the Geologists' Association, 98(4): 331–353. https://doi.org/10.1016/S0016-7878(87)80074-3
Echlin, C. 2009. Geological evaluation of a commercial ball clay deposit. Materials and Equipment-Whitewares, 22(2): 5.
Edwards, R.A. 1969. Preliminary results of the mapping of the Bovey Basin (Abstract), Proceedings of the Ussher Society, 2: 85.
Edwards, R.A. 1976. Tertiary sediments and structure of the Bovey Basin, south Devon. Proceedings of the Geologists' Association, 87(1): 1–26. https://doi.org/10.1016/S0016-7878(76)80032-6
Evans, D., Wilkinson, G.C., and Craig, D.L. 1979. The Tertiary sediments of the Canna basin, Sea of the Hebrides. Scottish Journal of Geology, 15(4): 329–332. https://doi.org/10.1144/sjg15040329
Evans, D., Hallsworth, C., Jolley, D.W., and Morton, A.C. 1991. Late Oligocene terrestrial sediments from a small basin in the Little Minch. Scottish Journal of Geology, 27(1): 33–40. https://doi.org/10.1144/sjg27010033
Fawcett, A.H. and Grimshaw, J. 1989. Carbon-13 NMR characterisation of Northern Ireland lignites, abstract, Irish Journal of Earth Sciences, 10.
Fitzgerald, J.A. 1999. Pollen and spore assemblages from the Oligocene Lough Neagh Group Vol. 1, PhD Thesis, University of Sheffield, UK.
Fowler, A. and Robbie, J.A. 1961. Geology of the country around Dungannon, Memoir of the Geological Survey of Northern Ireland: 274.
Fyfe, J.A., Long, D., and Evans, D. 1993. United Kingdom Offshore Regional Report: The Geology of the Malin-Hebrides Sea Area, HMSO for the British Geological Survey.
Fyfe, L.J.C., Schofield, N., Holford, S.P., Jerram, D.A., and Hartley, A. 2021. Emplacement of the Little Minch Sill Complex, Sea of Hebrides Basin, NW Scotland. Journal of the Geological Society, 178(3): 1–23. https://doi.org/10.1144/jgs2020-177
Griffith, A.E., Legg, I.C., and Mitchell, W.I. 1987. Mineral Resources, p. 43–58. In Buchanan, R.H. and Walker, B.M. (eds.) Province, City and People: Belfast and its Region, Greystone Books, Belfast.
Haq, B.U., Hardenbol, J., and Vail, P.R. 1987. Chronology of fluctuating sea levels since the Triassic. Science, 235(4793): 1156–1167. https://doi.org/10.1002/joc.4121
Heer, O. 1862a. XL. On the fossil flora of Bovey Tracey. Philosophical Transactions of the Royal Society of London, (152): 1039–1086. https://doi.org/10.1098/rstl.1862.0043
Heer, O. 1862b. XVI. The fossil flora of Bovey Tracey. Proceedings of the Royal Society of London, (11): 453–455. https://doi.org/10.1098/rspl.1860.0099
Herbert-Smith, M. 1979. The age of the Tertiary deposits of the Llanbedr (Mochras Farm) borehole as determined from palynological studies, Institute of Geological Sciences Report, 78/24: 15–29.
Holford, S.P., Green, P.F., and Turner, J.P. 2005. Palaeothermal and compaction studies in the Mochras borehole (NW Wales) reveal early Cretaceous and Neogene exhumation and argue against regional Palaeogene uplift in the southern Irish Sea. Journal of the Geological Society, 162(5): 829–840. https://doi.org/10.1144/0016-764904-118
Hubbard, R.N.L.B. and Boulter, M.C. 1983. Reconstruction of Palaeogene climate from palynological evidence. Nature, 301(5896): 147–150. https://doi.org/10.1038/301147a0
Huggett, J.M. and Knox, R.W.O'B. 2006. Clay mineralogy of the Tertiary onshore and offshore strata of the British Isles. Clay Minerals, 41(1): 5–46. https://doi.org/10.1180/0009855064110195

Islam, M.A., 1983. Dinoflagellate cyst taxonomy and biostratigraphy of the Eocene Bracklesham Group in southern England. Micropaleontology: 328–353.
Jenkins, D.G., Boulter, M.C., and Ramsay, A.T.S. 1995. The Flimston Clay, Pembrokeshire, Wales: a probable late Oligocene lacustrine deposit. Journal of Micropalaeontology, 14(1): 66.
https://doi.org/10.1144/jm.14.1.66
Johnson, T. 1941. List of fossil plants from Co. Tyrone.National Museum of Ireland, Dublin.
Johnson, T. and Gilmore, J.G. 1921. The occurrence of Dewalquea in the coal-bore at Washing Bay, The scientific proceedings of the Royal Dublin Society16: 323–333.
Johnson, T. and Gilmore, J.G. 1922. The lignite of Washing Bay, Co. Tyrone. The scientific proceedings of the Royal Dublin Society, 17: 59–64.
Jowsey, N.L., Parkin, D.L., Slipper, I.J., Smith, A.P.C., and Walsh, P.T. 1992. The geology and geomorphology of the Beacon Cottage Farm Outlier, St Agnes, Cornwall. Geological Magazine, 129(1): 101–121.
https://doi.org/10.1017/S0016756800008153
King, C., Gale, A.S., and Barry, T.L. 2016. A revised correlation of Tertiary rocks in the British Isles and adjacent areas of NW Europe, The Geological Society, Geological Society Special Report No. 27.
Manning, P.I., Robbie, J.A., Wilson, H.E., and Hull, E. 1970. Geology of Belfast and the Lagan Valley:(one-inch Geological Sheet 36), HMSO: 36.
Manum, S.B., Boulter, M.C., Gunnarsdottir, H., Rangnes, K., and Scholze, A., 1989. 32. Eocene to Miocene Palynology of the Norwegian Sea (ODP Leg 104). Proceedings of the Ocean Drilling Program, Scientific Results, 104: 611–662.
McCabe, A.M., Coope, G.R., Gennard, D.E., and Doughty, P. 1987. Freshwater organic deposits and stratified sediments between early and late Midlandian (Devensian) till sheets, at Aghnadarragh, County Antrim, Northern Ireland. Journal of Quaternary Science, 2(1): 11–33.
https://doi.org/10.1002/jqs.3390020104
McCann, N. 1991. Subsurface geology of the Lough Neagh-Larne basin, Northern Ireland. Irish Journal of Earth Sciences: 53–64.
McLean, D. 2002. The nature, age and origin of the Flimston Clay, Pembrokeshire: palynological and mineralogical analyses, Countyside Council for Wales, Report No. 0019: 1–26.
Munsterman, D.K. and Brinkhuis, H. 2004. A southern North Sea Miocene dinoflagellate cyst zonation. Netherlands Journal of Geosciences, 83(4): 267–285.
https://doi.org/10.1073/pnas.0505267102
O'Sullivan, K.N. 1979. The sedimentology, geochemistry and conditions of deposition of the Tertiary rocks of the Llanbedr (Mochras Farm) Borehole, HM Stationery Office, 78/24.
Parnell, J. and Meighan, I.G. 1989. Lignite and associated deposits of the Tertiary Lough Neagh Basin, Northern Ireland. Journal of the Geological Society, 146(2): 351–352.
https://doi.org/10.1144/gsjgs.146.2.0351
Parnell, J., Shukla, B., and Meighan, I.G. 1989. The lignite and associated sediments of the Tertiary Lough Neagh Basin. Irish Journal of Earth Sciences: 67–88.
Portlock, J.E. 1843. Report on the Geology of the County of Londonderry, and of Parts of Tyrone and Fermanagh. A. Milliken.
Powell. A.J., 1992. (ed) A Stratigraphic Index of Dinoflagellate Cysts.
Reid, C. and Reid, E.M. 1910. The lignite of Bovey Tracey, Philosophical Transactions of the Royal Society of London, 201(B): 161–178.
Smythe, D.K. and Kenolty, N. 1975. Tertiary sediments in the Sea of Hebrides, Journal of the Geological Society, 131: 227–233.
https://doi.org/10.1144/gsjgs.131.2.0227
Tappin, D.R., Chadwick, R.A., Jackson, A.A., Wingfield, R.T.R., and Smith, N.J.P. 1994. The geology of Cardigan Bay and the Bristol Channel, British Geological Survey, United Kingdom Offshore Regional Report.
Turner, C. 1979. Geology of the country around Bude and Bradworthy. Geological Survey of Great Britain, memoir 309.
Ussher, W.A.E. 1879. II.–Post-Tertiary Geology of Cornwall1. Geological Magazine, 6(3): 102–110.
https://doi.org/10.1017/S0016756800170074
Vincent, A. 1974. Sedimentary environments of the Bovey Basin, Unpublished M. Phil. Thesis, University of Surrey, UK.

Vinken, R. 1988. The Northwest European Tertiary Basin: results of the international geological correlation-programme, Project No. 124.

Walsh, P.T., Atkinson, K., Boulter, M.C., and Shakesby, R.A. 1987. The Oligocene and Miocene outliers of west Cornwall and their bearing on the geomorphological evolution of Oldland Britain. Philosophical Transactions of the Royal Society of London. Series A, Mathematical and Physical Sciences: 211–245.

Watts, W.A. 1962. Early Tertiary pollen deposits in Ireland. Nature, 193(4815): 600.

Watts, W.A. 1970. Tertiary and Interglacial floras in Ireland, p. 17–33. In Stephens, N. and Glasscock, R.E. (eds.) Irish Geographical Studies. Queen's University Belfast.

Wilkinson, G.C. and Boulter, M.C. 1980. Oligocene pollen and spores form the western part of the British Isles, Palaeontographica Abteilung B, 175B(1-3): 27–83.

Wilkinson, G.C., Bazley, R.A.B., and Boulter, M.C. 1980. The geology and palynology of the Oligocene Lough Neagh clays, Northern Ireland. Journal of the Geological Society, 137(1): 65–75.
https://doi.org/10.1144/gsjgs.137.1.0065

Wilson, S.J. 1996. High resolution comparative palynostratigraphy and palaeoecology of Oligocene sequences in the terrestrial basins of the western British Isles and the marine North Sea Basin, PhD thesis, University of Sheffield, UK.

Wolfe, J.A. 1978. A paleobotanical interpretation of Tertiary climates in the Northern Hemisphere: Data from fossil plants make it possible to reconstruct Tertiary climatic changes, which may be correlated with changes in the inclination of the earth's rotational axis. American Scientist, 66(6): 694–703.

Wolfe, J.A. 1979, Temperature parameters of humid to mesic forests of Eastern Asia and relation to forests of other regions of the Northern Hemisphere and Australasia: United States Geological Survey Professional Paper, 1106: 37.

Woodland, A.W. (ed.) 1971. The Llanbedr (Mochras Farm) Borehole, Institute of Geological Sciences, Report No. 71/18.

Wright, W.B. 1924. Age and origin of the Lough Neagh clays. Quarterly Journal of the Geological Society, 80(1-4): 468–488.
https://doi.org/10.1144/GSL.JGS.1924.080.01-04.23

Wynne, A.B. 1857. On the Tertiary Clay and Lignite at Ballymacadam. British Association Report.

UTESCHER ET AL. (2024)APPENDIX 2.

List of pollen types (with revised taxonomy) reported throughout Oligocene to Miocene palynological study of the British Isles, presented in a presence-absence matrix. Synonyms are listed, dependent on row number, shown in column: identification (ID). Nearest Living Relatives (NLRs) are listed, where possible, based on assignments listed by Stuchlik et al. (2001, 2002, 2009, 2014) and Utescher et al. (2024). Available as a spreadsheet at https://palaeo-electronica.org/content/2024/5275-mid-cenozoic-palaeoclimates-northwest-europe.

APPENDIX 3.

Taxonomic revision of fossil names, based on revisions by Stuchlik et al. (2001, 2002, 2009, 2014). Available as a spreadsheet at https://palaeo-electronica.org/content/2024/5275-mid-cenozoic-palaeoclimates-northwest-europe.

APPENDIX 4.

List of model outputs of palaeoclimate variables from each study site. Reconstructed optima and 50% uncertainties and the differences between optima and uncertainties have been listed. Available as a spreadsheet at https://palaeo-electronica.org/content/2024/5275-mid-cenozoic-palaeoclimates-northwest-europe.